NAVAL POSTGRADUATE SCHOOL

MONTEREY, CALIFORNIA

THESIS

OPTIMIZATION AND STATISTICAL EVALUATION OF GOES CLOUD-TOP PROPERTIES FOR NOWCASTING LIGHTNING INITIATION

by

Ryan J. Harris

March 2010

Thesis Advisors: Philip A. Durkee
Kurt E. Nielsen

REPORT DOCUMENTATION PAGE			*Form Approved OMB No. 0704-0188*
Public reporting burden for this collection of information is estimated to average 1 hour per response, including the time for reviewing instruction, searching existing data sources, gathering and maintaining the data needed, and completing and reviewing the collection of information. Send comments regarding this burden estimate or any other aspect of this collection of information, including suggestions for reducing this burden, to Washington headquarters Services, Directorate for Information Operations and Reports, 1215 Jefferson Davis Highway, Suite 1204, Arlington, VA 22202-4302, and to the Office of Management and Budget, Paperwork Reduction Project (0704-0188) Washington DC 20503.			
1. AGENCY USE ONLY *(Leave blank)*	**2. REPORT DATE** March 2010	**3. REPORT TYPE AND DATES COVERED** Master's Thesis	
4. TITLE AND SUBTITLE Optimization and Statistical Evaluation of GOES Cloud-Top Properties for Nowcasting Lightning Initiation			**5. FUNDING NUMBERS**
6. AUTHOR(S) Harris, Ryan J.			
7. PERFORMING ORGANIZATION NAME(S) AND ADDRESS(ES) Naval Postgraduate School Monterey, CA 93943-5000			**8. PERFORMING ORGANIZATION REPORT NUMBER**
9. SPONSORING /MONITORING AGENCY NAME(S) AND ADDRESS(ES) N/A			**10. SPONSORING/MONITORING AGENCY REPORT NUMBER**
11. SUPPLEMENTARY NOTES The views expressed in this thesis are those of the author and do not reflect the official policy or position of the Department of Defense or the U.S. Government. IRB Protocol number ______________.			
12a. DISTRIBUTION / AVAILABILITY STATEMENT Approved for public release; distribution is unlimited			**12b. DISTRIBUTION CODE** A

13. ABSTRACT

A cumulus cloud field may develop within a conditionally unstable environment, but only a fraction of the cumulus elements eventually develop into thunderstorms. Determining which of these convective elements is most likely to generate lightning—a critical need for the aviation community and Department of Defense—often starts with little more than a qualitative visual satellite analysis. To protect personnel and property, lightning nowcast tools (e.g., an automated geostationary satellite-based Lightning Initiation (LI) algorithm) require measurable research. This work quantifies the behavior of ten previously identified Geostationary Operational Environmental Satellite (GOES-12) Infrared (IR) Interest Fields (IFs) in the hour before LI. A total of 172 lightning-producing storms that occurred during the 2009 convective season are manually tracked and studied over four regions—Northern Alabama, Oklahoma, Kennedy Space Center and Washington D.C. Four-dimensional and cloud-to-ground lightning arrays provide precise lightning initiation points for each storm in both time and space. Individual tendencies are identified for the ten LI IFs. Statistical significance tests are conducted to determine the potential predictive capability and regional dependence of each IF. This study found that eight out of ten LI IFs exhibited at least 15 minutes of potential predictive capability and 35 minutes on average. Additionally, eight out of ten fields can likely be applied across a large geographical area with minimal error. Future operational applications identified and briefly explored in this work include the use of a lightning probability optimization tool.

14. SUBJECT TERMS			**15. NUMBER OF PAGES**
Lightning, Thunderstorm, GOES, Geostationary, Satellite, Convection, Convective Initiation, Lightning Initiation, Nowcast, Applied Meteorology			125
			16. PRICE CODE
17. SECURITY CLASSIFICATION OF REPORT	**18. SECURITY CLASSIFICATION OF THIS PAGE**	**19. SECURITY CLASSIFICATION OF ABSTRACT**	**20. LIMITATION OF ABSTRACT**
Unclassified	Unclassified	Unclassified	UU

NSN 7540-01-280-5500

Standard Form 298 (Rev. 8-98)
Prescribed by ANSI Std. Z39.18

THIS PAGE INTENTIONALLY LEFT BLANK

Approved for public release; distribution is unlimited

OPTIMIZATION AND STATISTICAL EVALUATION OF GOES CLOUD-TOP PROPERTIES FOR NOWCASTING LIGHTNING INITIATION

Ryan J. Harris
Captain, United States Air Force
B.S., State University of New York–Brockport, 2002

Submitted in partial fulfillment of the
requirements for the degree of

MASTER OF SCIENCE IN METEOROLOGY

from the

NAVAL POSTGRADUATE SCHOOL
March 2010

Author: Ryan J. Harris

Approved by: Philip A. Durkee
Advisor

Kurt E. Nielsen
Second Reader

Philip A. Durkee
Chairman, Department of Meteorology

THIS PAGE INTENTIONALLY LEFT BLANK

ABSTRACT

A cumulus cloud field may develop within a conditionally unstable environment, but only a fraction of the cumulus elements eventually develop into thunderstorms. Determining which of these convective elements is most likely to generate lightning—a critical need for the aviation community and Department of Defense—often starts with little more than a qualitative visual satellite analysis. To protect personnel and property, lightning nowcast tools (e.g., an automated geostationary satellite-based Lightning Initiation [LI] algorithm) require measurable research. This work quantifies the behavior of ten previously identified Geostationary Operational Environmental Satellite (GOES-12) Infrared (IR) Interest Fields (IFs) in the hour before LI. A total of 172 lightning-producing storms that occurred during the 2009 convective season are manually tracked and studied over four regions—Northern Alabama, Oklahoma, Kennedy Space Center and Washington D.C. Four-dimensional and cloud-to-ground lightning arrays provide precise lightning initiation points for each storm in both time and space. Individual tendencies are identified for the ten LI IFs. Statistical significance tests are conducted to determine the potential predictive capability and regional dependence of each IF. This study found that eight out of ten LI IFs exhibited at least 15 minutes of potential predictive capability and 35 minutes on average. Additionally, eight out of ten fields can likely be applied across a large geographical area with minimal error. Future operational applications identified and briefly explored in this work include the use of a lightning probability optimization tool.

THIS PAGE INTENTIONALLY LEFT BLANK

TABLE OF CONTENTS

THIS PAGE INTENTIONALLY LEFT BLANK

LIST OF FIGURES

LIST OF TABLES

LIST OF ACRONYMS AND ABBREVIATIONS

14WS	14th Weather Squadron, AF Combat Climatology Center
39rad	3.9-μm Radiance
4-D	Four-Dimensional
4DLSS	Four-Dimensional Lightning Surveillance System
45WS	45th Weather Squadron, Patrick AFB, FL
AF	Air Force
AL	Alabama
BLIDS	Blitz Informations Dienst von Siemens
CCAFS	Cape Canaveral Air Force Station
CDF	Cumulative Density Function
CG	Cloud-to-Ground
CGLSS	Cloud-to-Ground Lightning Surveillance System
CI	Convective Initiation
CIMMS	Cooperative Institute for Meteorological Satellite Studies
CIWS	Corridor Integrated Weather System
Cb	Cumulonimbus
Ch	Channel
CLASS	Comprehensive Large Array-Data Stewardship System
CTT	Cloud-Top-Temperature
DC	Washington District of Columbia
DoD	Department of Defense
FAA	Federal Aviation Administration
FAR	False Alarm Rate
FL	Florida
GOES	Geostationary Operational Environmental Satellite
GPS	Global Positioning System
IC	In-Cloud

IDL	Interactive Data Language
IF	Interest Field
IMPACT	Improved Accuracy from Combined Technology
IQR	Inter-Quartile Range
IR	Infrared
KSC	Kennedy Space Center
LDAR	Lightning Detection and Ranging
LI	Lightning Initiation
LI-60	60-minutes Before Lightning Initiation
LI-45	45-minutes Before Lightning Initiation
LI-30	30-minutes Before Lightning Initiation
LI-15	15-minutes Before Lightning Initiation
LI-0	Lightning Initiation Time
LMA	Lightning Mapping Array
L-P	Lightning-Producing
MATLAB	Matrix Laboratory
MB06	Mecikalski and Bedka (2006)
McIDAS-V	Man Computer Interactive Data Access System, Fifth Generation
MDF	Magnetic Direction Finding
MSG	Meteosat Second Generation
NASA	National Aeronautics and Space Administration
NLDN	National Lightning Detection Network
N-L-P	Non-Lightning-Producing
NM	New Mexico
NOAA	National Oceanic and Atmospheric Administration
NREL	National Renewable Energy Laboratory
OK	Oklahoma
PDF	Probability Density Function

POD	Probability of Detection
ref39	3.9-μm Reflectance
RASC	Royal Astronomical Society of Canada
SATCAST	Satellite Convective Analysis and Tracking
Tb	Brightness Temperature
Tb107	10.7-μm Brightness Temperature
Tb39	3.9-μm Brightness Temperature
Tb65	6.5-μm Brightness Temperature
Tb133	13.3-μm Brightness Temperature
Tb133107	13.3-10.7-μm Brightness Temperature Channel Difference
Tb39107	6.5-10.7-μm Brightness Temperature Channel Difference
Tb65107	6.5-10.7-μm Brightness Temperature Channel Difference
TBD	To Be Determined
TCL	Total Cloud Lightning
TOA	Time Of Arrival
USAF	United States Air Force
VHF	Very High Frequency
VIS	Visible

THIS PAGE INTENTIONALLY LEFT BLANK

ACKNOWLEDGMENTS

After months of seemingly endless work, one tends to accumulate a sizeable number of people whose assistance was paramount to completing a product like the Master's thesis before you. I'd first like to thank my advisor, Dr. Phil Durkee, and Second Reader, Kurt Nielsen, for first embracing my sometimes neurotic and crazy ideas and for providing the guidance necessary to create a well-grounded product. Furthermore, I would like to extend my sincere appreciation to Dr. John Mecikalski and Wayne MacKenzie from the University of Alabama-Huntsville for supplying this thesis topic and especially their vital collaboration. I would also like to thank Mr. William Roeder, the 45th Weather Squadron, and the Applied Meteorological Unit at Patrick AFB for providing funding and data support as well as accommodating my site visit to Cape Canaveral, Florida. Throughout my thesis, I often looked to and appreciated assistance from Dr. Pat Harr, Mary Jordan and Bob Creasey for help with deciphering statistical results, coding and data support. A similar thanks goes out to John Walker from UAH for his coding help. Additionally, I could not have done this project without the flash-grouping algorithm and lightning support provided by Dr. Bill McCaul at NSSTC. I'd also like to thank Dr. Bill Rison of New Mexico Tech, Dr. Bill Beasley from the University of Oklahoma, and Dr. Don MacGorman of NOAA/NSSL for help obtaining the OK lightning data archive. Jeff Zautner from the 14th Weather Squadron was also crucial in supplying the processed National Lightning Detection Network data as well. For nearly 18 months, my classmates have been a superb sounding board and absolutely awesome group to work with. I sincerely appreciate their help and friendship. Finally, my family deserves a shower of gratitude for putting up with the countless study and thesis hours I was forced to spend away from home. I want to thank you for motivating me, supporting me, and for being the rock upon which I can stand.

THIS PAGE INTENTIONALLY LEFT BLANK

I. INTRODUCTION

"Thunder is good, thunder is impressive;
but it is lightning that does the work."

— Mark Twain, 1908

A. MOTIVATION

Lightning is one of Earth's most awe-inspiring and highly researched atmospheric phenomena. Yet our knowledge of exactly how and when it will form remains an elusive research problem for atmospheric scientists. The ultimate goal of this study is to work toward predicting *when* lightning will form based on the behavior of satellite-sensed cloud-top properties.

While radar and lightning detection are excellent instruments for forecasting thunderstorms, satellite data are key and oftentimes the only tool available to assess weather in data-sparse or data-denied regions where the Department of Defense (DoD) may conduct future operations. A satellite-derived tool to forecast thunderstorm initiation on higher resolution temporal and spatial scales consistent with most mesoscale model data would be a tremendous asset over these data-sparse regions. Such a tool would help organizations like the National Aeronautics and Space Administration (NASA), 45th Weather Squadron (45WS), the United States Air Force (USAF), and the Federal Aviation Administration (FAA) to avoid or mitigate lightning's adverse impacts in the hopes of protecting people and resources.

1. Lightning Impact to People

Cloud-to-ground (CG) lightning is one of the two primary types of cloud-borne electrical discharge. In the next section, we discuss CG lightning and in-cloud (IC) lightning generation in more detail. While CG strikes make up a minority of total lightning, they significantly impact human populations. Lightning over the 10-year period 1999–2008 caused an average of 43 direct fatalities, 266

injuries and more than $47.2 million in property and crop damage per year across the United States (U.S.) and its territories (National Oceanic and Atmospheric Administration (NOAA) Hazards Statistics 2010). Curran et al. (2000) cited additional insurance reports that suggest the annual cost of lightning damage in the U.S. could be closer to $1 billion. Lightning also killed more people per year than tornadoes and hurricanes and was second only to flooding during the 30 years leading up to 1994 (Curran et al. 2000). In April 1996, the USAF re-evaluated their lightning watch and warning procedures after an Airman was killed while working on a C-130 aircraft at Hurlburt Field, Florida ([FL]; McNamara 2002; Nelson 2002). CG strikes also indirectly impact people via lightning-induced fires and power outages.

2. Lightning Impact to Federal Operations

In addition to human safety, the DoD, FAA and NASA are concerned about how and when CG and IC lightning will impact their respective operations.

a. DoD

The ability for the DoD to operate uninhibited during military operations and in peacetime crucially depends on knowing the weather. Lightning creates many adverse scenarios for military commanders. It delays missions, suspends refueling and maintenance on aircraft, forces re-routing of in-flight aircraft, disrupts sensitive communications and electronics, and often halts or delays surface personnel movements.

b. FAA

Lightning-induced aviation delays, diverts and cancellations cost commercial airlines tens of thousands of hours and hundreds of millions of dollars in lost revenue. Weather tools such as the Corridor Integrated Weather System (CIWS) have been developed in the last decade to help the FAA combat the adverse effects of weather, particularly convective weather (e.g., lightning). CIWS can save airlines 69,000 hours and $260 million in annual operating costs

(Robinson et al. 2004). Beyond lightning, thunderstorms also contain pockets of severe icing and turbulence that are detrimental to aircraft operation. Atmospheric convection causes the majority of aviation accidents blamed on turbulence (Kaplan et al. 2005).

c. NASA

The 45WS at Patrick Air Force Base works with NASA to launch vehicles—manned and unmanned—into space. The vehicles are launched at the Cape Canaveral Air Force Station (CCAFS) and Kennedy Space Center (KSC) complex on the east coast of FL. Figure 1 indicates why some consider FL as the lightning capital of the U.S. Higher lightning flash density has contributed to 30% of the mission scrubs due to weather at CCAFS/KSC (FAA 2003).

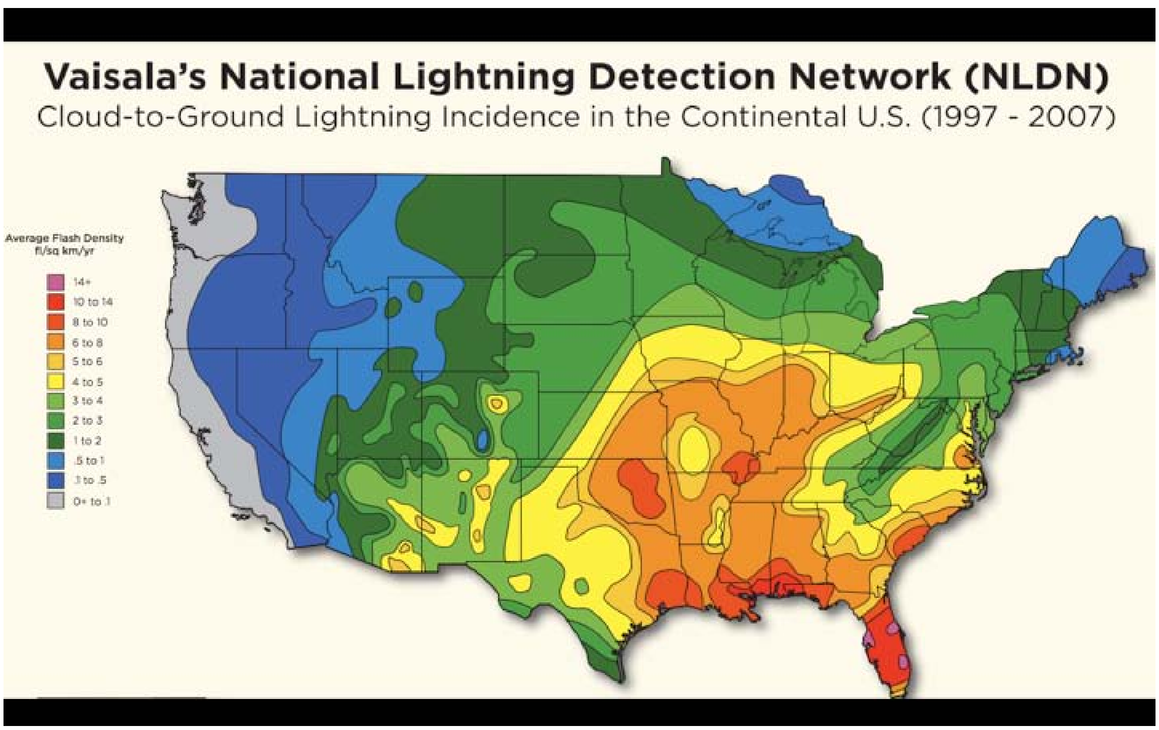

Figure 1. Average annual cloud-to-ground lightning flash density (flashes/km2/year) from 1997 to 2007 (From National Lightning Detection Network [NLDN] image courtesy of Vaisala).

A single launch scrub costs NASA $150,000 to $1 million depending on the launch vehicle. Lightning also directly impacts personnel

movements and operations at CCAFS/KSC. In fact, during this study, the Space Shuttle Discovery's movement to the launch pad was delayed by lightning, and the actual launch was scrubbed once due to nearby lightning. Additionally, direct lightning strikes to launch vehicles—whether natural or triggered by the vehicle—have disrupted system communication to the point of catastrophic rocket failure (Roeder et al. 1999).

B. THUNDERSTORM ELECTRIFICATION PROCESS

With lightning's impacts in mind, consider the thunderstorm electrification process. The electrification process is complex and still poorly understood. Lightning discharge processes span 15 orders of magnitude in scale from electrons on the sub-atomic level to thunderstorm dynamics tens or hundreds of kilometers in size (Williams 1988). Figure 2 depicts the thunderstorm electrification process, including a brief description.

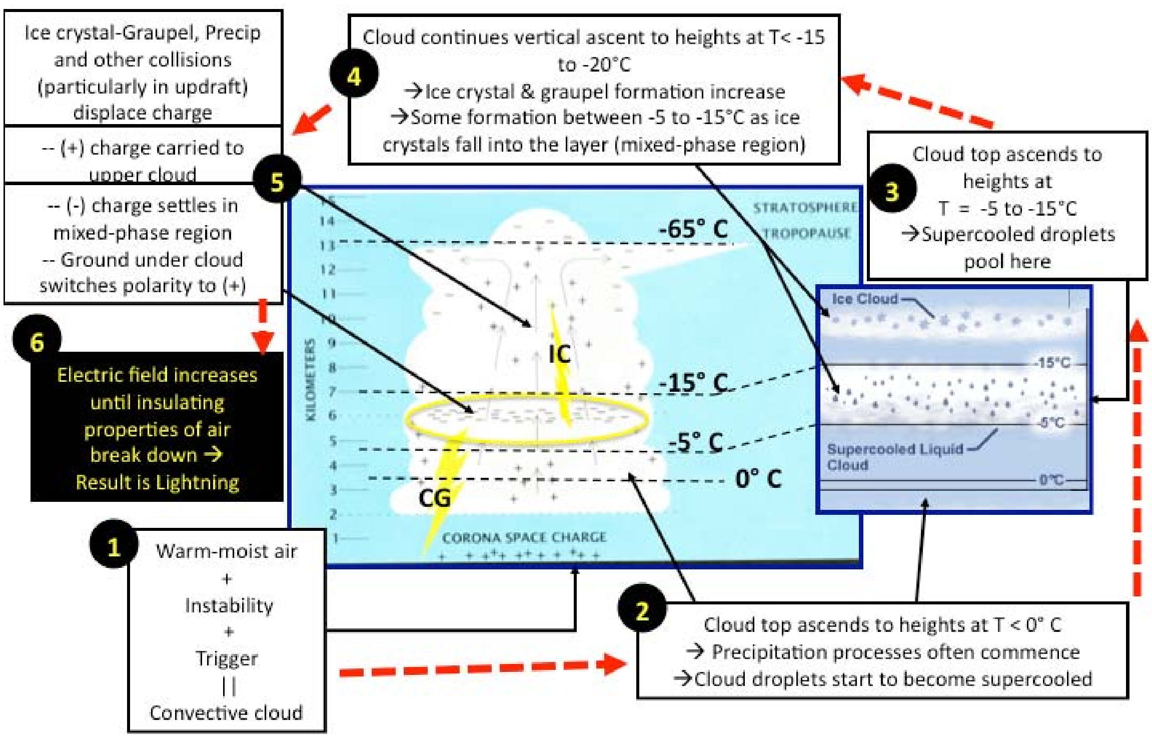

Figure 2. Six basic steps characterize the thunderstorm electrification process [Adapted from Williams (1988) and COMET (2005)].

The reader is directed to other well-documented literature for a more in-depth discussion on this topic (Krehbiel 1986; Williams 1988; Houze 1993; Saunders 1993).

1. Basic Thunderstorm Ingredients

Understanding lightning requires a basic understanding about thunderstorm formation. The pioneering thunderstorm research completed by Byers and Braham (1948)—although somewhat dated—relays a valid and still very relevant discussion on thunderstorm genesis.

Warm moist air, convective instability and a triggering mechanism work together and give rise to a convective cloud. The most common way to think of convective instability is a dense airmass overlying a less dense airmass. Gravity attempts to re-establish hydrostatic equilibrium—the balance between buoyancy force and gravity—by moving the more dense airmass underneath the less dense airmass via convective overturning. A triggering mechanism is a lifting focus for the convection to take place. Examples include frontal boundaries, orographic lift against higher terrain, or perhaps an outflow boundary from other thunderstorms.

The resulting buoyant column of air manifests itself as a cumulus cloud as the warm air rises, cools and condenses into tiny cloud droplets. If the lift and instability are sufficient to overcome any stable atmospheric layers, the buoyant energy powers the cloud's vertically growing updraft until equilibrium is reached. For strong convection like thunderstorms, this equilibrium level is often located at the stable layer between the troposphere and the stratosphere (i.e., tropopause). A typical thunderstorm life cycle averages between one and three hours (Byers and Braham 1948).

2. Thunderstorm Electrification

Many dynamical and microphysical processes occur to yield lightning before a strong vertically developing cumulus (i.e., cumulonimbus [Cb]) reaches

the tropopause. Recall first that a standard atmosphere generally cools with increasing height above ground level. Initially, a cumulus cloud contains only liquid cloud droplets. Precipitation processes usually begin as a cumulus cell rises through the 0° Celsius (°C) level while driven vertically by the updraft (Houze 1993). Additionally, the cloud droplets remain supercooled liquid until the cloud ascends to temperatures of around -15°C where they often start to freeze. As the Cb grows, a reservoir of supercooled droplets forms between -5 to -15°C. Cloud droplets freeze into ice crystals, graupel or hail—hereafter collectively referred to as ice particles—as the Cb continues to ascend through the -15 to -20°C level. Graupel forms when supercooled droplets freeze on contact with other ice particles. The heavier ice particles that can no longer be supported by the updraft fall within the cloud and often settle or fall through the supercooled droplet reservoir. The primary mystery of storm electrification occurs in this region, known as the mixed-phase region (Krehbiel 1986; Williams 1988; Houze 1993; Saunders 1993).

It is widely believed that collisions of supercooled droplets and ice particles in the mixed-phase region prompt transfers of electrical charge. Collisions are most abundant at the junction of the Cb's updraft and mixed-phase regions, and are proportional to the strength of the updraft. For reasons still unknown to scientists, the positive charges generally transfer to lighter cloud particles and are lofted by the updraft into the upper region of the Cb. Meanwhile, the heavier particles that remain in the mixed-phase region take on a negative charge. The earth and near-surface air beneath the cloud—which is normally negative in fair weather—acquires a positive charge to counter the negative charge accumulating in the mixed-phase region. The electric field, or gradient of an electric potential field, increases until the insulating properties of the air break down. The resultant lightning discharge briefly neutralizes the electric field (Krehbiel 1986; Williams 1988; Houze 1993; Saunders 1993).

3. Lightning Terminology

The lightning terminology used hereafter is also shared among the latest work in total cloud lightning (Krehbiel et al. 2000; Thomas et al. 2001; Koshak et al. 2004; Thomas et al. 2004; Goodman et al. 2005; MacGorman et al. 2008; Murphy et al. 2008; McCaul et al. 2009). For simplicity, a CG stroke is dissected below. A lightning stroke initiates at a source point (i.e., the parent source) where the air's insulating properties first break down. Additional sources arise as the gradient of electric charge increases. Narrow channels of electric current flow between the sources and traverse the space between the source region and the termination point of the lightning. In this example, the source point is a negative charge in the cloud, and the termination point is the positively charged earth. A surge of electric current connects all sources from the parent source to the termination point in a series of branches once the channel is connected. One surge of electric current is a lightning stroke. Hundreds to thousands of individual sources and multiple strokes make up a single flash. A typical flash may last more than one second and can extend tens of kilometers or more (McNamara 2002; Nelson 2002). A lightning stroke that initiates in the cloud and extends to the ground is a CG stroke, while a stroke that initiates in the cloud and extends to another region in the cloud is an IC stroke. In the developing stages of a thunderstorm, IC strokes normally precede the first CG stroke by five to ten minutes (Williams et al. 1989; Houze 1993).

C. THUNDERSTORMS: GEOGRAPHICAL AND TEMPORAL VARIATIONS

The NLDN flash density map in Figure 1 yields a few generalizations about the geographical variation of lightning. Lightning is favored in regions where there is an abundance of warm moist air like the southeastern U.S. Lightning occurrence generally decreases with latitude and is at a minimum for much of the intermountain west, the Pacific Coast, the Great Lakes region and northern New England States. The Appalachian and Rocky Mountains usually see less frequent lightning; however, a few isolated pockets of higher density

lightning are apparent over the Four Corners region of the southwestern U.S. due to the summer monsoon. Easterling (1989) and Changnon (2001; 2003) conducted thunderstorm rainfall climatologies of the U.S. and concluded similarly with the generalizations made above. Easterling (1989) identified four to five regional clusters that had nearly the same thunderstorm-induced rainfall pattern as the lightning flash density in Figure 1. He concluded that the region most likely to produce heavy rainfall from thunderstorms during the spring, summer and fall includes the southern Atlantic and Gulf Coasts and extends into the central and southern Great Plains. With regard to time, each author outlines in their research how thunderstorms generally peak in the afternoon hours and in the summer months when the solar heating is at a maximum.

Easterling (1989) also found that synoptic weather patterns play a large role in the precipitation occurrence from mesoscale thunderstorms. While this may be no surprise, it is interesting to note that summertime thunderstorms forming in the generally drier Plains region—Oklahoma (OK) for instance—are similar to storms forming in parts of the humid southeast—like Alabama (AL). Taken one step further, Krehbiel (1986) argued that although there may be regional differences in the size and extent of thunderstorms across synoptically, geographically and even seasonally different regions, the basic electrical structure of the storms leading up to lightning remains the same. Note in Figure 3 how the electrically active mixed-phase region is located in the same thermal region of each cloud (i.e., between -10 to -20°C). This is the case for deep, moist convection in Florida (FL), drier, high-based convection in New Mexico (NM), and cold core, low-topped wintertime convection in Japan.

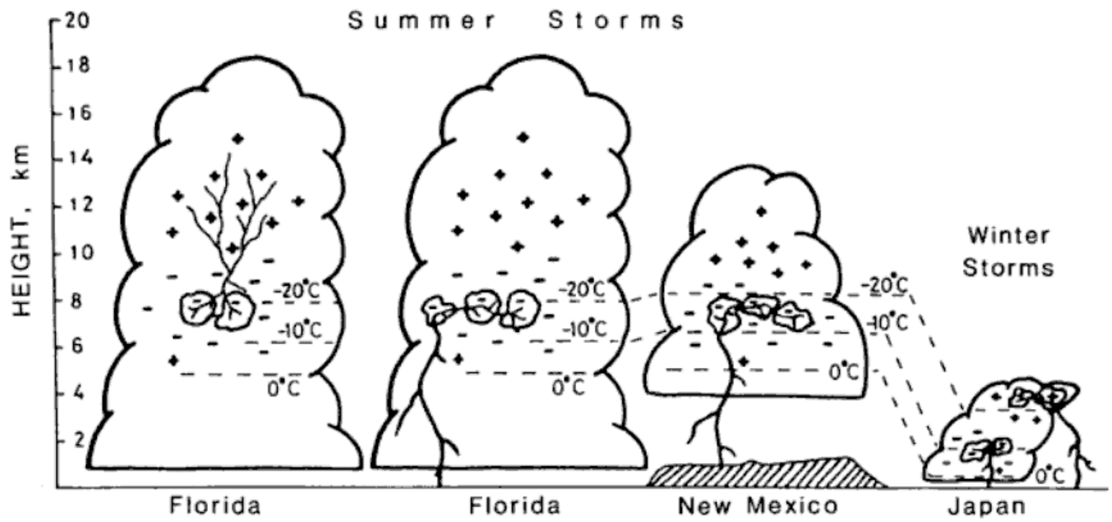

Figure 3. Electrical structure of thunderstorms across three varying regions and two varying seasons from Krehbiel (1986).

D. REMOTELY SENSING THUNDERSTORMS

Since the dawn of mankind, humans have remotely sensed thunderstorms. Watching a billowing Cb develop before us, our eyes are often forgotten as our most important remote sensing tool. Since then, man has developed satellite imaging and the latest in lightning and radar detection technology to remotely sense our environment for thunderstorms.

1. Geostationary Satellite Imager and Uses

a. Geostationary Operational Environmental Satellite

Geostationary satellites, such as the Geostationary Operational Environmental Satellite (GOES-12), remotely sense the atmosphere over nearly an entire hemisphere from pole to pole. As the name implies, the satellite is centered roughly 36,000 km away and stationary relative to a point on the Earth's equator. Distance from Earth places limitations on spatial resolution of the imagery received. However, a geostationary satellite's main advantage is nearly continuous environmental monitoring—currently on the order of approximately 15 minutes between images—key to weather analysis and forecasting (Kidder and Vonder Haar 1995).

Five channels (Ch) on GOES-12 retrieve radiance reflected or emitted by the Earth in various wavelength bands. Each band or range of wavelengths is centered on a single wavelength as noted for each channel below. Ch 1, or the visible (VIS) channel, senses reflected radiance in the visible part of the electromagnetic spectrum, or specifically 0.65 μm for Ch 1. Channels 2, 3, 4 and 6 retrieve terrestrially emitted radiance in the infrared (IR) portion of the electromagnetic spectrum. Ch 2 at 3.9 μm is unique amongst all of the IR channels in that it senses both reflected visible radiance—known as reflectance—as well as emitted IR energy or emittance. This channel encounters very little attenuation or absorption by atmospheric gases or aerosols. Furthermore, the 3.9-μm channel is highly sensitive to water versus ice. Ch 3 senses radiance emitted at 6.5 μm and is known as the water vapor channel since terrestrially emitted radiation is absorbed by water vapor at this wavelength. Ch 4 retrieves 10.7 μm radiance and is known as the "clean window" channel since it experiences very little atmospheric attenuation. 10.7 μm is also important in that the Earth's emitted energy peaks at this wavelength. GOES-12's Ch 6 collects radiance measurements at 13.3 μm including emission from carbon dioxide, a well-mixed atmospheric constituent.

A GOES user may perform a few post-processing procedures for a more usable data format. For instance, the IR radiance retrievals are often converted to a brightness temperature (Tb) value for easier comparison across the various spectral channels. The Tb is not an actual temperature, but rather the temperature an object would have if it were a perfect blackbody. Following Planck's and Kirchhoff's Law, a blackbody is an object that emits as much energy as it absorbs at a given wavelength. Finally, GOES-12 has 1-km spatial resolution for the VIS channel, 4-km resolution for Ch 2-4, and 8-km resolution for Ch 6. Kidder and Vonder Haar (1995) and CIMMS (2010) are two good sources for further review on the GOES platform.

b. Basic Convective Cloud Properties Viewed From GOES

When using GOES-12 imagery to study cloud properties of a convective cell, the user should be aware of the differences in spatial resolution from VIS imagery to IR imagery as seen in Figure 4.

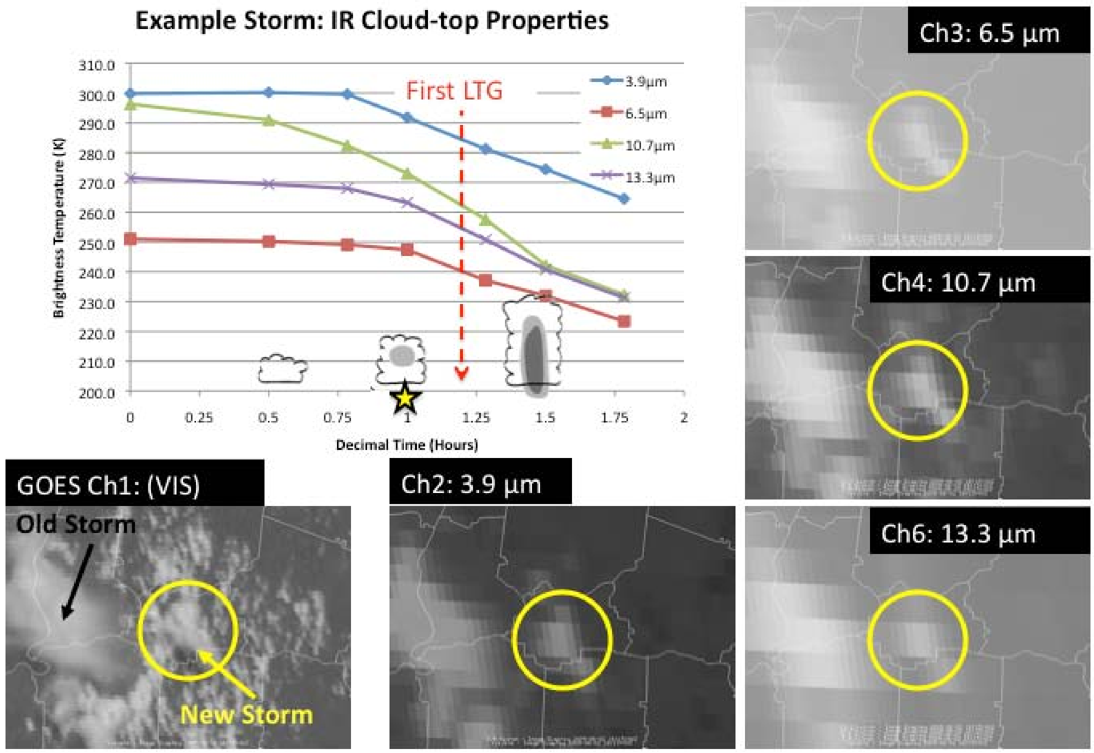

Figure 4. Convective cloud properties as depicted by GOES-12's visible channel (Channel 1), and GOES-12's infrared (IR) channels (Channels 2, 3, 4 and 6). The graph by time in the upper-left depicts general storm evolution of GOES IR cloud-top properties (i.e., Channels 2-4, and 6). Gray shading in the graph's clouds depicts precipitation. The star indicates approximately when each GOES image (Channels 1-4, 6) was taken.

Individual cumulus clouds can be identified in the VIS imagery, but not until the convective cloud has grown to sufficient size can we see the new storm developing on the IR channels. The 3.9-µm and 10.7-µm images appear very similar—each channel is located within highly transmissive, low atmospheric absorption windows—while the atmospheric path radiance attenuation are apparent in Channel 3 and 6. Radiance in these channels is absorbed by water

vapor and carbon dioxide respectively; thus we see colder Tbs and therefore lighter gray shades. This study attempts to quantify the satellite-derived cloud properties of known lightning-producing convective cells prior to lightning generation. Data like the example in Figure 4 are plotted and analyzed in this study.

c. Thunderstorm Research Using Geostationary Satellites

Thunderstorm research using geostationary satellites has often focused on linking the severity of thunderstorms with changes observed in satellite imagery. Adler and Fenn (1979) and Rosenfeld et al. (2008) for instance studied the vertical growth rate of tornadic and other severe thunderstorms using IR imagery. Adler and Fenn (1979) derived reasonable estimates of the vertical velocity and divergence fields associated with their cases. Rosenfeld et al. (2008) dissected microphysical precursors to hail and tornadic thunderstorms using the latest in multispectral geostationary satellite data. Other studies like those conducted by Goodman et al. (1988) and Roohr and Vonder Haar (1994) utilized geostationary imagery and lightning data to demonstrate general convective patterns. These four studies are just a few of the first to hint at nowcasting thunderstorm development and decay using satellite technology. A nowcast in this study is defined as a 0-1 hour forecast.

2. Remote Sensing Using Lightning Detection

Lightning detection is a burgeoning research field in remotely sensing thunderstorms. Storms that have already initiated lightning are central to such research. Focus has shifted from solely CG lightning studies to total cloud lightning (TCL) examination (i.e., combined CG and IC lightning) in the past decade. Goodman et al. (2005) and MacGorman et al. (2008) used TCL to infer storm severity. Additionally, McCaul et al. (2009) showed how TCL can help nudge mesoscale model resolution of microphysical processes related to lightning.

3. Thunderstorm Research Using Radar

A reference search for thunderstorm research using radar yields a vast library of literature. Dye et al. (1989) and Gremillion and Orville (1999) are just a couple of the studies that focus attention on using radar to study thunderstorm initiation. Gremillion and Orville (1999) studied the effectiveness of nowcasting thunderstorm initiation using radar echo top thresholds. Their study cross-referenced mixed-phase region thermal thresholds (i.e., -10°C, -15°C and -20°C) against radar returns over the CCAFS/KSC region with some success. With the help of studies like these, the USAF currently monitors radar echo tops nearing the mixed-phase region to nowcast thunderstorms.

E. HISTORY OF CONVECTIVE INITIATION AND LIGHTNING INITIATION

A cumulus cloud field may develop within a conditionally unstable environment, but only a fraction of the cumulus elements typically will develop into thunderstorms. Determining which of these convective elements is most likely to develop often starts with little more than a qualitative "eyeball" analysis of geostationary satellite imagery. Recent studies, however, have demonstrated that satellite imagery can provide more quantitative assessments of cumulus cloud growth leading to Convective Initiation (CI) and Lightning Initiation—abbreviated LI, not to be confused with lifted index.

Quantifying the behavior of GOES cloud-top properties to assess CI is relatively new in the last decade. Roberts and Rutledge (2003) and Mecikalski and Bedka (2006)—hereafter referred to as MB06—define CI as when a convective element attains 35 dBZ or more on radar. MB06 characterized the behavior of eight GOES-based IR Interest Fields (IF) and identified potential thresholds that are often precursors to CI. They based the IFs on combinations and time trends for three of the four GOES IR channels (Ch 3, 4 and 6). Mecikalski et al. (2008) evaluated the usefulness of a nowcasting tool modeled after the MB06 results. The statistics showed positive probability of detection

(POD) rates, but relatively high false alarm rates (FAR). More recently Siewert et al. (2010) applied a similar methodology to the Meteosat Second Generation (MSG) satellite system in Europe.

Setvak and Doswell (1991), Lindsey et al. (2006) and Rosenfeld et al. (2008) identified microphysical characteristics of growing convective elements using the 3.9-μm channel. These recent advances are important in providing additional microphysical clues to lightning generation given the increased water versus ice sensitivity of the 3.9-μm channel. In other words, the 3.9-μm channel can be used to help indicate whether cloud glaciation is occurring, or specifically the transition of supercooled cloud droplets to ice crystals. Siewert (2008) has most recently taken advantage of this work to demonstrate the usefulness of the 3.9-μm channel and other GOES IR channels in nowcasting LI. Table 1 summarizes the CI/LI IFs that MB06 and Siewert (2008) employed in their research. The table also includes two additional fields that this research explores. The IFs in this study are discussed later in Section II G.

Table 1. Convective initiation and lightning initiation interest fields and their respective thresholds used in MB06, Siewert (2008) and what this study considers. The last column summarizes each field's physical description.

Interest Field	MB06 Critical CI Value	Siewert LI Value	This study	Description
10.7 µm Tb	< 0°C	≤ - 13°C	*To be determined (TBD)*	Cloud tops cold enough to support supercooled water and ice mass growth; cloud-top glaciation
10.7 µm Tb Time Trend	< - 4°C / 15 min (ΔTb / 30 min < ΔTb / 15 min)	≤ - 10°C / 15 min (≤ - 15°C / 30 min)	*TBD*	Cloud growth rate (vertical)
Timing of 10.7-µm Tb drop below 0° C	Within prior 30 min	*Not used*	*TBD*	Cloud-top glaciation
6.5 - 10.7 µm Tb difference	Tb Diff: -35°C to -10°C	≥ - 17°C	*TBD*	Cloud top height relative to mid/upper troposphere
13.3 - 10.7 µm Tb difference	Tb Diff: -25°C to -5°C	≥ - 7°C	*TBD*	Cloud top height relative to mid/upper troposphere; better indicator of early cumulus development but sensitive to cirrus
6.5 - 10.7 µm Tb Time Trend	> 3°C / 15 min	≥ 5°C / 15 min	*TBD*	Cloud growth rate (vertical) toward dry air aloft
13.3 - 10.7 µm Tb Time Trend	> 3°C / 15 min	≥ 5°C / 15 min	*TBD*	Cloud growth rate (vertical) toward dry air aloft
3.9 - 10.7 µm Tb Difference**	*Not used*	*Not used*	*TBD*	Cloud-top glaciation
3.9 - 10.7 µm Tb Time Trend*	*Not used*	T - T(t-1) < -5°C and T - T(t+1) < - 5°C	*TBD*	Sharp decrease, then increase indicates cloud-top glaciation
3.9 µm Fraction Reflectance*	*Not used*	≤ 0.05	*TBD*	Cloud top consists of ice (ice is poorer reflector than water at 3.9 µm)
3.9 µm Fraction Reflectance Trend**	*Not used*	*Not used*	*TBD*	Cloud-top glaciation rate

* Added in Siewert's (2008) LI Study

** Added for this study

F. RESEARCH FRAMEWORK

Previous satellite and lightning research has focused primarily on identifying precursors to severe thunderstorms after lightning has already begun. In contrast, this study evaluates the effectiveness of specified GOES IR IFs in forecasting the onset of lightning in the 0–1 hour time period following initial satellite detection of a growing cumulus cloud. The research is built around the following framework of hypotheses:

- LI nowcasting from GOES is a viable capability, which can be improved with a better understanding of how to use and interpret quantified GOES data.
- Use of the 3.9-μm channel is underutilized. We expect the information this channel provides to be of significant value to 0–1 hour LI nowcasting.
- We presume that regional dependencies do exist in LI detection via GOES data.
- Improved methods and procedures can be developed to enhance existing GOES-based LI nowcasting methods.

To thoroughly test these hypotheses, this study builds on previous CI/LI research by providing a statistically significant number of cases in various regions of the U.S. for comparison in hopes of showing a predictive capability of each IF with regard to time before lightning. Secondly, a regional comparison of IF behavior leading up to LI will determine if LI thresholds can be applied over a broad geographical region. Overall, the primary goal of this work is to identify which field or combination of fields provides the most accurate and timely indication of imminent lightning-production in convective storms.

II. DATA AND METHODOLOGY

A. STUDY TIMEFRAME AND REGIONS

As a means of meeting this study's objectives and addressing the research hypotheses, the following data and analysis procedures are developed. This study considers summertime convection that occurred between 24 May 2009 and 23 August 2009. The summer season is optimal for building a sufficiently large dataset over a broad geographical area so as to allow for statistically significant results. With increasingly large datasets, more robust statistical tests may be performed toward quantifying the results. Four regions were selected based on the availability of four-dimensional (4-D) lightning array data: Huntsville, Alabama, CCAFS/KSC, FL, Washington D.C. (DC) and Oklahoma City, Oklahoma (OK).

B. REMOTE SENSING TOOLS

Geostationary satellite and surface-based lightning detection systems were the main remote sensing platforms used in this study. A brief description of how geostationary data were obtained is followed by a more detailed explanation of the lightning systems and data.

1. Geostationary Satellite

Using NOAA's Comprehensive Large Array-data Stewardship System (CLASS), we obtained post-processed GOES-12 data for further study (NOAA-CLASS 2010). 16-bit GOES Variable formatted data for all five GOES-12 imager channels were converted to the Man Computer Interactive Data Access System (McIDAS) Area file format via the NOAA-CLASS site and downloaded. The McIDAS Area file format contains calibrated radiance and Tb data among other fields for each channel. Additionally, a McIDAS Area file is easily analyzed in the Fifth Generation McIDAS (McIDAS-V) software beta version 1.03 created by the University of Wisconsin-Madison Space Science and Engineering Center.

2. National Lightning Detection Network

Vaisala's NLDN is an arrangement of 113 IMProved Accuracy from Combined Technology (IMPACT) sensors spaced every 200–350 km throughout the U.S. McNamara (2002), Cummins et al. (2006) and Ward et al. (2008) provide good synopses of how the system operates. To pinpoint CG lightning activity, the latest NLDN upgrade uses Global Positioning System (GPS) technology and a new location identification technique combining Time of Arrival (TOA) and Magnetic Direction Finding (MDF) technologies. The system provides time, location, polarity, and peak current information for each individual return stroke. A flash-grouping algorithm collects spatially and temporally similar strokes and groups them into flashes. A stroke must be within one second and 10 km of the initial stroke and each stroke must be within 500 microseconds of the previous stroke in this algorithm (McNamara 2002). Cummins et al. (2006) identified the NLDN's CG flash detection efficiency as 90–95% and the location accuracy as 500 m, well within the spatial resolution of GOES imagery. We retrieved post-processed NLDN CG flash data from the USAF's 14WS—formerly the AF Combat Climatology Center—in Asheville, North Carolina.

3. Lightning Mapping Array

Remotely sensing TCL data has been a growing research field since the first Lightning Detection and Ranging (LDAR) system was installed at CCAFS/KSC, FL in the 1970s. Since then, the Lightning Mapping Array (LMA) was born out of new lightning research at New Mexico Tech (Krehbiel et al. 2000; Thomas et al. 2001). The LMA locates lightning radiation sources in three spatial dimensions and time. The array is a mesoscale network of GPS-TOA sensors that detect Very High Frequency (VHF) signals at unused television frequencies. The arrays are approximately 60x80 km in size. For this study, we used the 4-D TCL data from three of the four existing LMAs. The Oklahoma LMA (OKLMA) and the North Alabama LMA (NALMA) consist of 11 and 13 GPS VHF receivers, respectively, that sense lightning source radiation in the 54–88 MHz range. The

Washington D.C. LMA (DCLMA) is the newest operational LMA, and it contains ten sensors that detect lightning sources in the 192-198 MHz radio frequency range. The higher VHF channel is used in DC to limit the effects of increased radio frequency noise in an urban environment (Krehbiel et al. 2006). The LMA's flash detection efficiency approaches 100% within the 60x80-km array and decreases outside of the array area. The location accuracy degrades quadratically with distance from the center (Koshak et al. 2004; Thomas et al. 2004). NALMA, as noted by Goodman et al. (2005), is nominally accurate to within 50 m inside the 150-km array center.

Because of time constraints, this study used pre-processed "decimated" LMA data, which is available much faster than the post-processed data. While the images generated using this decimated data are not as detailed as fully post-processed images, the decimated data are sufficiently detailed for most uses (Rison et al. 2003; E. McCaul, personal communication). From the decimated data, the following information was used for each source detected by the array: decimal time, latitude, longitude, and altitude. Appendix A shows an example of the LMA and other 4-D lightning file formats. The DCLMA (2010) and NALMA (2010) websites provided the two-minute decimated lightning files for DC and AL respectively for each day in this study. New Mexico Tech provided daily (UTC) decimated OKLMA data by request.

4. 4-D Lightning Surveillance System (4DLSS)

The legacy LDAR system at CCAFS/KSC, FL was recently replaced by the 4DLSS. The 4DLSS has both a CG and TCL sensor array. Like the LMA, the 4DLSS's TCL array uses VHF and TOA techniques to pinpoint lightning sources. The array consists of nine 60-66 MHz VHF sensors spread across an estimated 45x65-km area that includes the CCAFS/KSC complex. The flash detection efficiency is 100% within the array itself and is 90% at 111 km from the center of the array. Like the LMA, the location accuracy degrades quadratically with distance from the center. The location error is less than 2 km at 111 km

from the center (Murphy et al. 2008). The 4DLSS is slightly less accurate than the LMA since the 4DLSS array area is smaller. NASA has a convenient site that was used to download the 4DLSS data (TRMM-4DLSS 2010). The following information was used for each source detected by the array: Julian day, x-y-z position coordinates, and only LDAR events. The x-y-z coordinates identify the location of a source on a Cartesian map with the center of the array located at the origin, <0,0,0>. The Cloud-to-Ground Lightning Surveillance System (CGLSS) that is part of the 4DLSS was not used in this study. Appendix A shows an example of the 4DLSS and other 4-D lightning file formats.

C. POTENTIAL STORM DAYS CATALOG

1. Study Region Considerations

Before building a storm catalog, we considered the accuracy of each 4-D lightning platform to narrow the focus areas. Similar to the work conducted by Goodman et al. (2005), potential storm cases were limited to within 150 km of each LMA array center. Specific LMA detection efficiencies were not available to compare with FL; however, since FL has a smaller array area, its effective range is smaller. Therefore, we arbitrarily chose the 90% detection efficiency radius (i.e., 100 km) to restrict the FL cases in this study. A few exceptions to these restrictions were allowed, which are discussed later in Section III A. Figure 5 below shows the regions of interest for this study. The center points for each array are as follows: a) NALMA (34.7246 N, 86.6450 W), b) OKLMA (35.3365 N, 97.7474 W), c) DCLMA (38.9218 N, 77.0208 W) and d) FL 4DLSS (28.5385 N, 80.6426 W).

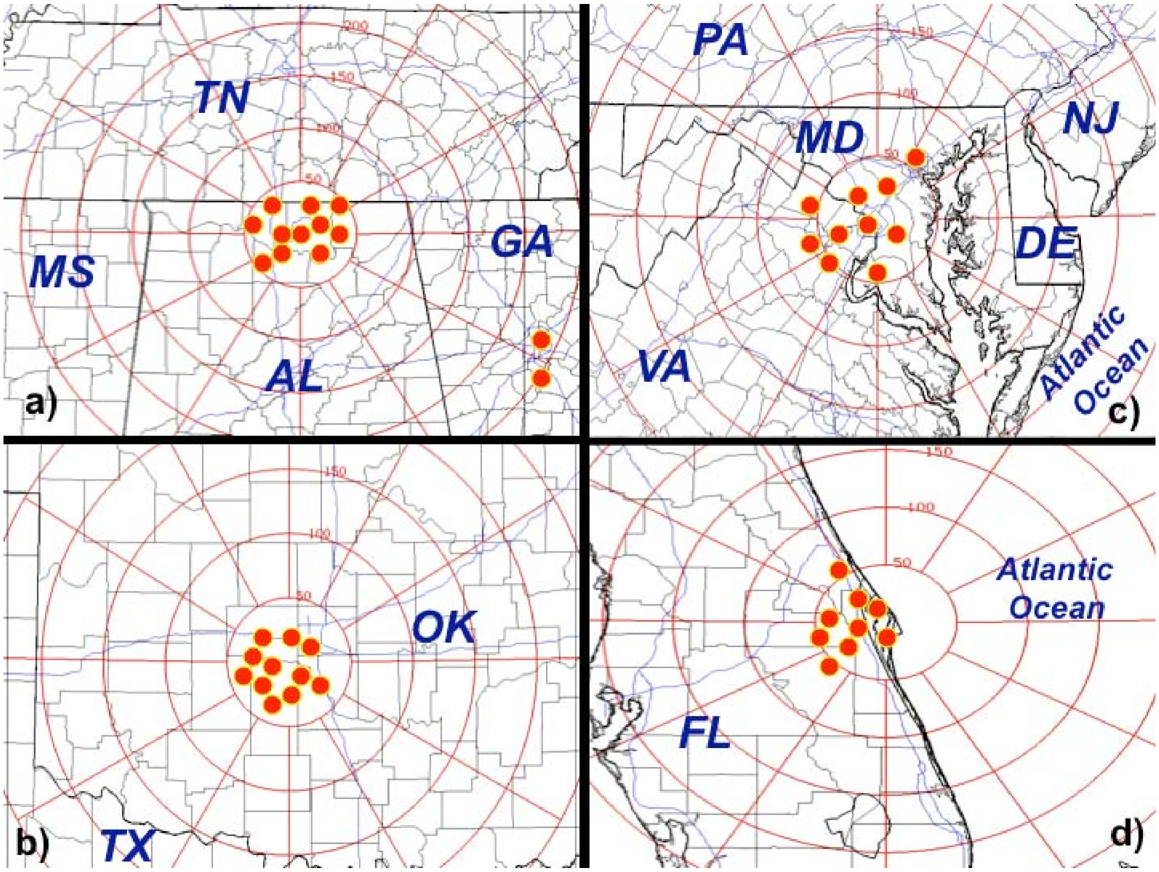

Figure 5. Four-dimensional (4-D) lightning arrays used in this study. Red circles represent individual VHF sensors in each array. The a) NALMA uses 11 sensors near Huntsville, AL and two sensors near Atlanta, GA. The b) OKLMA uses 11 sensors south and west of Oklahoma City, OK. The c) DCLMA uses 10 sensors around Washington D.C. Finally, the d) 4DLSS uses nine sensors around Cape Canaveral, FL. Range rings are spaced every 50 km.

2. Storm Days Catalog: Identifying Potential Lightning Initiators

After the usable radii for each 4-D lightning region were determined, GOES-12 VIS imagery was examined each day to look for potential LI regions. To do this, we subjectively searched for speckled cumulus fields that later developed into convective storms. Key to the search were newly-initiated convective storms occurring between 1230 and 2359 UTC. Storms with nearby pre-existing convection (i.e., within 10 km) were generally excluded from this study due to possible satellite measurement contamination. Potential storm days for each region were catalogued based on the criteria in Table 2. Eventually,

some days were excluded due to unavailable satellite or lightning data. To minimize observational satellite error, every effort was made to avoid days that clearly contained cirrus. Contamination by cirrus and pre-existing convection reduces the accuracy of satellite-interpreted radiance. For example, a cirrus cloud that is located at 35,000 ft may have a cloud-top-temperature (CTT) of -40°C. The cirrus will cause any clouds developing underneath—like a new cumulus cloud—to appear colder to the satellite than their actual CTT. Once the catalog was complete, we obtained GOES-12 data for all "Excellent" cases. Some "Good" and a few "Fair" cases were eventually used as well after closer examination revealed less contamination than initially assessed.

Table 2. Initial VIS satellite imagery criteria used to identify and catalog potential lightning-initiating convection.

QUALITY	*Inside 100-150-km Domain*	*Pre-existing Convection*	*Cirrus Contamination*
Excellent	Yes	No	No
Good	Yes	Minimal	Minimal
Fair	No	Likely	Likely

D. PROCESSING LIGHTNING DATA

Lightning data, particularly 4-D TCL data, are extremely voluminous. A single storm can have tens to hundreds of thousands of individual lightning radiation source events, and single flashes within a storm can contain anywhere from a few sources to over a thousand. Many of the potential storm days easily had a million or more source events. Thousands of source events or more can occur in only a second or two. The purpose of this research was not to study the complicated lightning structure, but to identify when LI occurred. To reduce the data volume but still maintain data integrity, the 4-D lightning data was processed using two flash-grouping algorithms similar to the NLDN flash-grouping algorithm. One algorithm processed 4-D lightning data for the three LMA regions, and the second algorithm grouped lightning sources into probable flashes for the FL 4DLSS. Also tracked was CG LI using NLDN data to verify the 4-D lightning data

and additionally to measure the time lag from IC to CG LI. Data processing for each 4-D lightning array is discussed in the next two sub-sections.

1. LMA Data

To process the LMA data, we used Matrix Laboratory (MATLAB) version 7.8 and a Fortran flash-grouping algorithm. Before running the flash-grouping algorithm, the two-minute LMA files were combined into a single daily (UTC) LMA file. Dr. Bill McCaul at the National Space Science Technology Center provided the LMA flash-grouping algorithm for this research. The algorithm employs time and space proximity criteria to identify the sources belonging to a given flash. Sources are assumed to belong to the same flash if they occur less than 0.3 s apart in time and also satisfy a spatial separation requirement. He documents the specific criteria and background behind the algorithm further in McCaul et al. (2009).

After the sources were assigned a flash number, we further filtered out what McCaul et al. (2009) termed “singletons.” Most researchers in the TCL field consider a flash containing only one source to be either erroneous or likely atmospheric VHF noise. Therefore, TCL researchers filter out singletons by considering flashes with two to ten or more sources for an accurate flash measurement (E. McCaul, personal communication). This study assumes that a flash contains at least four sources. A sensitivity analysis produced very similar results using two to five sources as the threshold. After all flashes were filtered, we then assumed the first source within the flash to be the parent or originating source. Subsequently, flash-grouped LMA files were created for each potential storm day. Each newly processed LMA file contained a list of each flash by time and location (latitude, longitude, and altitude) represented by the parent source of each flash. Finally, a simple header was added on each file so the LMA flash files could be read quickly into McIDAS-V. Reference Appendix A for a closer look at the lightning file formats.

2. 4DLSS Data

Since the 4DLSS file format is much different than the LMA format, it was necessary to use a different flash-grouping algorithm. McNamara (2002) and Nelson (2002) used a flash-grouping algorithm to cluster lightning sources for the original LDAR sensor. However, the LDAR array, its software, and processing were recently updated. The updates provide a much more accurate 4DLSS array. We used the original Interactive Data Language (IDL) flash-grouping algorithm from Nelson and the new 4DLSS accuracy numbers identified by Murphy et al. (2008) to cluster lightning sources into probable flashes.

To account for the improved 4DLSS accuracy, we altered Nelson's range error (i.e., 12% for a given source) and the 1-km branch bounds accuracy. The algorithm was updated using Murphy's location accuracy equation, which increases range error quadratically with distance from the center of the array. We also changed the 1-km branch bounds accuracy from 40 km to 72 km—also based on Murphy's location accuracy equation—given the increased accuracy range of the updated 4DLSS. Finally, for consistency, we changed the 4DLSS clustering thresholds to more closely match those used in the LMA algorithm. Table 3 shows the original LDAR flash-grouping algorithm's clustering thresholds alongside the new 4DLSS flash-grouping algorithm as well as the LMA thresholds for comparison.

Before the 4DLSS flash-grouping algorithm was run, we filtered out all of the calibration and CGLSS events. Additionally, the 4DLSS's day/time format was converted to the old LDAR I day/time format. These changes successfully converted the original 4DLSS file format into a format that could be read by our adapted 4DLSS flash-grouping algorithm, all without any degradation to the data. MATLAB was then used to combine all of the half-hourly 4DLSS files into a single daily (UTC) 4DLSS file.

IDL version 7 was used to run the updated 4DLSS flash-grouping algorithm once the pre-processing steps were complete.

Table 3. Clustering thresholds for each 4-D lightning flash-grouping algorithm including the original LDAR, the new 4DLSS, and the LMA.

CRITERIA	*Flash-grouping Algorithm Thresholds*		
	LDAR[1]	*4DLSS[2]*	*LMA[3]*
Maximum Flash Time	3 s	3 s	ND
Maximum Time Between Sources	0.5 s	0.3 s	0.3 s
Maximum Time Between Branches	0.03 s	0.03 s	ND
Maximum Flash Coverage	5 km	1 km	1 km
Maximum Allowable Angle Error	1 deg	2.9 deg	2.9 deg
Additional Criteria	ND	ND	Various[3]

ND = Not defined/used
1 Nelson (2002)
2 Matched McCaul et al. (2009) for consistency in this study
3 McCaul et al. (2009)

The resulting file yielded a new list of all the daily lightning sources over CCAFS/KSC that were also assigned a probable flash number. As with the LMA data, we considered a valid flash to contain at least four sources; all flashes with less than four sources were thus filtered out. After the flash-grouped 4DLSS file was created, we converted the x-y-z spatial coordinates to latitude-longitude-altitude coordinates. Since this is not a simple one-to-one transformation, we used geodetic approximation calculations that take the Earth's curvature into consideration (RASC 2010). Subsequently, flash-grouped 4DLSS files were created for each potential storm day using MATLAB. The new 4DLSS file contained a list of each flash by time and location (latitude, longitude and altitude) represented by the parent source of each flash. Finally, a simple header was appended onto each file so the 4DLSS flash files could be read quickly into McIDAS-V. Reference Appendix A for a closer look at the lightning file formats.

E. IDENTIFYING INDIVIDUAL STORM CASES

Once the lightning and satellite data were prepared, we set forth to identify individual storm cases. For each day with active lightning, individual cells were studied from the pre-cumulus stage to LI. Convective cells that failed to produce lightning were generally ignored for this study. Recall that the individual storm

search in this study was focused on the 100-150-km array for each region. At this point, we also limited the sample storm set to a specific time window each day for each region. The 3.9-μm reflectance (ref39) becomes undefined as the solar zenith angle approaches 90°. Lindsey et al. (2006) determined the ref39 field to be most usable when the solar zenith angle is less than or equal to 68°. The usable time window changes throughout the day, with latitude/longitude, and from season to season. The solar zenith angle is lowest near midday and during the summertime. During our period of study, individual storm cases were selected within the following approximate time windows in each region based on Lindsey et al.'s (2006) 68° rule: AL (1305-2230 UTC), FL (1242-2208 UTC), OK (1351-2315 UTC), and DC (1230-2152 UTC). From here, we loaded the GOES-12 imagery into McIDAS-V one storm day at a time. Additionally, both the 1-minute grouped NLDN and 4-D lightning data—hereafter referred to as CG and IC data respectively—were overlaid on top of the satellite images. Note that the NLDN picks up a small percentage of IC flashes and a 4-D lightning array picks up CG flashes.

With the VIS and 10.7-μm imagery side-by-side and the lightning data overlaid, each satellite image was scanned for initiating convection. Figure 6 on the next page shows an example of how each case was tracked. Once potential lightning-initiating convection was located, the analysis was started one satellite image time-step prior to the first sign of a speckled cumulus cloud field. After a few cases were evaluated, we determined the analysis starting point should be at least one hour prior to the earliest of the following: the storm's first lightning occurrence or the storm's 10.7-μm CTT reaching 253 K. Krehbiel (1986) referenced the -20°C level as the point at which storms become strongly electrified. We ended each storm's analysis 30 minutes after the earliest occurrence of the following: final lightning flash, the storm's 10.7-μm CTT reaching 253 K or after rapid storm dissipation.

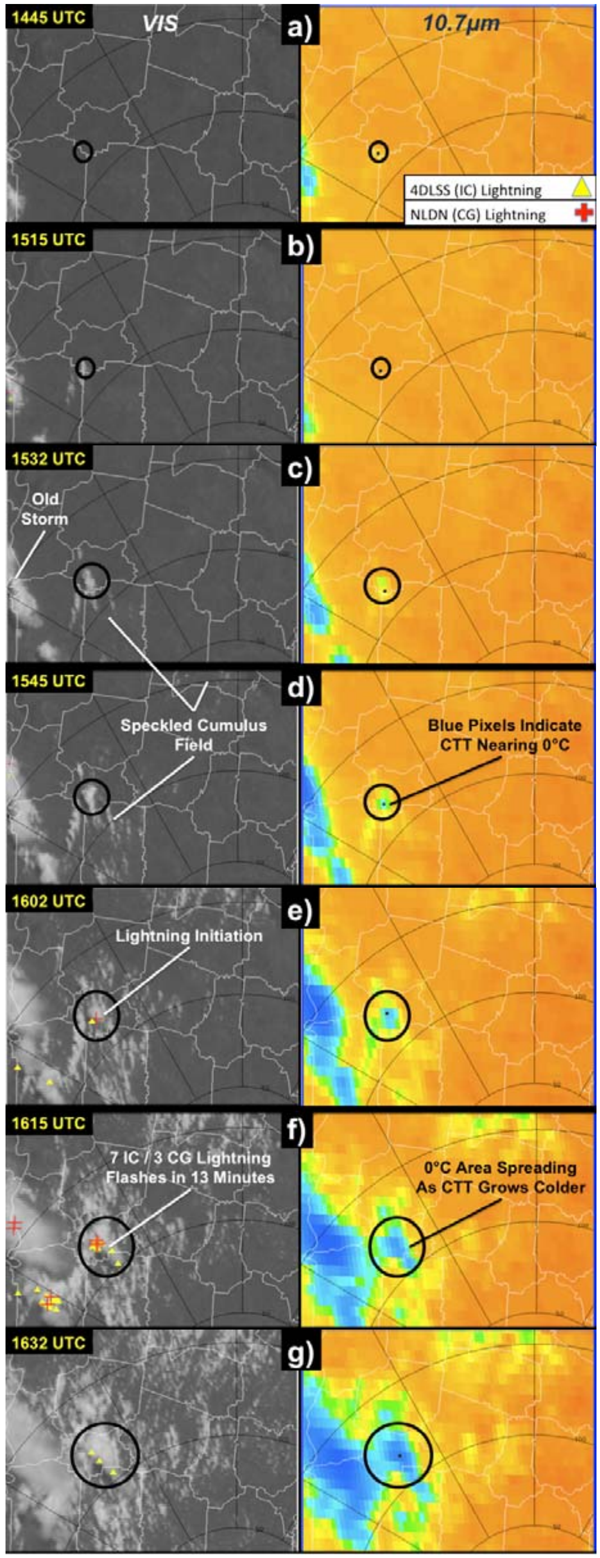

Figure 6. Example of storm tracking from one hour before LI (a) 1445 UTC to 30 minutes after LI (g) 1632 UTC. Pictured are GOES-12 VIS at left and 10.7-μm imagery at right with lightning also depicted.

Similar to Siewert (2008), we identified the storm centroid as the coldest 10.7-μm Tb. Assuming minimal cirrus contamination, the coldest CTTs typically indicate the region of strongest storm updraft. Using Lagrangian methods, we tracked a storm's coldest CTT throughout each case's analysis. Strong vertical wind shear complicates CTT measurements as the stronger winds aloft displace the coldest CTTs downstream of the storm's main updraft. Therefore, we limited the number of strong vertical wind shear cases. Finally, the convective environment for each case was also identified based on the synoptic and mesoscale setup. Each storm was characterized by one of the following: isolated/general storm (i.e., minimal synoptic forcing), organized mesoscale storm or synoptic/linear storm (e.g., cold frontal convection).

F. COLLECTING STORM MEASUREMENTS

After the appropriate storm time window was established for each case, we gathered pre- and post-LI environmental measurements for the hour before and half-hour after LI. We used McIDAS-V's data probe tool to interrogate the following GOES-12 IR parameters: 3.9-μm Tb (Tb39), 3.9-μm radiance (39rad), 6.5-μm Tb (Tb65), 10.7-μm Tb (Tb107), and 13.3-μm Tb (Tb133). Each channel's parameters were measured by placing the data probe's cursor over the coldest Tb107 pixel for a given storm. The Tb readings were recorded to the nearest tenth of a degree K, and the radiance readings were recorded to the nearest 0.001 W/m^2/str for each satellite image. Next, we estimated the area of each storm's lightning potential based on the coverage of the 273 K Tb107 as eluded to in Figures 6d and 6f. Due to time constraints, though, we were unable to analyze the lightning response to storm growth. Finally, the LI initiation time was identified as the first IC and CG flash times to the nearest minute for each storm. Subsequently, the number of IC and CG flashes were counted between each successive satellite image as shown in Figure 6f.

G. GOES LIGHTNING INITIATION INTEREST FIELDS

1. Interest Field Selection

Previous CI/LI work—as outlined in Chapter I—provided a solid foundation for this LI study to be built upon. We explored the same eight GOES LI IFs used in Siewert (2008), and added two additional fields for further study (refer back to Table 1 for a summary of each field): Tb107, 15-minute Tb107 trend, 6.5-μm-10.7-μm difference (Tb65107), 13.3-μm-10.7-μm difference (Tb133107), 15-minute Tb65107 trend, 15-minute Tb133107 trend, 3.9-μm-10.7-μm difference (Tb39107), 15-minute Tb39107 trend, ref39, and 15-minute ref39 trend. All difference fields refer to a simple Tb subtraction for the two respective channels. For instance, the Tb65107 difference in Figure 4's graph at the 0.5-hour mark is 250 K – 290 K = -40 K. Since satellite data exhibit disparate time intervals between images (e.g., 10, 13, 17, 30, 5 minutes), we chose to use a 15-minute time tendency for the trend IFs. MB06 and Siewert (2008) used the same methodology. For simplicity, we assume linear storm growth between successive satellite images even though thunderstorms exhibit highly non-linear atmospheric tendencies. Finally, the 3.9-μm, 6.5-μm and 13.3-μm channels were not included in this study as stand-alone IFs. Previous CI/LI research, as well as other studies relating these fields to cloud properties, determined that the aforementioned channels show little to no significant "stand-alone" signal leading up to LI (MB06; Mecikalski et al. 2008; Siewert 2008). Before progressing toward building the LI databases, we explain the background behind the ref39 calculation.

2. 3.9 Micron Reflectance Calculation

Previous research demonstrated the ref39's usefulness, particularly with regard to water versus ice delineation in convective clouds (Setvak and Doswell 1991; Lindsey et al. 2006; Siewert 2008). The total 3.9-μm radiance received at the satellite, $R_{3.9\mu m}$, can be summed up in one simple equation:

$$R_{3.9\mu m} = ref39 + \varepsilon_{3.9\mu m} \mathrm{R}_{\mathrm{emit}3.9\mu\mathrm{m}}(T), \qquad (1)$$

where ref39 is the 3.9-μm reflectance and the second term is the product of an object's 3.9-μm emittance and its emissivity, $\varepsilon_{3.9\mu m}$. The sensed objects—namely cloud mass—are assumed to be perfect blackbodies at 3.9 μm, and thus $\varepsilon_{3.9\mu m}$=1. Unlike the other IFs, subtracting out the reflected component is not a simple channel difference or time trend calculation. Below we summarize how to remove the ref39 from the total 3.9-μm radiance using Setvak and Doswell's (1991) and Lindsey et al.'s (2006) original work.

The sun radiates energy at all wavelengths of the electromagnetic spectrum. We first calculated the total amount of Earth-absorbed solar radiance at 3.9-μm assuming the sun's blackbody temperature is 5800 K and using the GOES-12 Planck function constants and solar radiance equation:

$$\mathrm{R}_{\mathrm{emit}3.9\mu\mathrm{m}}(T_{sun}) = \frac{\mathrm{fk1}_{3.9\mu\mathrm{m}}}{\exp\left(\dfrac{\mathrm{fk2}_{3.9\mu\mathrm{m}}}{\mathrm{bc1}_{3.9\mu\mathrm{m}}+\left(\mathrm{bc2}_{3.9\mu\mathrm{m}}Tsun\right)}\right)-1}, \quad (2)$$

where fk1, fk2, bc1 and bc2 are all 3.9-μm GOES-specific constants defined at CIMMS (2010). Next, the 3.9-μm solar flux at the top of the atmosphere was calculated:

$$S_{3.9\mu\mathrm{m}}(r,\xi) = [\mathrm{R}_{\mathrm{emit}3.9\mu\mathrm{m}}(T_{sun})](R_{sun}/r_E)^2\cos\xi , \quad (3)$$

where R_{sun} is the sun's radius (6.96 x 10^8 km), r_E is the earth's orbit radius (1.496x10^{11} km), and $\cos\xi$, or μ as it is sometimes referred, uses the solar zenith angle. Next, the solar zenith angle is converted to radians to calculate μ:

$$\mu = \cos[\xi(\pi/180)]. \quad (4)$$

Solar zenith angle, ξ, may be computed using the solar position algorithm at NREL (2010). Recall that the solar zenith angle depends on the storm's latitude, longitude and occurrence time. The following parameters are input into the NREL (2010) algorithm for storms in this study: 0-m location elevation, 1000-hPa average pressure, 20°C average temperature, and 64.797 s (default) delta-T (difference of Earth time and UTC). Varying the first three parameters provided no major shift in the retrieved solar zenith angles.

With the solar flux calculated, the 3.9-μm emitted Planck blackbody radiance was estimated as noted from Kidder and Vonder Haar (1995)

$$B_{3.9\mu m}\left(Tb_{107}\right)=\frac{c_1\lambda^{-5}}{\exp\left(\dfrac{c_2}{\lambda Tb_{107}}\right)-1}\ , \tag{5}$$

where c_1 = 1.19104 x 10^{-16} W m^2/str, c_2 = 0.01438769 m K, and λ = 3.9x10^{-6} μm. The result of Equation 5 was then multiplied by 10^{-6} to obtain the emitted Planck radiance in terms of W m^2/str/μm. Here the Planck curve is based on the GOES-obtained Tb107 measurement. The corresponding 3.9-μm point on the Planck curve is the 3.9-μm emittance assuming the Tb107 measurement emanated from a perfect blackbody. For optically thick clouds like a developing Cb, this is a safe assumption (Setvak and Doswell 1991; Lindsey et al. 2006). Finally, the ref39 field is calculated using

$$ref\,39=\frac{R_{3.9\mu m}-B_{3.9\mu m}(Tb_{107})}{S_{3.9\mu\mathrm{m}}(r,\xi)-B_{3.9\mu m}(Tb_{107})}\ . \tag{6}$$

In more simple terms,

$$3.9\text{-}\mu\text{m Reflectance} = \frac{3.9\text{-}\mu\text{m Total Radiance - } 3.9\text{-}\mu\text{m Emitted Radiance}}{3.9\text{-}\mu\text{m Solar Flux - } 3.9\text{-}\mu\text{m Emitted Radiance}} \tag{7}$$

Some minimal error is introduced in assuming only isotropically-scattering spherical cloud and precipitation particles (Setvak and Doswell 1991; Lindsey et al. 2006). For each case, the following GOES inputs were obtained for the 3.9-μm reflectance calculations: the solar zenith angle (ξ), the satellite-retrieved total 3.9-μm radiance ($R_{3.9\mu m}$), and the satellite-retrieved Tb107.

3. Building Lightning Initiation Databases

After gathering the satellite and lightning data for all cases, five databases were prepared for temporal and regional comparison analysis. First, all storms were oriented to the same temporal plane by converting them to decimal hour.

The initial time—whether cases started at 1402 UTC or 2231 UTC for example—is set to zero. This temporal standardization allowed for easier comparative storm analysis.

Next, the hour prior to LI is sub-divided into 15-minute intervals to eventually measure the predictive capability of each IF. Quarter-hour intervals were chosen since GOES data is currently available every 15 minutes on average. In addition, most of the cases in this study developed from the pre-cumulus stage to LI in an hour or less. The five time increment databases consisted of IF data at 60 minutes before LI (LI-60), 45 minutes before LI (LI-45), 30 minutes before LI (LI-30), 15 minutes before LI (LI-15), and finally the LI time (LI-0). For the initial investigation, we presumed an IC flash represented LI.

Satellite image intervals and LI time never consistently matched up in the hour leading up to first lightning. Therefore, we performed linear interpolation methods on each IF between satellite data points. An example of the linear interpolation methods is shown in Figure 7. Squares, circles, triangles and diamonds mark the actual satellite data points for the four IR channels.

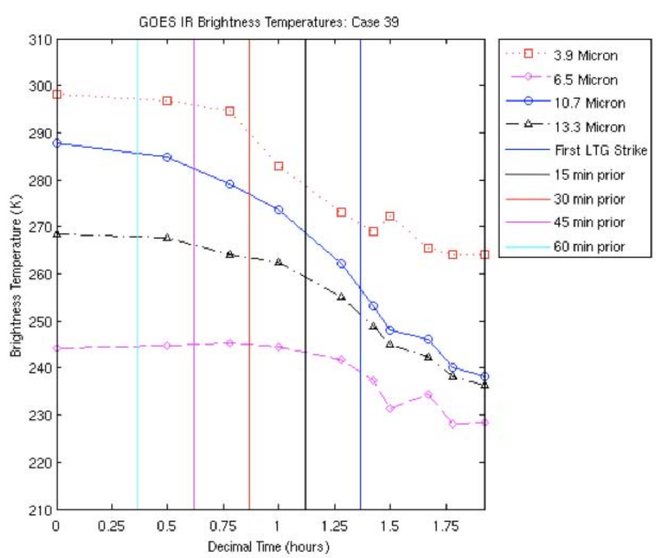

Figure 7. Example of IF interpolation between satellite data points. Interpolations occur at four 15-minute time intervals in the hour before and including LI and are identified by where the vertical lines cross the IF curves. In this example, Brightness Temperature (K) is represented on the y-axis and the x-axis is time in decimal hours.

Each time increment database was built by interpolating between the satellite data points where the five time intervals—the vertical lines—intersect each IF. For instance, the Tb107 value 30 minutes prior to LI is interpolated as 265 K. Due to non-linearity common with thunderstorm development, other non-linear methods were considered including a cubic and cubic-spline interpolation. The cubic interpolation results were very similar to the linear interpolation. Since the cubic-spline interpolation introduces additional error at the ends of each curve, we chose the linear interpolation for simplicity. We expect some introduced interpolation error where some IFs exhibit more non-linear tendencies than others. However, this method approximates the IF behavior very well in a standardized time-interval data comparison with minimal interpolation error.

THIS PAGE INTENTIONALLY LEFT BLANK

III. RESULTS AND ANALYSIS

A. CASE BREAKDOWN

Following the methodology explained in Chapter II, we built and analyzed 172 total cases over four geographical regions as depicted in Figure 8. At least 30 cases were collected for each region to build statistically sound databases. Before the results are analyzed, we discuss two exceptions made while building the storm databases.

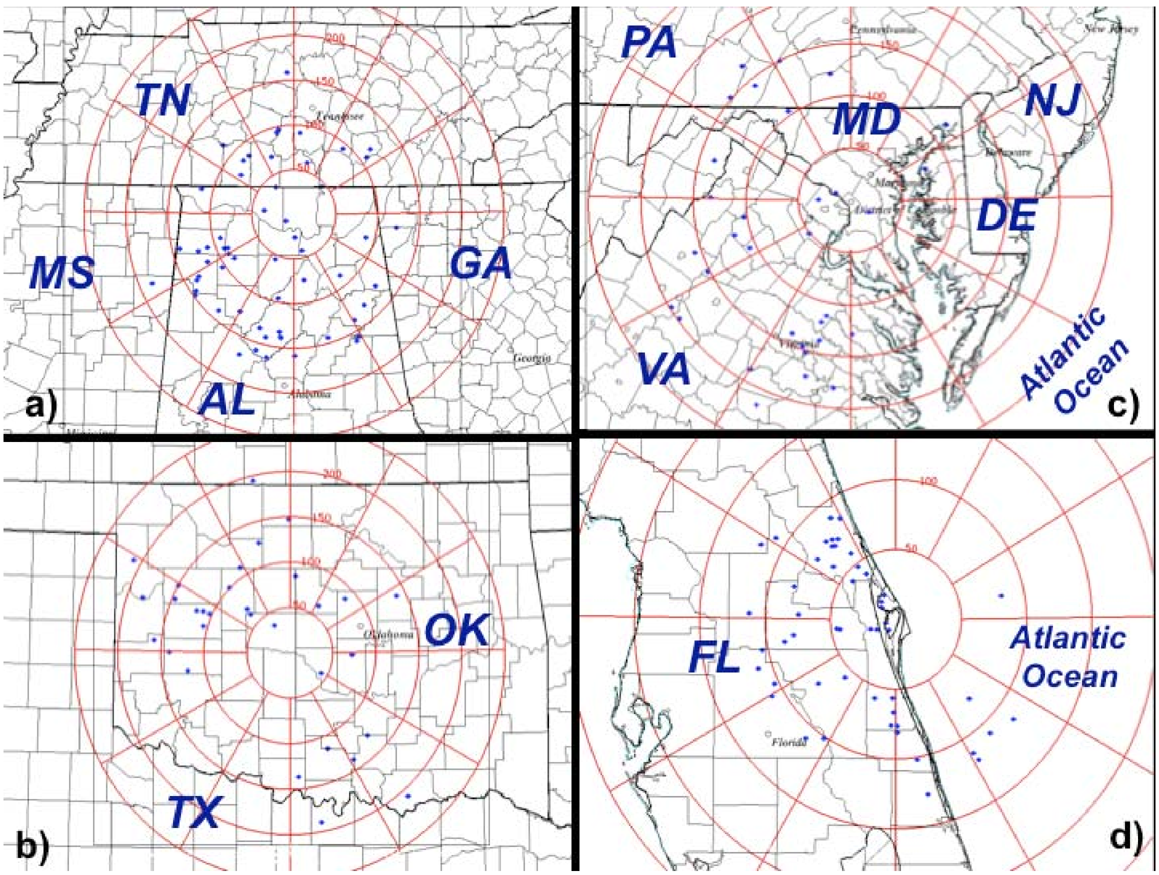

Figure 8. Total of 172 LI storm cases—denoted as blue dots—analyzed over four regions: a) 58 AL cases, b) 31 OK cases, c) 32 cases and 51 FL cases.

Due to a lack of data, the first five AL cases contain only partially complete data with respect to time. Specifically, AL's LI-60 distribution has 53/58 cases (i.e., five less than the total) and the LI-45 distribution has 57/58 cases (i.e., one

less than the total). Insignificant degradation to our results is expected given the relatively large sample size. Secondly, 22/172 cases (i.e., 12.8%) occurred outside of our self-restricted 100 to 150-km array areas. The aforementioned exception was made only if the 4-D lightning array in question appeared to handle the individual storm case well. “Well” was defined as when a CG flash occurred within 4.6 to 6.9 minutes of an IC flash depending on the region. The average time between IC and CG flashes in this study—6.9 minutes for AL, 6.8 minutes for FL, 4.6 minutes for DC and 4.7 minutes for OK—matched very closely with the approximate five- to ten-minute interval noted by Williams et al. (1989) and Houze (1993). Any potential lightning timing error due to this exception is determined to be no more than a couple minutes and has little to no effect on our analysis. One final lightning note that had no bearing on our results was that some storms in three of the four regions—13.8% for AL, 9.8% for FL, 0.0% for DC and 25.8% for OK—exhibited zero CG flashes within 30 minutes after the first IC flash.

B. QUALITATIVE ASSESSMENT OF INDIVIDUAL CASES

Before the predictive capability of each IF was explored, we reviewed every storm case within each region for quality control and to make general IF behavior notes. Figures 9–15 depict the IF results for storm 39 in the FL region. All 172 cases do not necessarily follow the exact path to LI as storm 39; however, the qualitative descriptions based on storm 39 generally represent the entire dataset very well. Therefore, only FL storm 39’s individual results are discussed below.

1. Behavior of Individual GOES IR Channels

Although this study ignores the stand-alone Tb39, Tb65 and Tb133 channels as IFs, some general comments are appropriate. Figure 9 shows all four GOES IR channels’ behavior in the hour before. LI-0—when lightning has initiated in the storm—is furthest right of all vertical lines. Each vertical line to the

left of the LI-0 line represents a 15-minute increment prior to LI. Thus, the vertical line at far left represents the LI-60 timeframe.

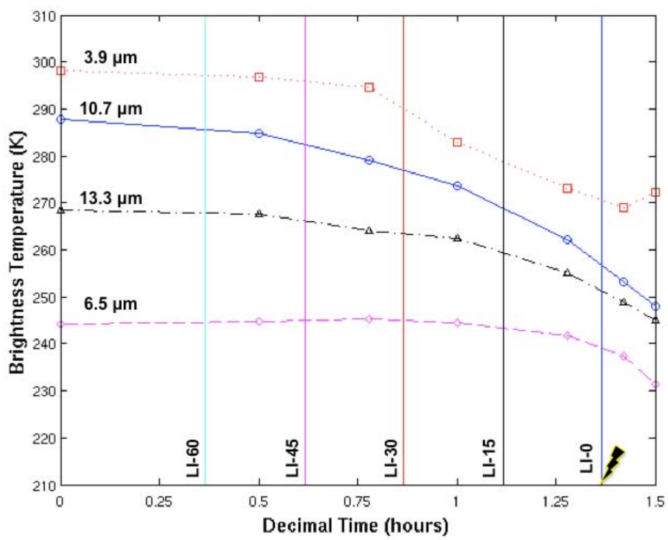

Figure 9. Behavior of four GOES-12 IR brightness temperatures over time for FL case 39. The vertical LI-0 line represents the first lightning strike, with each vertical line left of LI-0 representing 15-minute increments before lightning up to 60 minutes before LI (i.e., LI-60).

The Tb39 field—the top line in Figure 9—not surprisingly has the highest Tb of all channels due to the 3.9-μm's combined reflective and emissive components in this atmospheric window region. Between LI-60 and LI-30, note the steady to gradually decreasing Tb39 trend. As more ice appears in the growing convective cloud, the Tb39 field indicates less reflectance and therefore sees a steeper Tb decrease in the 30 minutes before LI.

The Tb65 field—the bottom curve in Figure 9—exhibits the lowest Tbs of all channels due to water vapor absorption. The early Tb65 values even before the cumulus forms approximate the 400-600-hPa ambient air temperature where the greatest water vapor absorption occurs. Thus, the Tb65 field experiences little change until the steady drop about 15 minutes prior to LI when the convective cloud has risen vertically into or past the 400-600-hPa layer. The Tb133 field—the second curve from the bottom—exhibits similar behavior. However, the Tb133 temperatures are slightly warmer and the late decrease is

slightly steeper than the Tb65 field due to carbon dioxide absorption. Finally, the Tb107 field—the solid blue curve second from the top—exhibits the most noteworthy trends in the hour before LI. As the cumulus forms generally between LI-60 and LI-45, a gradual Tb107 decrease is seen. A more precipitous drop occurs occasionally after LI-45 but most often after LI-30 as the convective cloud rapidly grows into a colder environment. The precipitous Tb107 drop for some cases—particularly in the FL region—did not occur until the last 15 minutes before LI. Very few cases exhibited only gradual decreases in the 15 minutes prior to LI, indicating that our dataset contains primarily rapidly developing storms (i.e., less than one hour) versus slow-building lightning initiators. One final regional note is that OK experiences the most precipitous Tb107 decreases of all regions, and the drops also occur earlier in the storm's development. One possible reason for this may be that OK had more explosively developing severe thunderstorms than any of the other three regions.

2. Tb107 Trend

The 15-minute Tb107 trend—shown in Figure 10—appears weakly negative (i.e., between 0 and -6 K per 15 minutes) for most cases until about the LI-30 point.

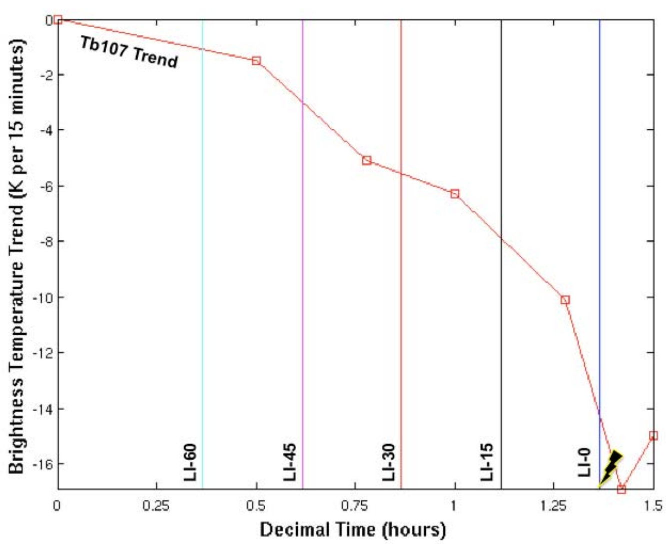

Figure 10. Same as Figure 9, except for Tb107 15-minute trend.

The trend decreases significantly (i.e., dropping more than 6 K per 15 minutes) in the 15 to 30 minutes before LI as the thunderstorm's updraft rapidly pushes the cloud to colder atmospheric levels. Unlike the other three regions, OK's Tb107 trend maintained a relatively strong decrease (i.e., falling more than 6 K per 15 minutes) from early in the storm's development leading up to LI, also possibly due to stronger developing storms in that region. Tb107 decreases of more than 10 K per 15 minutes at LI-0 were common for all regions. Compared to other IFs, the Tb107 trend exhibited moderate variability between cases.

3. Tb65107 and Tb133107 Difference Fields

The Tb65107 and Tb133107 difference IFs, as seen in Figure 11, display similar characteristics. Each of the aforementioned IFs start low and the Tb65107 difference starts lower than the Tb133107 difference due to the Tb65 field having a much colder Tb with respect to the Tb107 field.

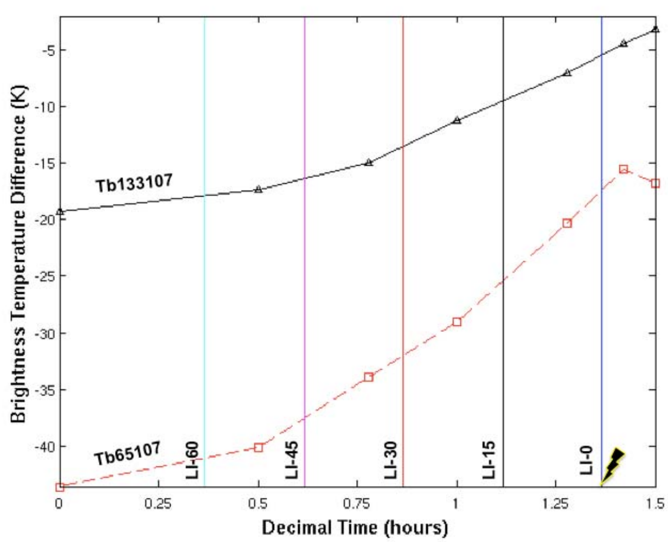

Figure 11. Same as Figure 9, except for Tb65107 and Tb133107 difference fields.

Both the Tb65107 and Tb133107 IFs show steady increases (i.e., becoming less negative) for all four regions, as the convective cloud grows closer to LI. Some Tb65107 and Tb133107 data occasionally became neutral around the LI-30 mark before continuing to increase shortly after. Although case 39 does not exhibit

this behavior in Figure 11, one potential cause for this temporarily steady behavior in other cases may be linked to the convective cloud reaching a capped or stable atmospheric layer and briefly slowing the storm's growth. Finally, the Tb65107 and Tb133107 difference IFs display very little variability between storms when compared to the other IFs.

4. Tb65107 and Tb133107 Trends

Figure 12 shows the Tb65107 and Tb133107 trend IFs. Note the weakly positive tendency of both IFs during the early storm development stage (i.e., less than 4 K per 15 minutes). By the LI-30 timeframe, most storms exhibited a sharper positive trend. Notice the separation between the two IFs though as the Tb65107 trend outpaces the Tb133107 trend (i.e., greater than 4-6 K per 15 minutes versus 3-5 K per 15 minutes) after LI-45. As the Tb107 decreases rapidly after LI-30, the gap between it and Tb65 closes more quickly than the Tb107 and Tb133 curves. Like the Tb65107 and Tb133107 IFs, their respective trends show little variability between storms when compared to the other IFs.

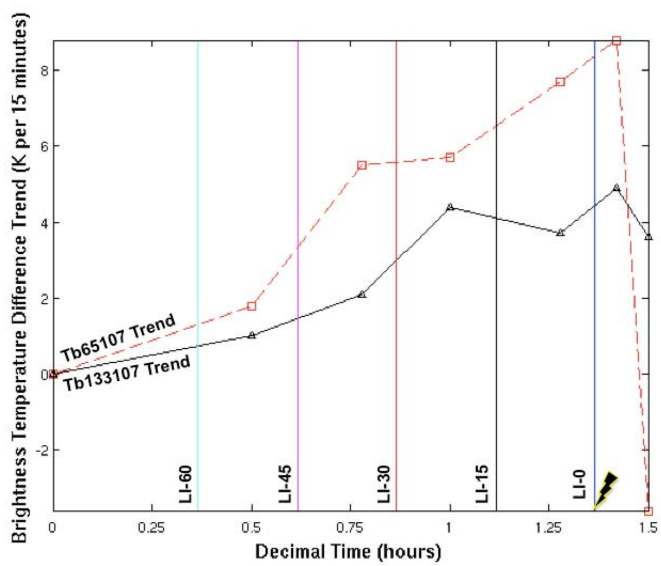

Figure 12. Same as Figure 9, except for Tb65107 and Tb133107 trend fields.

5. Tb39107 Difference and ref39 IFs

The Tb39107 difference IF typically had a steady or perhaps a slight increase in the early storm development stage. The increase is often followed by a sharp decrease then further increase about 15-30 minutes prior to LI as exhibited by the Tb39107 curve. The sharp increase was not as apparent for DC and typically did not occur until the last 15 minutes before LI. Similarly, the FL cases showed this increase most often in the last 15 minutes. Siewert (2008) suggested the sharp Tb39107 increase that follows a slight dip or steadiness indicates a rapid ice flux increase within the storm. Since higher ice content decreases the Tb39's reflective component more rapidly than the emitted component—as approximated by the Tb107 field—his hypothesis makes sense. We discuss this hypothesis in further detail later. The Tb39107 difference exhibited the largest variability between storms when compared to the other IFs.

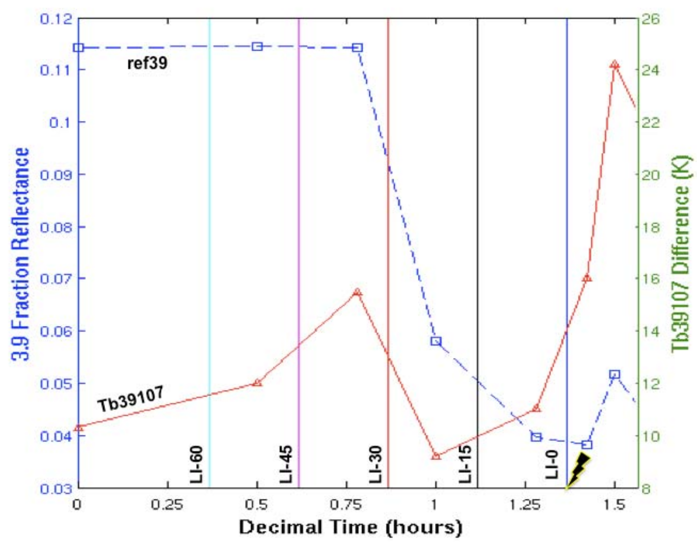

Figure 13. Same as Figure 9, except for Tb39107 difference and ref39 fields.

The ref39 IF—shown as the dashed line in Figure 13—exhibited some of the least variability between storms when compared to the other IFs. A steady and sometimes even a sharp ref39 decrease was often noticed in the hour before LI. The sharpest drops generally occurred 15-45 minutes prior to LI. The ref39 IF occasionally mirrored the slight increase-before-decreasing-trend that the

Tb39107 difference IF exhibits, particularly in FL. Furthermore, nearly all of the 172 storms had ref39 values of 0.05 or less in the last 15 minutes before LI. Setvak and Doswell (1991) suggest the Cb has reached complete glaciation at this fraction reflectance threshold. A glaciated cloud infers greater lightning potential since charge separation occurs rapidly with ice crystal and supercooled droplet collisions.

6. Tb39107 and ref39 Trends

The Tb39107 and ref39 trends exhibit characteristics similar to those we discussed in the previous section. Note the weakly positive Tb39107 trend in Figure 14 between LI-60 and LI-45 followed by a quick decrease then strong increase by the LI-15 point. We noted much less Tb39107 trend variability between storms when compared to the Tb39107 difference IF.

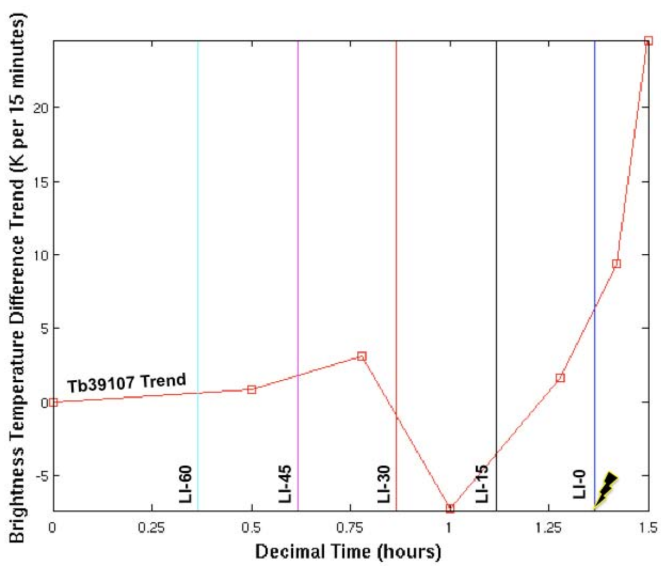

Figure 14. Same as Figure 9, except for Tb39107 trend field.

The 15-minute ref39 trend—as seen in Figure 15—also exhibited very little variability between storms when compared to the other IFs. The ref39 trend generally remains negative throughout the hour leading up to LI and has the most pronounced negative trend 15-45 minutes before LI.

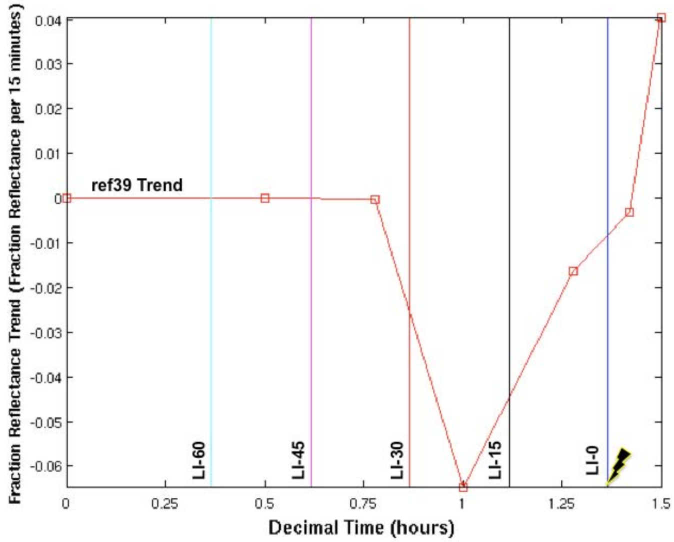

Figure 15. Same as Figure 9, except for ref39 trend field.

C. PREDICTIVE CAPABILITY OF EACH INTEREST FIELD

After each of the 172 cases was qualitatively analyzed, we compiled statistics for each of the five LI databases from LI-60 to LI-0. The full set of statistics (i.e., median, mean, inter-quartile range [IQR], and standard deviation [st dev]) for all regions is listed in Appendix B. To determine each IF's lightning potential predictive capability, we first sought answers to two important questions. Within each region 1) does each IF appear to have lightning predictive capability and if so, 2) how far in advance—time wise—can each IF predict lightning? "Potential" is used to qualify the predictive capability since the results are limited by the fact that all of the cases in this study are lightning-producers. Thus, we do not have an independent non-lightning convection dataset to compare with this study. Later in Section III E, the results are compared with a small independent dataset. For now, each IF's potential predictive capability was determined in the following manner.

While the raw LI statistics in Appendix B are useful to pick out specific numbers, we used boxplots to qualitatively assess each LI IF's predictive capability. Boxplots—like the ones in Figure 16—display useful information such

as the dataset's median and spread, and their format allows for easy qualitative comparison analysis between times and later in this study, regions.

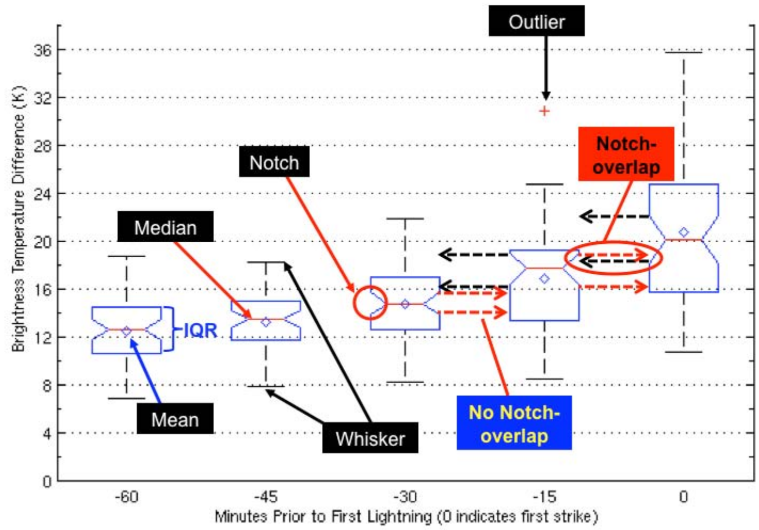

Figure 16. Boxplot tools used in this study.

Each boxplot—otherwise known as a box and whisker plot—has a notched box representing the middle 50% of the data or the IQR. A larger IQR indicates higher spread and therefore data variability. The horizontal red line splitting the box in two equal segments—assuming a Normal distribution—represents the median. For reference, we denote each database's mean by a diamond near each median. The median and IQR are resistant statistics, whereas outliers adversely impact the mean and standard deviation (Wilks 2006). The vertical dashed lines on either side of the IQR (i.e., the whiskers) represent approximately 99% of a distribution from whisker to whisker. Any pluses beyond the whiskers signify outlier data points. The notch within each boxplot's IQR represents a visual statistical significance test. Notch-overlap checks whether each database is significantly different than the other databases. For instance, the LI-0 notch in Figure 16 overlaps the LI-15 notch. Therefore, the two databases are deemed statistically the same at the α=0.05 significance level. The 5% test level, which is the most common α threshold, means that we are willing to accept that the notch-overlap hypothesis test may incorrectly assess

the results 5% of the time or less. If the notches do not overlap—like LI-15 compared to LI-30—then the two databases are deemed significantly different. The width of each notch varies based on each distribution's spread.

A two-sample t-test hypothesis test was also run for more firm results beyond the visual notch-overlap test. A parametric statistical significance test such as the t-test is appropriate since nearly all IFs exhibit a nearly Gaussian or Normal distribution. We ran the t-test knowing that the notch-overlap uses the median, and the t-test uses the mean in its hypothesis testing. A two-sample t-test hypothesis checks whether two sample means are significantly different from each other, assuming the samples are more or less Gaussian. Like the notch-overlap test, the t-test was run at the α=0.05 significance level. The null hypothesis is that the means from one distribution time to the next (e.g., LI-0 versus LI-15) *are* significantly different. Thus, the alternate hypothesis is that the means are *not* significantly different (Wilks 2006). In other words, the means are the same.

The notch-overlap and two-sample t-test are used to answer the two predictive capability questions outlined earlier. For an IF to demonstrate predictive capability, we first look for no notch-overlap between LI-0 and LI-15. In other words, if a storm exhibits distinctive IF properties 15 minutes before LI compared to LI-0, then we are more likely to identify a unique IF predictor. However, any notch-overlap between LI-0 and LI-15 indicates minimal predictive capability, even if no notch-overlap exists at other times prior to LI. If for instance LI-0 and LI-15 data are not significantly different from each other, then we cannot know if a random storm's satellite reading belongs to one time increment or the other. Secondly, consecutive zero notch-overlap further out in time from LI (i.e., from right to left) signifies how far in advance the IF might predict LI. For instance, if no notch-overlap is noted between the LI-0/LI-15 and LI-15/LI-30 databases, then the IF has unique potential predictive capability as much as 30 minutes prior to LI.

In addition to the notch-overlap and two-sample t-test, we identify each IF's characteristics prior to LI in the following sub-sections. The five boxplots in Figures 17 to 26 represent the four 15-minute increment databases before LI and the first lightning time (i.e., LI-0) database. All four geographical regions showed similar characteristics; therefore, the following qualitative assessment based on FL's boxplots applies to all four regions unless otherwise noted. On the other hand, all four regions are shown in the t-test tables, Tables 4 to 13. Note that a few t-test results vary from the notch-overlap test since the t-test is testing against a distribution and its mean, while the notch-overlap tests against a distribution and its median. A final determination was based on the t-test results.

1. Tb107

The pre-LI Tb107 characteristics for all 51 FL cases, as seen in Figure 17, closely resemble the behavior of individual case example 39 discussed in Section III B. In fact, all IF distributions discussed below match very closely with FL case 39.

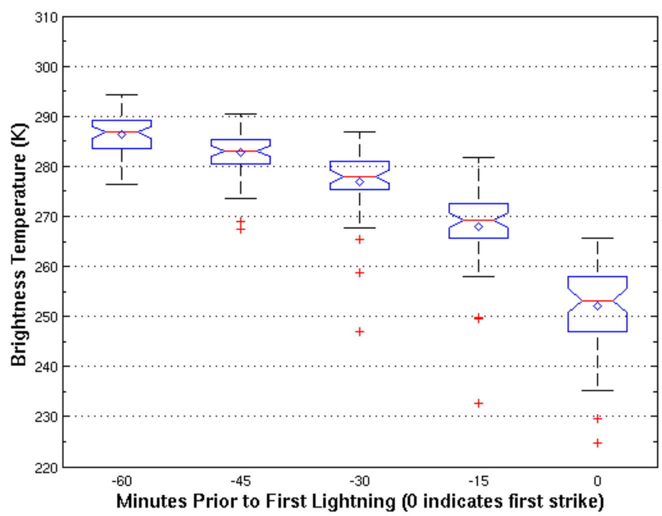

Figure 17. Tb107 behavior in the hour prior to LI as represented by 51 FL cases. Zero at the far right represents the 51 cases at the first lightning strike time increment. Each of the four boxplots preceding LI-0 represents the 51 FL cases in 15-minute increments prior to lightning up to one hour before LI.

In Figure 17, first note the early linear Tb107 decrease leading up to LI with a distinctly accelerated drop in the last 15 to 30 minutes. The notch-overlap test clearly shows no overlap.

Table 4 shows the predictive capability hypothesis test results for the Tb107 IF. The t-test results in Table 4 also indicate that the Tb107 IF has very good potential predictive capability out to 60 minutes prior to LI. Furthermore, all regions show LI by the time the cloud reaches a Tb107 of 253 K or -20°C. The Tb107's spread increases by LI-0, which implies a larger degree of variability in cloud microphysical and dynamical interactions at the time of the first lightning occurrence.

Table 4. Predictive capability hypothesis test results for Tb107 IF in AL, FL, OK and DC. In each region, the 51-case LI-15 sample is compared to the 51-case LI-0 sample; then LI-15 is compared to LI-30 and so on. A "YES" indicates the two samples are significantly different. A "NO" indicates the two samples are *not* significantly different. Predictive capability is qualified based on the LI-0/LI-15 comparison. "Likely" indicates mostly "YES"s among regions. "Marginal" indicates half "YES"s and half "NO"s, and "Minimal" indicates mostly "NO"s among regions. An IF's potential predictive capability lead time is determined by the number of consecutive "YES"s from LI-15 to LI-60.

Interest Field	**Tb107**			
Region	**AL**	**FL**	**OK**	**DC**
LI-15	YES	YES	YES	YES
LI-30	YES	YES	YES	YES
LI-45	YES	YES	YES	YES
LI-60	YES	YES	YES	YES
Predictive Capability	***Likely***			
Potential Lead Time	*60-min*	*60-min*	*60-min*	*60-min*
"Average" Lead Time	***60-min***			

2. Tb107 Trend

Like the Tb107 IF, the pre-LI Tb107 trend is characterized by an accelerating downward trend, becoming more negative closer to LI. Figure 18 also shows increasing spread from LI-60 to LI-0, indicating a variability pattern

similar to the Tb107 field. As seen in Table 5, all regions show good potential predictive capability with respect to the Tb107 trend IF. AL and FL appear to have better predictive capability beyond 30 minutes compared to DC and OK.

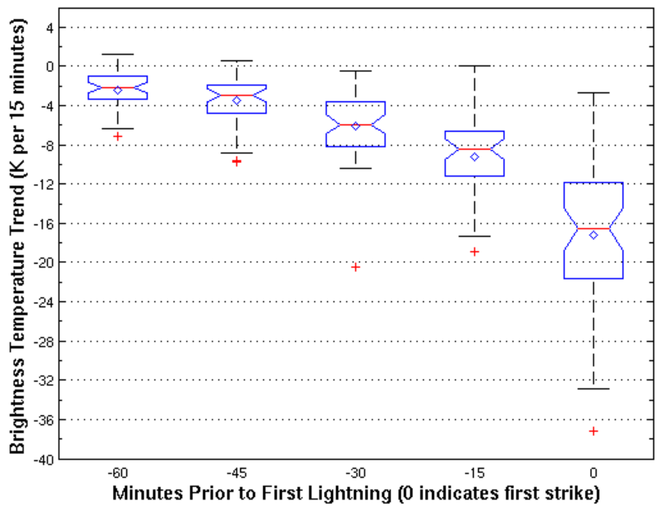

Figure 18. Same as Figure 17, except for Tb107 trend IF.

Table 5. Same as Table 4, except for Tb107 trend IF.

Interest Field	**107_trend**			
Region	**AL**	**FL**	**OK**	**DC**
LI-15	YES	YES	YES	YES
LI-30	YES	YES	YES	YES
LI-45	YES	YES	NO	NO
LI-60	YES	YES	YES	YES
Predictive Capability	***Likely***			
Potential Lead Time	*60-min*	*60-min*	*30-min*	*30-min*
"Average" Lead Time	***45-min***			

3. Tb65107 and Tb133107

Figure 19 and Table 6 depict the Tb65107's predictive capability, and Figure 20 and Table 7 show the Tb133107 results. Each of these IFs depicts a clear increase over time, becoming slightly more accelerated near the last 15 to 30 minutes before LI. Tb65107 experiences higher spread compared to Tb133107, possibly since atmospheric water vapor is not as well mixed as

carbon dioxide. A well-mixed gas like carbon dioxide may provide more consistent satellite readings for the 13.3-μm channel.

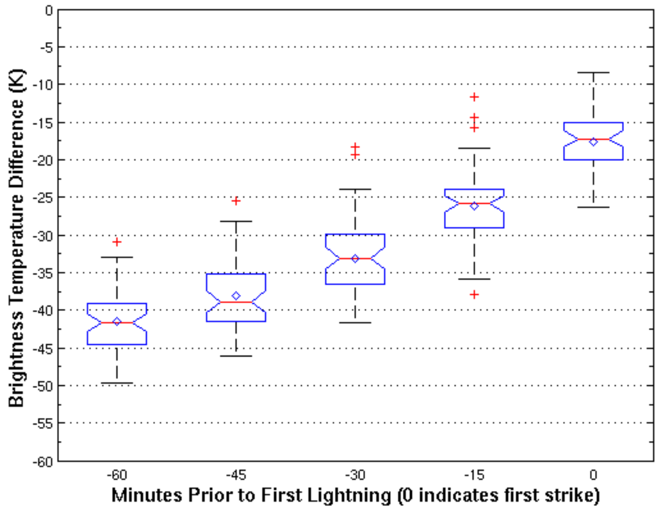

Figure 19. Same as Figure 17, except for Tb65107 difference IF.

Table 6. Same as Table 4, except for Tb65107 difference IF.

Interest Field	**65-107**			
Region	**AL**	**FL**	**OK**	**DC**
LI-15	YES	YES	YES	YES
LI-30	YES	YES	YES	YES
LI-45	YES	YES	YES	YES
LI-60	YES	YES	YES	YES
Predictive Capability	***Likely***			
Potential Lead Time	*60-min*	*60-min*	*60-min*	*60-min*
"Average" Lead Time	***60-min***			

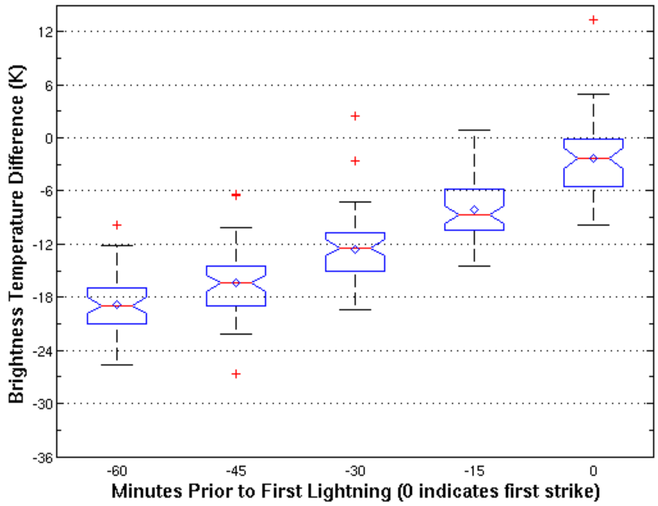

Figure 20. Same as Figure 17, except for Tb133107 difference IF.

Table 7. Same as Table 4, except for Tb133107 difference IF.

Interest Field	**133-107**			
Region	**AL**	**FL**	**OK**	**DC**
LI-15	YES	YES	YES	YES
LI-30	YES	YES	YES	YES
LI-45	YES	YES	YES	YES
LI-60	YES	YES	YES	YES
Predictive Capability	***Likely***			
Potential Lead Time	*60-min*	*60-min*	*60-min*	*60-min*
"Average" Lead Time	***60-min***			

The Tb65107 and Tb133107 IFs appear to have very good predictive capability with 60-minute potential lead times for all four regions based on the notch-overlap and t-test results.

4. Tb65107 Trend

The pre-LI Tb65107 trend increases linearly as seen in Figure 21. We attribute the increasing spread with time to the same cloud microphysics and dynamics that affect the Tb107 field. Any potential LI-15/LI-30 and LI-45/LI-60 notch overlap is difficult to discern. Therefore, the results in Table 8 are

referenced for a clearer predictive capability answer. While FL appears to have excellent predictive capability with respect to the Tb65107 IF, all three other regions experience varying degrees of predictability. AL, FL, and DC exhibit at least a 15-minute predictive capability, while OK shows minimal predictive capability. If the predictive lead times are averaged for all four regions, the Tb65107 trend IF has a 15 to 30-minute predictive lead time. Although all regions exhibit a clear trend increase, less predictive capability exists prior to LI since the change in that trend is not substantial enough from one time to the next particularly at longer time ranges prior to LI.

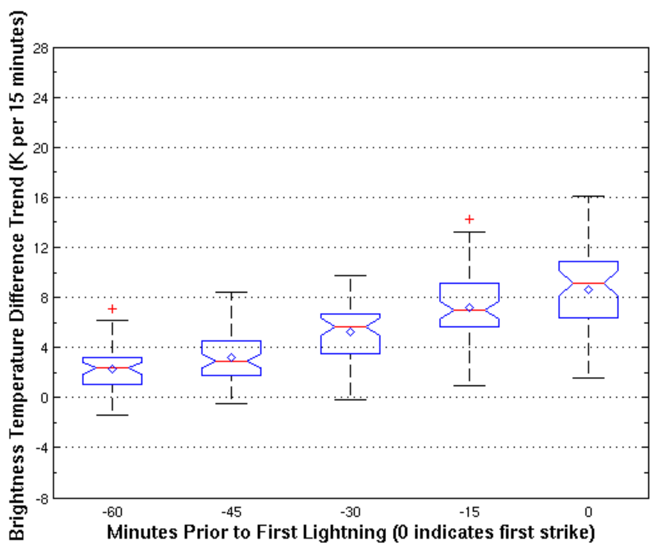

Figure 21. Same as Figure 17, except for Tb65107 difference trend IF.

Table 8. Same as Table 4, except for Tb65107 difference trend IF.

Interest Field	**65-107_trend**			
Region	**AL**	**FL**	**OK**	**DC**
LI-15	YES	YES	NO	YES
LI-30	YES	YES	NO	NO
LI-45	NO	YES	NO	NO
LI-60	YES	YES	YES	YES
Predictive Capability	***Likely***			
Potential Lead Time	*30-min*	*60-min*	*0-min*	*15-min*
"Average" Lead Time	***15 to 30-min***			

5. Tb133107 Trend

The Tb133107 trend's increase is even subtler than the Tb65107 trend. Figure 22 also indicates much less spread than the Tb65107 trend for the same reason discussed in Section III C 3 above. Less spread reduces potential notch-overlap and therefore should increase predictive capability likelihood; however, Figure 22 and Table 9 indicate plenty of notch-overlap and little predictive capability due to the subtlety of the Tb133107 trend's increase. Although the Tb133107 trend exhibits relatively weak predictive capability at longer lead times, three of the four regions (i.e., AL, OK, and DC) show at least some predictive capability with a 15-minute average lead time.

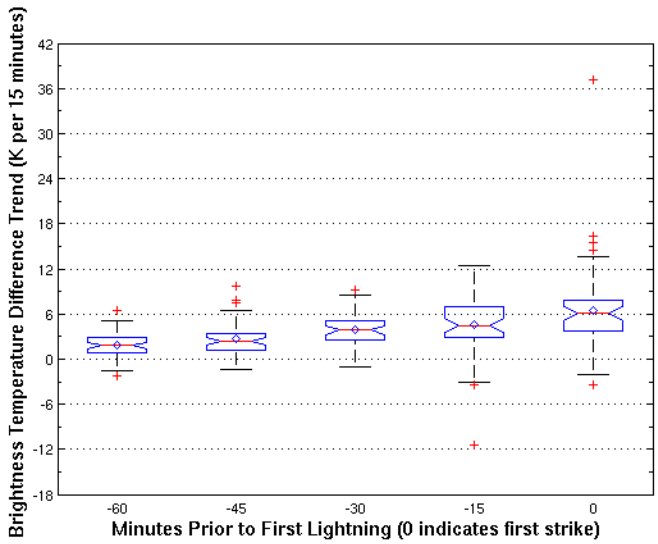

Figure 22. Same as Figure 17, except for Tb133107 difference trend IF.

Table 9. Same as Table 4, except for Tb133107 difference trend IF.

Interest Field	**133-107_trend**			
Region	**AL**	**FL**	**OK**	**DC**
LI-15	YES	NO	YES	YES
LI-30	NO	NO	NO	NO
LI-45	NO	YES	NO	NO
LI-60	YES	YES	YES	YES
Predictive Capability	***Likely***			
Potential Lead Time	*15-min*	*0-min*	*15-min*	*15-min*
"Average" Lead Time	***15-min***			

6. Tb39107

In Figure 23, the Tb39107 IF increases linearly at first and then accelerates in the last 15 to 30 minutes before LI. Any notch-overlap between LI-0 and LI-15 for FL is subtle. Hence, Table 10 is referenced for a clearer answer on the Tb39107's predictive capability. Table 10 indicates potential predictive capability for AL, FL and OK but to varying degrees in the hour prior to LI. The accentuated Tb39107 increase at 15–30 minutes before LI matches the average lightning lead time that the Tb39107 IF may provide as noted in Table 10.

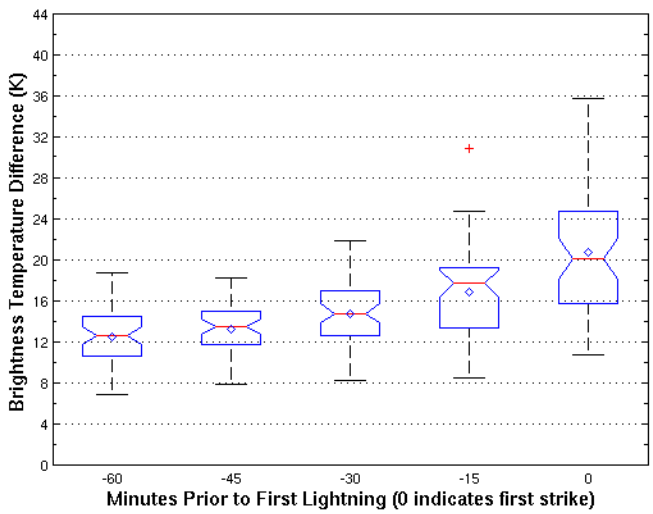

Figure 23. Same as Figure 17, except for Tb39107 difference IF.

Table 10. Same as Table 4, except for Tb39107 difference IF.

Interest Field	**39-107**			
Region	**AL**	**FL**	**OK**	**DC**
LI-15	YES	YES	YES	NO
LI-30	YES	YES	NO	NO
LI-45	NO	YES	NO	NO
LI-60	NO	NO	NO	YES
Predictive Capability	***Likely***			
Potential Lead Time	*30-min*	*45-min*	*15-min*	*0-min*
"Average" Lead Time	***15 to 30-min***			

7. Tb39107 Trend

The Tb39107 trend generally increases leading up to LI as seen in Figure 24. The individual trend seen earlier in FL case 39 is somewhat apparent in each region's plots—although to a much lesser degree for FL in Figure 24.

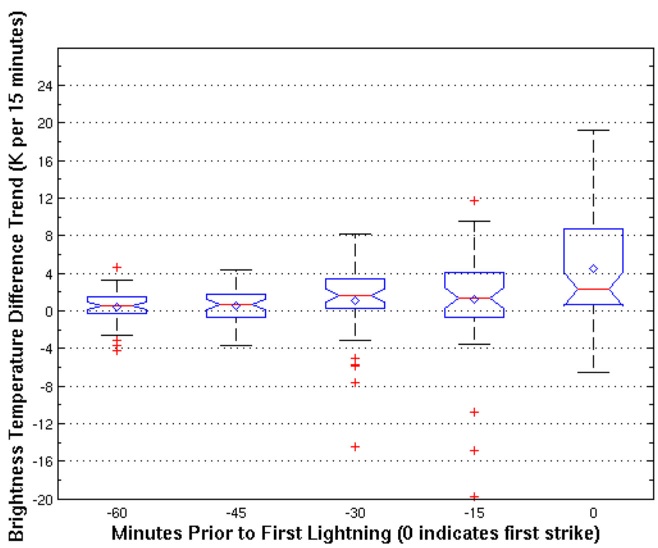

Figure 24. Same as Figure 17, except for Tb39107 difference trend IF.

The characteristic increase-decrease-increase signal documented by Siewert (2008) is somewhat apparent in the Tb39107 trend distributions. However, we cannot statistically validate this increase-decrease-increase tendency here due to marginal notch-overlap and t-test results as seen in Figure 24 and Table 11.

Table 11. Same as Table 4, except for Tb39107 difference trend IF.

Interest Field	**39-107_trend**			
Region	**AL**	**FL**	**OK**	**DC**
LI-15	YES	YES	NO	NO
LI-30	NO	NO	NO	NO
LI-45	NO	NO	NO	YES
LI-60	NO	NO	NO	NO
Predictive Capability	***Marginal***			
Potential Lead Time	*15-min*	*15-min*	*0-min*	*0-min*
"Average" Lead Time	***0 to 15-min***			

Although the aforementioned increase-decrease-increase tendency was noted previously in individual cases, this tendency is likely washed-out when combined into a larger dataset since the Tb39107 trend tendency often takes place at different times for each case in the 15 to 45 minutes prior to LI. In addition, the Tb39107 trend shows some predictive capability for AL and FL, yet little in the way of predictive quality out beyond 0 to 15 minutes.

8. ref39

As ice content increases volumetrically within a growing storm, the ref39 decreases as depicted in Figure 25.

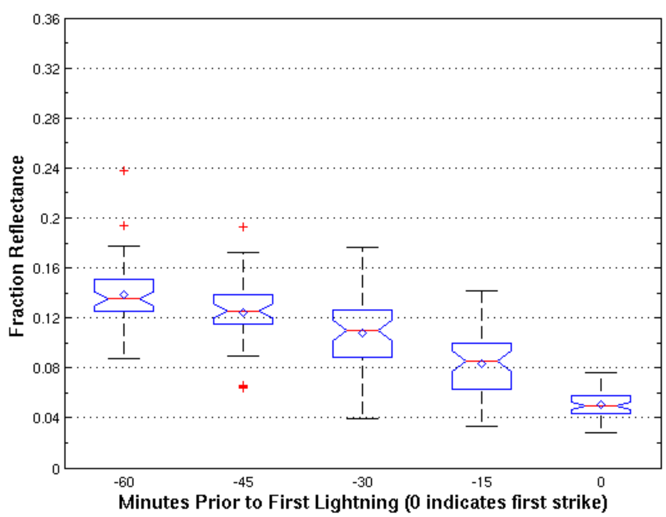

Figure 25. Same as Figure 17, except for ref39 IF.

The decrease is primarily linear and perhaps very slightly accelerated in the last 15 to 30 minutes for each region. AL, FL and DC reach complete cloud-top glaciation (i.e., ref39≤0.05) by LI-0, while OK is close with a 0.07 3.9-μm fraction reflectance. The ref39's notch-overlap in Figure 25 and the t-test results in Table 12 indicate very good predictive capability with at least 45 minutes lead time before LI.

Table 12. Same as Table 4, except for ref39 IF.

Interest Field	**ref39**			
Region	**AL**	**FL**	**OK**	**DC**
LI-15	YES	YES	YES	YES
LI-30	YES	YES	YES	YES
LI-45	YES	YES	YES	YES
LI-60	YES	YES	NO	NO
Predictive Capability	***Likely***			
Potential Lead Time	*60-min*	*60-min*	*45-min*	*45-min*
"Average" Lead Time	***45 to 60-min***			

9. ref39 Trend

Although a general decreasing tendency is noted in the ref39 trend, Figure 26 and Table 13 indicate that the decreases are too subtle from one time increment to the next.

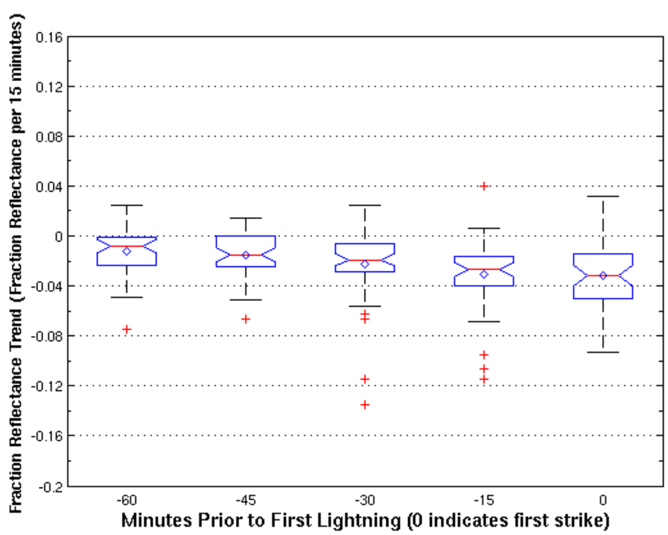

Figure 26. Same as Figure 17, except for ref39 trend IF.

DC is the only region to demonstrate predictive capability. Overall the ref39 trend demonstrates very little predictive capability in terms of both prediction and obviously time before LI.

Table 13. Same as Table 4, except for ref39 trend IF.

Interest Field	**ref39_Trend**			
Region	**AL**	**FL**	**OK**	**DC**
LI-15	NO	NO	NO	YES
LI-30	NO	NO	NO	NO
LI-45	NO	NO	NO	YES
LI-60	NO	NO	YES	NO
Predictive Capability	***Minimal***			
Potential Lead Time	*0-min*	*0-min*	*0-min*	*15-min*
"Average" Lead Time	***0 to 15-min***			

10. IF Predictive Capability Analysis

Overall, eight out of the ten IFs that were considered appear to have at least some predictive capability for most regions. The Tb39107 trend and ref39 trend were the two fields that showed relatively poor predictive capability results. Additionally, the Tb65107 and Tb133107 trends did not perform much better as noted in their lower average lead time. While the 15-minute trend IFs likely provide more awareness to imminent lightning, the individual case changes from one time increment to the next may be cancelling each other out when combined into a larger distribution of cases. Individual cases appear to have very similar tendencies—as mentioned for example with the Tb39107 trend earlier in Section III C 7. However, those tendencies may be taking place at different times in the storm's development. This trend disparity may explain some of the marginal results. All in all, we noticed distinct predictive capability trends for most IFs.

In addition, most fields appear fairly predictive at 15 to 45 minutes before LI with an average lead time for all fields and regions around 35 minutes. Like MB06 and Siewert (2008), we drew specific IF thresholds from the results above (see Table 14).

Table 14. Same as Table 1 except the thresholds based on a 15 to 30-minute nowcast are identified from this study's results.

Interest Field	MB06 Critical CI Value	Siewert LI Value	15 to 30-min Threshold (This LI Study)	Description
10.7 µm Tb	< 0°C	≤ - 13°C	*< 0° C*	Cloud tops cold enough to support supercooled water and ice mass growth; cloud-top glaciation
10.7 µm Tb Time Trend	< - 4°C / 15 min (ΔTb / 30 min < ΔTb / 15 min)	≤ - 10°C / 15 min (≤ - 15°C / 30 min)	*< - 6° C / 15 min*	Cloud growth rate (vertical)
Timing of 10.7-µm Tb drop below 0° C	Within prior 30 min	*Not used*	*Not Used*	Cloud-top glaciation
6.5 - 10.7 µm Tb difference	Tb Diff: -35°C to -10°C	≥ - 17°C	*> - 30° C*	Cloud top height relative to mid/upper troposphere
13.3 - 10.7 µm Tb difference	Tb Diff: -25°C to -5°C	≥ - 7°C	*> - 13° C*	Cloud top height relative to mid/upper troposphere; better indicator of early cumulus development but sensitive to cirrus
6.5 - 10.7 µm Tb Time Trend	> 3°C / 15 min	≥ 5°C / 15 min	*> 5° C / 15 min*	Cloud growth rate (vertical) toward dry air aloft
13.3 - 10.7 µm Tb Time Trend	> 3°C / 15 min	≥ 5°C / 15 min	*> 4° C / 15 min*	Cloud growth rate (vertical) toward dry air aloft
3.9 - 10.7 µm Tb Difference**	*Not used*	*Not used*	*> 17° C*	Cloud-top glaciation
3.9 - 10.7 µm Tb Time Trend*	*Not used*	T - T(t-1) < -5°C and T - T(t+1) < - 5°C	*> 1.5° C / 15 min*	Sharp decrease, then increase indicates cloud-top glaciation
3.9 µm Fraction Reflectance*	*Not used*	≤ 0.05	*< 0.11*	Cloud top consists of ice (ice is poorer reflector than water at 3.9 µm)
3.9 µm Fraction Reflectance Trend**	*Not used*	*Not used*	*< - 0.02 / 15 min*	Cloud-top glaciation rate
* Added in Siewert's (2008) LI Study				
** Added for this study				

Given the roughly 35-minute average IF lead time, we focused on the median and mean IF values for 15 to 30 minutes prior to LI to come up with the thresholds above. The LI IF thresholds in this study are less restrictive than Siewert's (2008) LI values since his study identified thresholds less than 15 minutes before LI. This study looks at thresholds up to 30 minutes prior to LI. The LI-0 and LI-15 median values in this study match Siewert's (2008) IF thresholds very closely. The IF thresholds listed in Table 14 should be used with caution since further study is required that incorporates an independent dataset containing non-lightning producing convection. Additionally, some IFs do not perform as well as others as we have shown. Further statistical study is recommended to identify POD and FAR performance before our thresholds are used operationally. Finally, while most IFs may be predictive out to 30 minutes in any given field, we cannot conclude here how they compare regionally. The regional IF characteristics are compared in the next section.

D. REGIONAL COMPARISON OF EACH INTEREST FIELD

By regionally comparing each IF, we hope to answer the following question: if a threshold were applied to a given IF, would the threshold potentially hold true for a large geographical region or are unique thresholds needed for varying regions? To answer this question, we again analyze notched-boxplots and two-sample t-tests to determine if each region's IFs are significantly different from one another. The null hypothesis is that the median/mean IF value from one region to the next *are* significantly different. Thus, the alternate hypothesis is that the medians/means are *not* significantly different (i.e., they are the same). If notches overlap and the t-test results show no difference between two regions, the regions are assumed to have the same predictive capability for a given IF. Furthermore, the regional comparison is focused on the final half-hour before LI since most IFs demonstrated predictive capability out to about 30 minutes. The notch-overlap tests—as seen in Figures 27 to 36—match very closely with the two-sample t-test results that are displayed in Tables 15 to 24; therefore, only LI-15 boxplots for each IF are shown for visual comparison.

1. Tb107

DC, FL and OK have very similar Tb107 characteristics in the half-hour prior to LI according to Figure 27 and Table 15. The DC and FL overlap in Figure 27 is quite apparent.

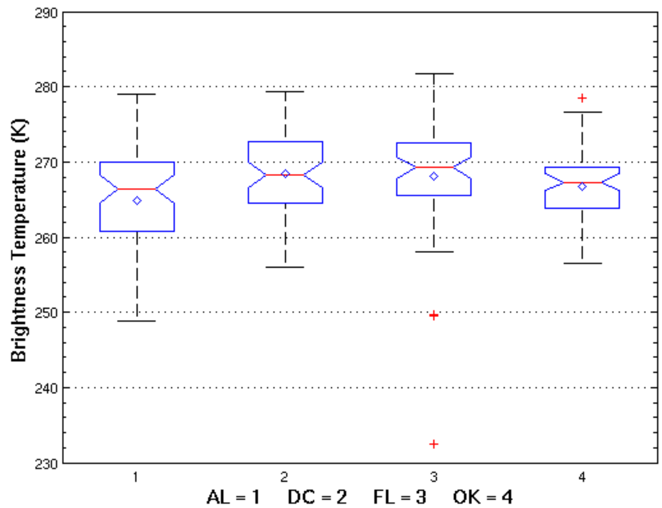

Figure 27. Regional comparison of (1) 58 AL cases, (2) 32 DC cases, (3) 51 FL cases and (4) 31 OK cases. The snapshot compares each region's Tb107 IF distribution 15 minutes prior to LI.

Table 15. Regional comparison hypothesis test results for Tb107 IF. Two specified regions in column 1 are compared at 30 and 15 minutes before LI and at LI-0. A "YES" indicates the two regions are significantly different. A "NO" indicates the two regions are *not* significantly different. The *YIELD* column identifies whether each set of regions is overall significantly different based on a "YES" or "NO" majority from LI-30 to LI-0.

Interest Field	**Tb107**			
Time	**LI-30**	**LI-15**	**LI-0**	***YIELD***
AL vs. DC	NO	YES	NO	***NO***
AL vs. FL	YES	YES	NO	*YES*
AL vs. OK	YES	NO	NO	***NO***
DC vs. FL	NO	NO	NO	***NO***
DC vs. OK	NO	NO	NO	***NO***
FL vs. OK	NO	NO	NO	***NO***

Also note the slight OK overlap with each of the aforementioned regions. AL is the only region that consistently yielded less overlap and therefore less similarity compared to the other regions. AL's consistently lower pre-LI Tb107s might suggest that a colder cloud-top and perhaps a taller thicker cloud are necessary for lightning to initiate in this region. Overall, the Tb107 IF appears useful across a broad geographical area.

2. Tb107 Trend

In Figure 28, AL, DC and FL have comparable cloud-top cooling rates right around -7 to -9 K per 15 minutes at LI-15. OK has minimal notch-overlap with FL at LI-15, but OK is typically the outlier when compared to the other three regions as seen in Table 16.

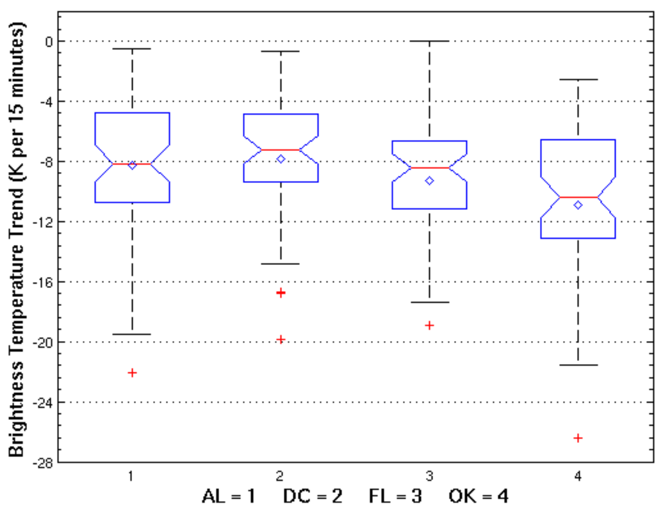

Figure 28. Same as Figure 27, except for Tb107 trend IF.

Since OK had a few more severe thunderstorm cases than the other regions, the OK region's stronger Tb107 trends, and thus stronger implied updrafts, possibly skewed the results. Otherwise, the Tb107 trend IF also performed well across a broad geographical area.

Table 16. Same as Table 15, except for Tb107 trend IF.

Interest Field	**107_trend**			
Time	**LI-30**	**LI-15**	**LI-0**	***YIELD***
AL vs. DC	NO	NO	NO	***NO***
AL vs. FL	NO	NO	YES	***NO***
AL vs. OK	YES	YES	NO	*YES*
DC vs. FL	NO	NO	NO	***NO***
DC vs. OK	YES	YES	NO	*YES*
FL vs. OK	YES	NO	NO	***NO***

3. Tb65107 and Tb65107 Trend

Interestingly, OK tends to be the only outlier when comparing each region's Tb65107 and Tb65107 trend IFs—as seen in Figures 29 and 30. AL, DC and FL have plenty of notch-overlap, suggesting these regions exhibit the same traits with respect to the Tb65107 and Tb65107 trend IFs. Once again, the consistently lower absolute Tb65107 values and stronger Tb65107 trends may be due to the few extra severe thunderstorm cases for OK.

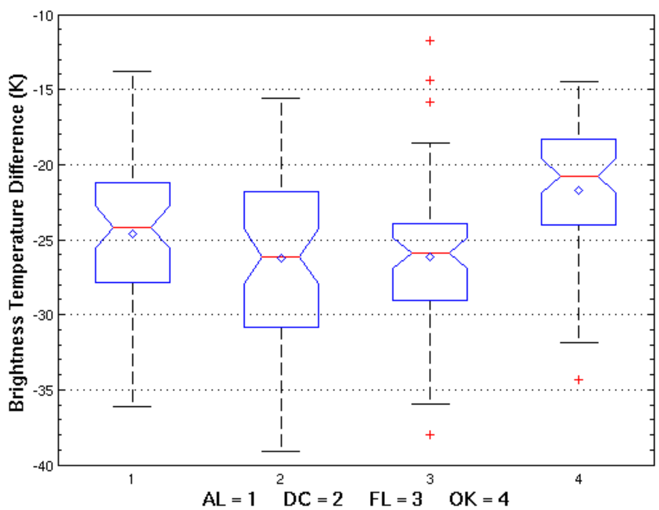

Figure 29. Same as Figure 27, except for Tb65107 difference IF.

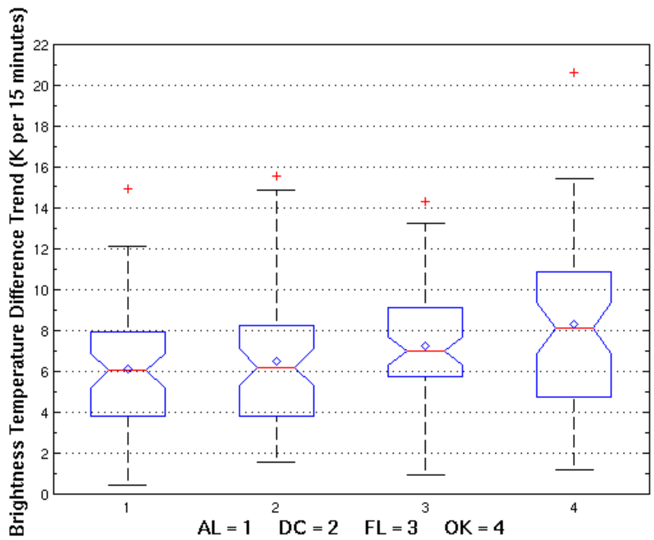

Figure 30. Same as Figure 27, except for Tb65107 trend IF.

Also, since OK sits just east of the Rocky Mountains, we may be seeing a slight reduction in water vapor due to middle tropospheric drying and therefore less water vapor absorption within the 6.5-μm channel. Less water vapor hence allows for higher 6.5-μm Tbs. Tables 17 and 18 also indicate how OK is the only region that differs from the other three in the Tb65107 and Tb65107 trend's regional comparisons.

Table 17. Same as Table 15, except for Tb65107 difference IF.

Interest Field	**65-107**			
Time	**LI-30**	**LI-15**	**LI-0**	***YIELD***
AL vs. DC	NO	NO	NO	***NO***
AL vs. FL	YES	NO	NO	***NO***
AL vs. OK	NO	YES	NO	***NO***
DC vs. FL	NO	NO	NO	***NO***
DC vs. OK	NO	YES	YES	*YES*
FL vs. OK	YES	YES	YES	*YES*

Table 18. Same as Table 15, except for Tb65107 trend IF.

Interest Field	**65-107_trend**			
Time	**LI-30**	**LI-15**	**LI-0**	***YIELD***
AL vs. DC	NO	NO	NO	***NO***
AL vs. FL	YES	NO	NO	***NO***
AL vs. OK	YES	YES	NO	*YES*
DC vs. FL	NO	NO	NO	***NO***
DC vs. OK	YES	NO	YES	*YES*
FL vs. OK	YES	NO	YES	*YES*

4. Tb133107

As seen in Figure 31, AL, FL and OK exhibit more consistent Tb133107 notch-overlap versus DC. AL and DC are the two regions most often different with respect to the Tb133107 IF. Table 19 also indicates that DC experiences the least in common with the other three regions.

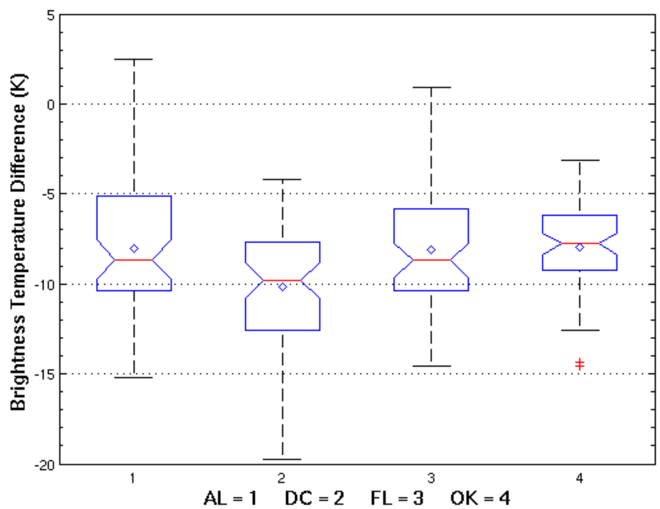

Figure 31. Same as Figure 27, except for Tb133107 difference IF.

Note the significant difference between DC and the other regions at least once during the half-hour before LI. One possible reason higher absolute Tb133107 values are seen for DC might be because DC is the most urban of all four regions and may have higher carbon dioxide levels. Increased carbon dioxide

would decrease the GOES-12 retrieved 13.3-μm radiance. Overall though, the Tb133107 IF performs well across a broad geographical area.

Table 19. Same as Table 15, except for Tb133107 difference IF.

Interest Field	**133-107**			
Time	**LI-30**	**LI-15**	**LI-0**	***YIELD***
AL vs. DC	YES	YES	NO	*YES*
AL vs. FL	NO	NO	NO	***NO***
AL vs. OK	YES	NO	NO	***NO***
DC vs. FL	NO	YES	NO	***NO***
DC vs. OK	NO	YES	NO	***NO***
FL vs. OK	NO	NO	NO	***NO***

5. Tb133107 Trend

Figure 32 and Table 20 indicate good general agreement between the four regions' Tb133107 trend comparisons. Surprisingly, DC falls back in line after being significantly different from the other three regions in the Tb133107 IF. Instead, OK once again compares somewhat poorly with the other regions, particularly AL. Like before, the only likely explanation is the effect severe storm cases might have on the OK region. All in all though, the Tb133107 trend appears useful across a large area.

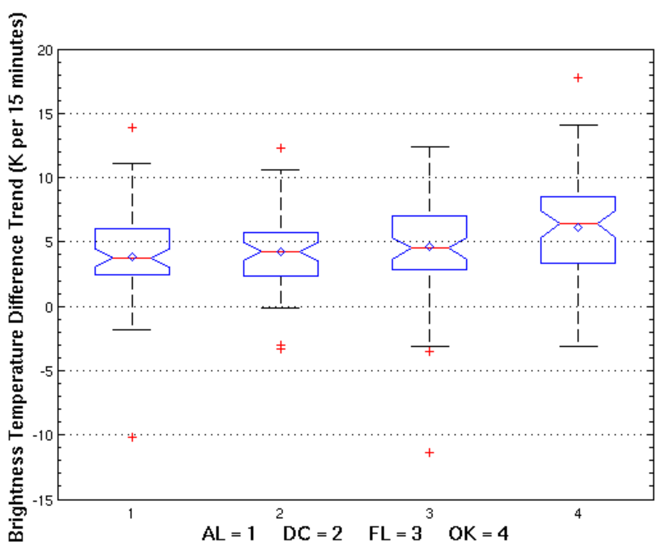

Figure 32. Same as Figure 27, except for Tb133107 trend IF.

Table 20. Same as Table 15, except for Tb133107 trend IF.

Interest Field	**133-107_trend**			
Time	**LI-30**	**LI-15**	**LI-0**	***YIELD***
AL vs. DC	NO	NO	NO	***NO***
AL vs. FL	YES	NO	NO	***NO***
AL vs. OK	YES	YES	YES	*YES*
DC vs. FL	NO	NO	NO	***NO***
DC vs. OK	NO	NO	YES	***NO***
FL vs. OK	NO	NO	YES	***NO***

6. Tb39107 and ref39

The Tb39107 and ref39 IFs display strikingly similar characteristics in Figures 33 and 34, and most likely due to changes in the 3.9-µm reflectance component. Note how AL and FL match closely to each other and DC and OK match closely to each other. This pattern repeats for the LI-30 and LI-0 timeframes as well.

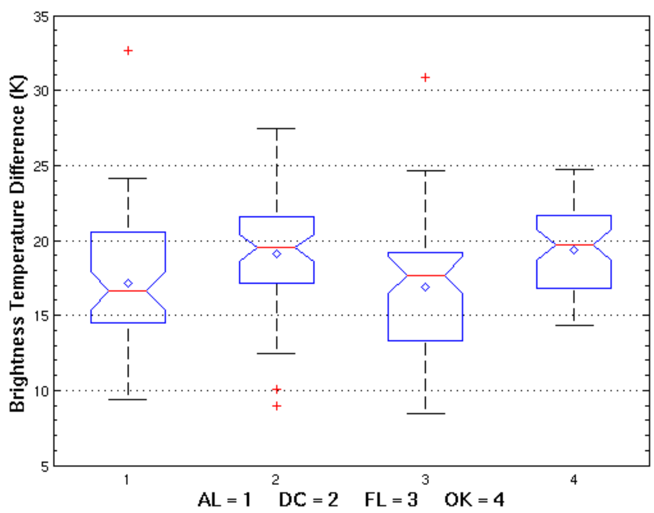

Figure 33. Same as Figure 27, except for Tb39107 difference IF.

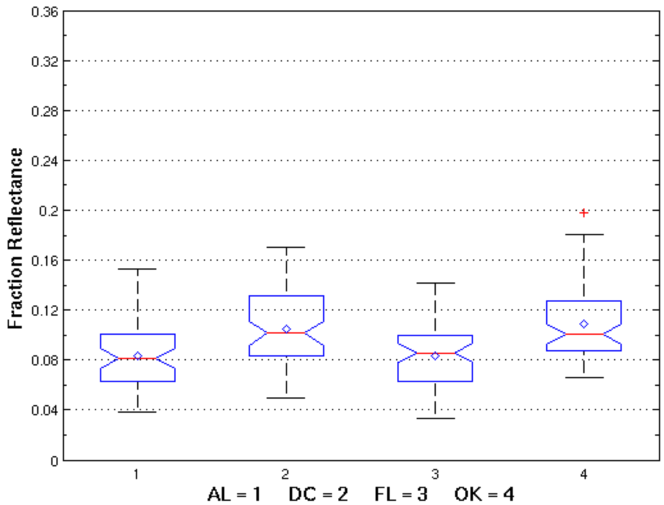

Figure 34. Same as Figure 27, except for ref39 IF.

Tables 21 and 22 validate the notch-overlap tests discussed above. The only consistently similar regions are the AL-FL combination and OK-DC combination. The most likely reason for this similarity has to do with GOES-12's viewing angle, which is discussed further in Sub-section 9 below. Of the fields discussed thus far, the Tb39107 and ref39 fields perform the poorest across broad geographical boundaries.

Table 21. Same as Table 15, except for Tb39107 difference IF.

Interest Field	**39-107**			
Time	**LI-30**	**LI-15**	**LI-0**	***YIELD***
AL vs. DC	YES	YES	NO	*YES*
AL vs. FL	NO	NO	NO	***NO***
AL vs. OK	YES	YES	NO	*YES*
DC vs. FL	YES	YES	NO	*YES*
DC vs. OK	NO	NO	NO	***NO***
FL vs. OK	YES	YES	NO	*YES*

Table 22. Same as Table 15, except for ref39 IF.

Interest Field	**ref39**			
Time	**LI-30**	**LI-15**	**LI-0**	***YIELD***
AL vs. DC	YES	YES	NO	*YES*
AL vs. FL	NO	NO	YES	***NO***
AL vs. OK	YES	YES	YES	*YES*
DC vs. FL	YES	YES	YES	*YES*
DC vs. OK	NO	NO	NO	***NO***
FL vs. OK	YES	YES	YES	*YES*

7. Tb39107 Trend

All four regions indicate clear Tb39107 trend notch-overlap in Figure 35. Of all the IFs discussed so far, the Tb39107 trend seems to show the best broad geographical agreement. Note in Table 23 the lack of a single “YES,” which indicates statistical similarity between all regions.

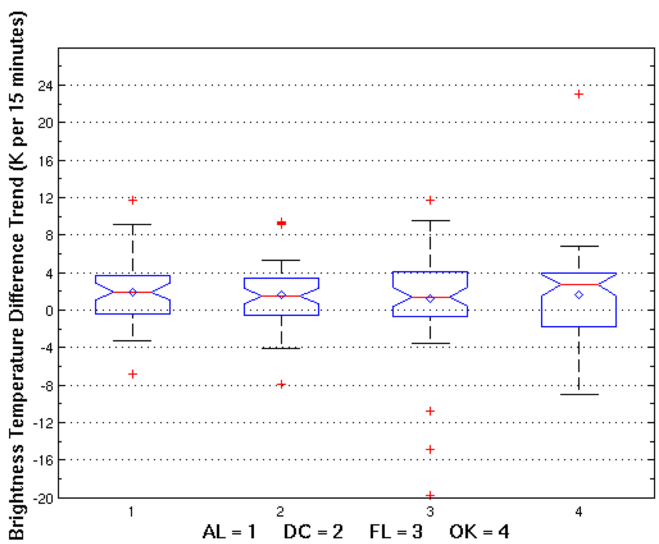

Figure 35. Same as Figure 27, except for Tb39107 trend IF.

Table 23. Same as Table 15, except for Tb39107 trend IF.

Interest Field	**39-107_trend**			
Time	**LI-30**	**LI-15**	**LI-0**	***YIELD***
AL vs. DC	NO	NO	NO	***NO***
AL vs. FL	NO	NO	NO	***NO***
AL vs. OK	NO	NO	NO	***NO***
DC vs. FL	NO	NO	NO	***NO***
DC vs. OK	NO	NO	NO	***NO***
FL vs. OK	NO	NO	NO	***NO***

8. ref39 Trend

Like all previous trends, the ref39 trend in Figure 36 shows good general agreement between AL, DC and FL. Once again, OK is the only outlier. OK most consistently indicates stronger ref39 trend tendencies in the last half-hour before LI, which may be another indication that the stronger convection might be skewing the data.

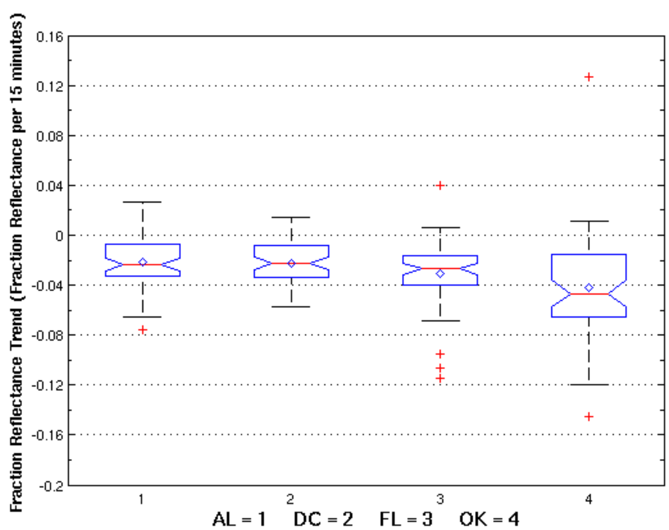

Figure 36. Same as Figure 27, except for ref39 trend IF.

Another possible reason for the stronger OK ref39 trends is that OK's 3.9-μm reflectance is almost always higher than the other three regions, particularly in the early storm development stages. OK's ref39 trend would have to be stronger to reach complete glaciation (i.e., ref39$\leq$0.05) and full lightning potential in the

minutes leading up to LI. Overall, the ref39 trend performs well across a broad geographical region.

Table 24. Same as Table 15, except for ref39 trend IF.

Interest Field	**ref39_Trend**			
Time	**LI-30**	**LI-15**	**LI-0**	***YIELD***
AL vs. DC	NO	NO	YES	***NO***
AL vs. FL	NO	YES	NO	***NO***
AL vs. OK	YES	YES	YES	*YES*
DC vs. FL	NO	NO	NO	***NO***
DC vs. OK	NO	YES	NO	***NO***
FL vs. OK	NO	NO	NO	***NO***

9. Regional Comparison Analysis

Overall, eight out of the ten IFs compared favorably well across broad geographical boundaries. This indicates that most IFs can be applied over a large area, and it also indicates that AL, DC, OK and FL have somewhat similar thunderstorm development as identified by GOES-12 IR properties. These results match closely with the summertime thunderstorm-induced rainfall study conducted by Easterling (1989). The Tb39107 and ref39 IFs showed the weakest regional comparison of the ten IFs.

Most of the IFs indicate OK and DC are similar and AL and FL are very similar. Geographically speaking, it makes sense for AL and FL to match most of the time. The similar IR satellite retrievals imply the two regions have similar thunderstorm development tendencies. Indeed, AL and FL see abundant moisture availability and summertime instability for thunderstorm occurrence. It makes less sense for OK and DC to have similar thunderstorm tendencies as is suggested by the results above. One possible reason is that this study included about 20 fewer OK and DC cases versus AL and FL. The OK-DC similarity was most apparent when the 3.9-μm channel was part of the IF. Therefore, a more likely explanation is that OK and DC are at GOES-12's edge of scan, the former at the westernmost edge of scan and the latter at a higher latitude edge of scan. Since the satellite looks at OK and DC at a more oblique angle than AL and FL,

the satellite-received radiance—especially reflectance measurements—may be skewed. Also, OK's data may be slightly biased due to a few additional stronger convection cases.

As mentioned, most of the IFs behave well across a broad geographical area. However, some fields that exhibit good predictive capability within each respective region may not be applied to large geographical areas without some additional false alarms or missed forecasts. For instance, the Tb39107 difference IF appears to perform well within each region in the half-hour prior to LI as indicated by the predictive capability results in the previous section. As hinted at earlier though, a Tb39107 threshold may not perform well when applied to a larger geographical region as indicated by the poor Tb39107 results in the regional comparison. To formally conclude that the regions have the same storm qualities, more study is needed that incorporates storm environment data (i.e., stability indices, lapse rates, available moisture, etc.) with our results.

E. OPTIMIZING GOES CLOUD-TOP PROPERTIES

Applying thresholds to large geographical regions may cause some storms to go either undetected or detected too late when lightning is imminent within minutes. However, some IF thresholds—like the Tb107 IF discussed in the regional comparison—may allow more advance warning for AL and yet possibly higher FARs due to less restrictive thresholds than is normal for that region. As seen in the boxplots above, one size, or in our case, one threshold certainly does not fit all storms. One possible option besides using concrete IF thresholds is to provide a probabilistic estimate of imminent lightning that considers a continuum of possible storms like the ones collected for this study. The lightning probability could combine storm data from many geographical regions, or small geographical regions could use their own tailored probabilistic lightning estimate based on their individual storm distribution. The latter option is briefly explored below. Due to limited time, the following exercise was run only

for the AL region. The primary goal was to find the likelihood of lightning at each satellite time, given a set of GOES-12 satellite readings (i.e., Tb107, Tb39, etc.).

1. Lightning Probability Methodology

Like the regional comparison conducted in the previous section, we focused the lightning probability exercise on the 30 minutes prior to LI (i.e., LI-30, LI-15 and LI-0). For each IF, all three time-increment distributions were combined into one large distribution. This yielded 10 IF distributions, each containing 174 data points (i.e., 58 AL cases multiplied by three time distributions yields 174). Thus, the 10 IF distributions describe the lightning-producing storm characteristics in the final half-hour before lightning. Like the boxplot used in previous sections, it is also possible to display a distribution as a probability density function (PDF), or Gaussian bell curve. The PDF, though, only describes the probability of occurrence at a single point. Knowing that the probability of lightning is 0.0035% when the instantaneous Tb107 satellite reading is 273 K is not useful. To obtain the total probability, the area under the PDF curve must be calculated. For instance, integrating the PDF from the median to the furthest outlier yields a total probability of 50%. PDF integration gives us a more useful curve that describes total probability, the cumulative density function (CDF). By using a CDF, we can hypothetically identify the total probability of lightning in the next 30 minutes given a GOES-12 reading. The 273 K Tb107 example now yields a more useful 40% probability of lightning for instance.

Since analytic integration of a PDF to yield a CDF is practically impossible, we used numerical approximations to obtain CDFs that describe the 10 IF distributions (Wilks 2006). Matlab's distribution fit tool (i.e., *dfittool* command) and curve fit tool (i.e., *cftool* command) were used to obtain CDFs for each IF. Figure 37 depicts the results of applying Matlab's non-parametric fits to one of our IF's distributions. Results for the other IFs looked very similar. The distribution fit tool yielded new coordinates, [x, F(x)], for each CDF. The x-coordinates represent the interpolated Tb107 values—as in Figure 37—and the

F(x) coordinates represent the cumulative probabilities at each respective Tb107 value. The coordinates were interpolated from the minimum to the maximum data point over 1000 increments. We list the maximum, minimum and increment values used to calculate each IF distribution in Appendix C. All [x,F(x)] coordinates form the complete CDF curve represented by the thicker blue non-parametric distribution fit curve in Figure 37.

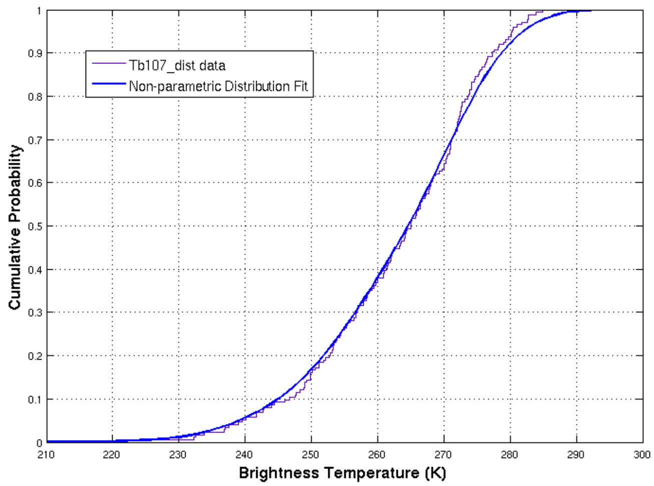

Figure 37. Non-parametric cumulative distribution function fit to Tb107 data—represented by the stair-step distribution—as performed using Matlab's distribution fit tool.

Next, the new CDF coordinates were plugged into Matlab's curve fit tool to obtain an actual equation for the CDF for further analysis. Matlab has a series of curve fit options to choose from. CDF equations for each IF were approximated using a Fourier series with the following generic form:

$$\begin{aligned} f(x) &= a_0 + a_1\cos(x*w) + b_1\sin(x*w) + a_2\cos(2*x*w) + b_2\sin(2*x*w) + \ldots \\ &\ldots + a_n\cos(n*x*w) + b_n\sin(n*x*w) \end{aligned} \quad . \quad (8)$$

The Fourier series is a linear combination of sine and cosine functions that fit a given curve based on each term's coefficients (i.e., a_n and b_n), weighting values, w, and input values, x. Increasing the number of linear combinations, n, increases the goodness of fit as measured by its R-square value. These Fourier series consist of six or eight linear combinations for each IF (i.e., n = 6 or 8). All curves had R-square values of at least 0.9997, where the best-fit curve is an

R-square value equal to one. The full list of coefficient values and goodness of fit statistics for each IF can be found in Appendix C. Figure 38 shows the results of the Fourier series curve fit analysis for the Tb107 IF. All other IF curve fits appear to be similar. Using the distribution and curve fit tool provided 10 sets of CDF equations and coefficients to analyze lightning probability for a few AL storms. For some fields like the Tb107 IF, probabilities were converted to 100-complement probabilities. Doing so makes more sense for colder cloud tops to exhibit higher lightning probability than warmer cloud tops. Thus for a Tb107 value of 253 K in Figure 38, instead of a 20% chance of lightning, the 100-complement probability of 80% was used.

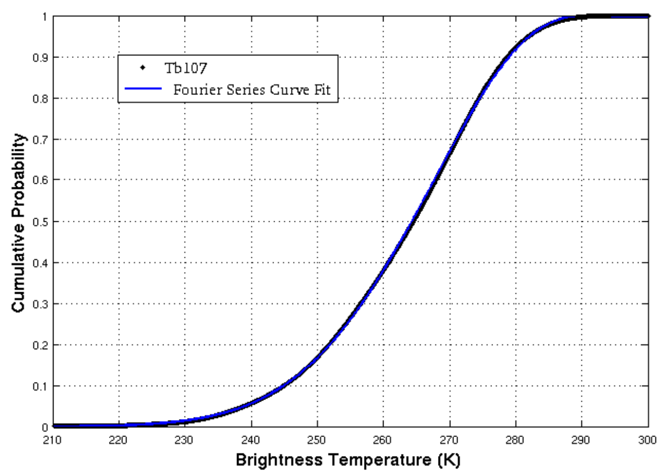

Figure 38. Tb107 data—as interpolated using the distribution fit tool—are plotted as black dots. Matlab's curve fit tool was used to fit the Tb107 data to Fourier series equation with eight linear sine/cosine combinations.

2. Lightning Probability Results

Since time was limited, the lightning probability analysis was restricted to six different AL storms: three lightning-producing (L-P) storms and three non-lightning-producing (N-L-P) storms. The three L-P storms were part of the 58 AL cases studied earlier. L-P Case 1 occurred 2 June 2009, and L-P Cases 2 and 3 occurred 19 August 2009. To minimize bias, we also chose N-L-P storms that occurred on 2 June and 19 August 2009. We assume the N-L-P storms did not in fact produce lightning since surrounding storms exhibited NALMA-sensed lightning.

With lightning nowcast optimization in mind, we chose to evaluate 30-minute probabilities based on the IFs in this study. Tables 25-27 show the probabilities of lightning in the next 30 minutes based on each IF for the three L-P cases. The first column is at least 60 minutes prior to LI and represents the actual satellite time with respect to LI-0. The last column represents the 10 LI IF probabilities at or just after the first lightning strike. After reviewing all L-P and N-L-P cases, we decided to highlight the 40-50% probabilities as probable lightning producers. Likely lightning producers were identified as those containing lightning probabilities greater than 50% and highlighted in red. While significant conclusions cannot be extracted from just three cases, we can certainly make some realistic observations for further study based on the results.

The most prevalent common thread between the three L-P cases can be seen with the trend IFs. The trend IFs, particularly the Tb39107 trend, consistently provide the first awareness of increased lightning potential. At least four of the five trend IFs show enhanced lightning potential within and sometimes just beyond the 30 minutes before lightning. While the Tb39107 trend stands out as a potential early lightning indicator, recall from earlier in Chapter III that the Tb39017 trend IF demonstrated relatively weak predictive capability for the other regions besides AL. In addition, the elevated Tb65107 and Tb133107 trend probabilities appear to contradict the relatively weak overall predictive capability results as noted in Chapter III. However, recall that the AL region showed the most promising 15 to 30-minute predictive capability of all four regions using these IFs. Also, the three L-P storms that were chosen may be some of the better performing cells with respect to the Tb65107 and Tb133107 trend fields. These two possible reasons may explain the apparent contradiction. As expected, the number of probable and likely lightning IF indicators increases closer to LI, particularly within the 30 minutes before LI. At least seven of ten IFs indicate probable lightning within the next 30 minutes by about LI-15.

Table 25. Thirty-minute lightning probability estimate for 10 GOES-12 LI IFs for lightning-producing storm Case 1, which occurred on 2 June 2009 over AL. The table is broken into satellite time columns with respect to the first lightning strike. LI-76 represents 76 minutes before LI and LI+1 represents one minute after LI. Probabilities between 40% and 50% are yellow; probabilities greater than 50% are red. The average lightning probability of all 10 IFs is calculated at the bottom of each satellite increment. For example, the average probability of lightning in the next 30 minutes at LI-46 is 12.2%.

LTG Case 1	***PROBABILITY AT GIVEN TIME BEFORE LIGHTNING***				
	LI-76	***LI-46***	***LI-29***	***LI-16***	***LI+1***
Tb107	0.0%	0.2%	4.4%	24.3%	67.7%
Tb107 Trend	2.6%	12.7%	48.0%	68.4%	80.1%
Tb65107	30.0%	2.3%	15.4%	43.0%	65.5%
Tb133107	5.0%	2.4%	9.7%	33.8%	52.2%
Tb65107 Trend	0.0%	12.7%	61.9%	83.0%	36.5%
Tb133107 Trend	9.1%	22.6%	77.3%	66.1%	33.6%
Tb39107	0.0%	5.2%	48.4%	59.0%	82.9%
Tb39107 Trend	27.1%	56.9%	89.6%	46.0%	70.7%
ref39	9.3%	2.3%	0.0%	15.7%	50.5%
ref39 Trend	13.8%	4.6%	2.3%	97.9%	78.1%
AVERAGE PROB	*6.7%*	*12.2%*	*35.7%*	*53.7%*	*61.8%*

Table 26. Same as Table 25 except for lightning-producing storm Case 2, which occurred on 19 August 2009 over AL.

LTG Case 2	***PROBABILITY AT GIVEN TIME BEFORE LIGHTNING***				
	LI-77	***LI-47***	***LI-30***	***LI-17***	***LI-0***
Tb107	0.6%	24.3%	45.4%	61.7%	65.1%
Tb107 Trend	7.9%	51.7%	36.5%	42.7%	5.9%
Tb65107	0.0%	14.3%	35.6%	57.6%	58.4%
Tb133107	3.6%	8.0%	27.1%	46.1%	66.9%
Tb65107 Trend	5.5%	67.4%	50.1%	53.8%	0.6%
Tb133107 Trend	18.7%	53.2%	44.5%	45.8%	40.9%
Tb39107	5.2%	57.8%	45.6%	49.8%	20.7%
Tb39107 Trend	46.0%	75.0%	13.5%	34.2%	2.5%
ref39	0.8%	6.4%	42.9%	64.3%	84.7%
ref39 Trend	25.1%	30.5%	90.5%	56.0%	43.9%
AVERAGE PROB	*11.3%*	*38.9%*	*43.2%*	*51.2%*	*39.0%*

Table 27. Same as Table 25 except for lightning-producing storm Case 3, which occurred on 19 August 2009 over AL.

LTG Case 3	***PROBABILITY AT GIVEN TIME BEFORE LIGHTNING***					
	LI-81	***LI-51***	***LI-34***	***LI-21***	***LI-4***	***LI+9***
Tb107	2.8%	31.0%	38.4%	61.7%	83.1%	65.1%
Tb107 Trend	2.6%	41.1%	9.6%	61.7%	57.2%	5.9%
Tb65107	0.5%	18.0%	24.1%	52.7%	86.5%	58.4%
Tb133107	1.9%	14.3%	15.7%	25.3%	58.6%	66.9%
Tb65107 Trend	0.0%	55.0%	8.0%	77.7%	71.4%	0.6%
Tb133107 Trend	9.1%	45.8%	11.2%	27.9%	61.6%	40.9%
Tb39107	31.9%	58.4%	62.2%	75.5%	42.9%	20.7%
Tb39107 Trend	27.1%	48.2%	32.1%	57.9%	0.8%	2.5%
ref39	0.0%	10.5%	20.0%	43.2%	91.3%	84.7%
ref39 Trend	13.8%	71.9%	35.9%	70.0%	88.1%	43.9%
AVERAGE PROB	*9.0%*	*39.4%*	*25.7%*	*55.4%*	*64.1%*	*39.0%*

In general, the average lightning probability increases closer to LI as well. Storm fluctuations—such as the drop in 30-minute lightning probabilities for Case 3 at LI-34—present challenges for this type of lightning product. The 30-minute lightning appears useful, but the L-P results should be compared with storms that did *not* produce lightning.

The 30-minute lightning probability estimates for the three N-L-P storm cases are shown in Tables 28-30. The N-L-P storms were tracked in the same manner as the L-P storms. Since no lightning reference point existed for the N-L-P storms, we tracked the storm from pre-cumulus stage—the first time column—until the cell began to dissipate—the last column. Like the L-P storms, the trend IFs exhibit the most promising response for potential lightning, particularly in Case 3. All five trend IFs for Case 3 show likely lightning. If we only looked at trend IFs as a potential lightning indicator, Case 3 would falsely be flagged for lightning. The other two N-L-P cases do not show any more than three of five trend IFs indicating probable lightning.

Table 28. Thirty-minute lightning probability estimate for 10 GOES-12 LI IFs for *non*-lightning-producing storm Case 1, which occurred on 2 June 2009 over AL. Since lightning was not observed for this storm, the table is broken into satellite time columns that represent the duration of the storm. Probabilities between 40% and 50% are yellow; probabilities greater than 50% are red. The average lightning probability of all 10 IFs is calculated at the bottom of each satellite increment. Times are in UTC.

NO LTG Case 1	PROBABILITY AT GIVEN TIME					
	17:45	*18:15*	*18:45*	*19:02*	*19:15*	*19:32*
Tb107	0.0%	0.4%	4.4%	11.4%	26.1%	11.9%
Tb107 Trend	2.6%	15.0%	19.4%	20.1%	39.6%	0.3%
Tb65107	0.2%	2.7%	17.4%	30.2%	48.2%	30.5%
Tb133107	0.0%	2.6%	4.2%	17.2%	31.9%	7.7%
Tb65107 Trend	0.0%	20.3%	29.2%	23.5%	43.9%	0.0%
Tb133107 Trend	9.1%	29.0%	36.0%	42.1%	38.4%	0.3%
Tb39107	4.3%	21.2%	32.5%	42.9%	62.2%	35.9%
Tb39107 Trend	27.1%	50.4%	36.3%	40.6%	62.1%	4.0%
ref39	6.1%	0.0%	11.9%	17.3%	20.2%	18.8%
ref39 Trend	13.8%	3.5%	45.5%	25.5%	20.4%	11.8%
AVERAGE PROB	*6.3%*	*14.5%*	*23.7%*	*27.1%*	*39.3%*	*12.1%*

Table 29. Same as Table 28 except for *non*-lightning-producing storm Case 2, which occurred on 19 August 2009 over AL.

NO LTG Case 2	PROBABILITY AT GIVEN TIME							
	15:15	*15:32*	*15:45*	*16:02*	*16:15*	*16:32*	*16:45*	*17:02*
Tb107	1.3%	6.2%	10.0%	11.6%	25.8%	26.1%	41.5%	33.5%
Tb107 Trend	2.6%	28.7%	12.7%	4.3%	37.2%	2.8%	34.1%	0.2%
Tb65107	1.7%	9.2%	13.6%	14.6%	32.8%	33.2%	47.4%	40.5%
Tb133107	1.7%	4.0%	9.0%	13.8%	34.4%	28.9%	52.8%	25.3%
Tb65107 Trend	0.0%	43.9%	11.8%	1.3%	58.5%	0.3%	29.2%	0.0%
Tb133107 Trend	9.1%	33.6%	29.0%	17.8%	54.4%	4.8%	56.8%	0.1%
Tb39107	11.0%	19.6%	25.4%	66.3%	71.7%	42.9%	62.2%	64.5%
Tb39107 Trend	27.1%	43.9%	39.5%	81.0%	39.5%	2.0%	62.1%	31.1%
ref39	2.6%	11.9%	17.2%	1.0%	9.7%	32.5%	37.2%	26.9%
ref39 Trend	13.8%	50.9%	29.4%	1.1%	72.8%	65.7%	22.2%	4.5%
AVERAGE PROB	*7.1%*	*25.2%*	*19.8%*	*21.3%*	*43.7%*	*23.9%*	*44.6%*	*22.7%*

Table 30. Same as Table 28 except for *non*-lightning-producing storm Case 3, which occurred on 19 August 2009 over AL.

NO LTG Case 3	PROBABILITY AT GIVEN TIME						
	15:15	15:32	15:45	16:02	16:15	16:32	16:45
Tb107	0.4%	1.0%	12.3%	27.9%	26.4%	40.9%	28.5%
Tb107 Trend	2.6%	10.6%	71.8%	28.7%	1.5%	21.4%	0.2%
Tb65107	0.8%	2.3%	22.1%	42.6%	42.2%	56.7%	40.5%
Tb133107	2.2%	1.7%	21.4%	38.1%	34.4%	52.2%	35.0%
Tb65107 Trend	0.0%	12.7%	93.2%	40.2%	0.0%	18.3%	0.0%
Tb133107 Trend	9.1%	25.7%	90.7%	32.5%	5.2%	33.6%	0.0%
Tb39107	6.8%	14.5%	35.9%	13.5%	21.2%	15.4%	6.3%
Tb39107 Trend	27.1%	46.0%	70.7%	4.0%	45.0%	18.1%	6.5%
ref39	0.7%	1.5%	13.2%	57.2%	48.5%	71.6%	71.2%
ref39 Trend	13.8%	20.1%	79.0%	90.4%	5.0%	46.9%	13.2%
AVERAGE PROB	*6.4%*	*13.6%*	*51.0%*	*37.5%*	*22.9%*	*37.5%*	*20.1%*

Generally speaking, the number of LI indicators is fewer, and the average lightning probabilities are less for the N-L-P storms. The N-L-P cases show no more than six probable IF lightning indicators at any given time. Overall, the 30-minute lightning probability estimate is able to delineate between L-P and N-L-P storms reasonably well. A more thorough study that incorporates many more L-P and N-L-P storms is certainly recommended.

THIS PAGE INTENTIONALLY LEFT BLANK

IV. CONCLUSIONS AND RECOMMENDATIONS

A. CONCLUSIONS

This study looked at the behavior of convective cloud-top properties in the hour preceding a storm's first remotely sensed lightning strike. We visually analyzed GOES-12 imagery—both VIS and IR—to first build a set of potential storm days over four geographical regions. After careful analysis, 172 total storms—58 AL, 32 DC, 51 FL and 31 OK—were identified for further study. 4-D lightning—as identified by LMA and 4DLSS arrays—and CG lightning—as identified by the NLDN—provided precise lightning initiation points for each storm in both time and space. After noting the LI time, we collected satellite measurements from the four GOES-12 IR channels for the hour prior to LI and the half-hour after LI.

Ten GOES-12 LI IFs were identified using previous studies and analyzed for each storm. The IFs—Tb107, Tb107 trend, Tb65107, Tb133107, Tb165107 trend, Tb133107 trend, Tb39107, Tb39107 trend, ref39 and ref39 trend—represent various channel differencing and 15-minute time trend techniques. Individual storm results were similar to that found in MB06 and Siewert (2008). Generally, each storm exhibited a notable drop in Tb107 and stronger CTT cooling rates as identified by the Tb107 trend. The Tb65107 and Tb133107 difference fields increased steadily as LI became imminent. The Tb65107 trend and Tb133107 trend IFs were positive and generally increased steadily as well. The Tb39107 difference generally increased as well. The Tb39107 trend for many individual storms often increased, then decreased slightly, then increased again leading up to LI. Siewert (2008) noted a similar trend. The ref39 IF decreases as LI nears due to lower reflectance of increased ice in the storm. The ref39 trend was most often negative in the last half-hour before LI. The most noteworthy tendencies for all ten fields often took place in the 15 to 30 minutes prior to LI. Figure 39 shows the basic conceptual model of how the ten LI IFs change during the hour preceding the first lightning strike.

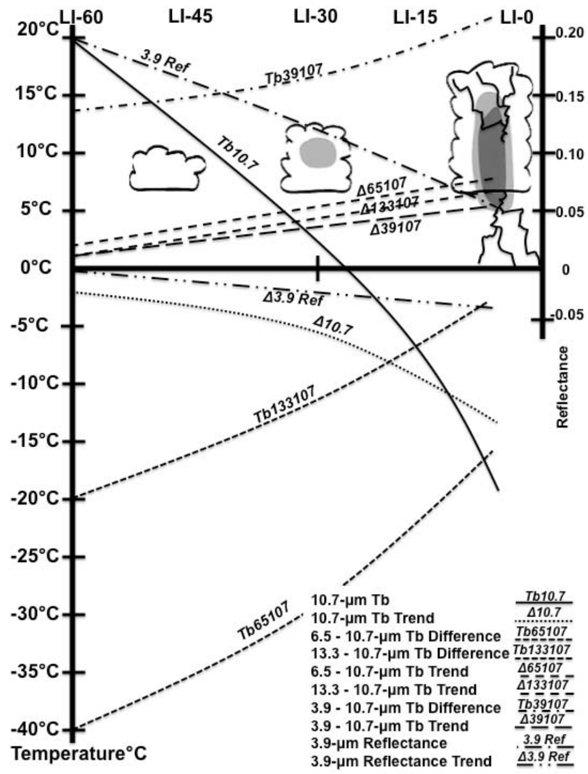

Figure 39. Conceptual model of LI IF behavior in the hour preceding first lightning, adapted from MB06. Typically, no cloud exists at LI-60. Cumuli begin to appear by LI-45, and precipitation—the gray shading—often forms within the cloud once the CTT reaches about 273 K. Lightning initiates at LI-0. 15-minute trend IFs are indicated by Δ.

After the individual cases were analyzed, we looked at each region's combined storm data to determine the predictive capability of each IF. Five time increments were used to compare IF characteristics. We linearly interpolated between satellite data points to parse data into LI-60, LI-45, LI-30, LI-15 and LI-0 distributions with LI-0 being the time of first lightning strike. To demonstrate predictive capability, each IF's LI-15 distribution had to be uniquely different than its LI-0 distribution. In addition, the extent of predictive capability—with regard to increasing time before LI—indicated how much time before LI each IF may be predictive in nature. Notched-boxplots and two-sample t-test hypothesis tests were used to show predictive capability for each field. Overall, eight out of the ten IFs demonstrated at least some predictive capability for most regions. The Tb39107 trend and ref39 trend showed the weakest predictive capability results

of the ten fields. Although individual storms exhibited similar tendencies, occasionally such tendencies occurred at different times during each storm's development. This is one possible reason why the Tb39107 and ref39 trends did not perform well in the predictive capability test. Additionally, most fields predict lightning 15 to 45 minutes before LI with an average lead time of about 35 minutes for all regions' storms. Therefore, the remainder of the study was focused on the 30 minutes prior to LI. Similar to MB06 and Siewert (2008), we picked out 15 to 30-minute LI IF thresholds that were common among most storms. Further study is recommended before these IF thresholds are used operationally.

When comparing the regional dependence of each IF, eight out of ten IFs performed well. Therefore, we concluded that most IFs can be applied over a large geographical area with minimal forecast busts or false alarms. The Tb39107 and ref39 field performed weakest of the ten fields during the regional comparison. AL and FL compared very well as expected; however, DC and OK were common outliers from the other two regions, and oftentimes they compared favorably well only with each other. Each of these regions had fewer cases than AL and FL, but more importantly each reside at GOES-12's edge of scan. Thus view angle may be skewing some of the results for OK and DC. This may only be an issue with the reflectance portion of the 3.9-μm channel. Another interesting note is that although some fields may exhibit good predictive capability within each respective region—such as the Tb39107 difference IF—a threshold for those fields may not be applied to a large geographical region without some additional false alarms or missed forecasts. All in all though, most IFs showed both good predictive capability and favorable regional compatibility for operational LI nowcast use.

Finally, we briefly explored a proposed lightning probability estimate product as one example of how this research might be optimized for forecast operations. The final three time distributions of AL data—LI-30, LI-15 and LI-0—were combined into one distribution for each IF. We used numeric approximation

tools built into Matlab to then approximate a CDF equation for each IF. The CDF equations were next applied to a limited sample of six storms—three L-P storms and three N-L-P storms—to find any common patterns. The proposed 30-minute lightning probability estimate performed reasonably well as a trial product. It appears that the product identified lightning-producing storms and more or less eliminated non-lightning-producing storms. The trend IFs, the number of probable IF lightning indicators, and to a lesser extent the average IF probability were three important delineators between L-P and N-L-P storms. Much more work and study are necessary before any such product is incorporated into operations; however, the lightning estimate product is just one avenue of further applied research.

B. RECOMMENDATIONS AND FUTURE RESEARCH

Lightning is a hazard to both operational agencies—like the DoD, NASA and FAA—and personnel. Having the tools to accurately predict the initiation of lightning, particularly in the 0–1 hour timeframe, is vital to operations and personnel safety. Last year, the USAF's Operational Weather Squadrons performed fairly well in forecasting lightning. Air Force Weather issued accurate lightning watches—which normally require at least 30 minutes of advanced warning—78.4% of the time. Additionally, Air Force Weather missed 6.7% lightning events and experienced a 53.2% FAR. Tools like the lightning probability estimate product discussed at the end of Chapter III have the capability of reducing the FAR and thus reducing the negative impact on delaying or halting important training and operational missions. Additionally, such tools can also significantly mitigate the number of missed lightning forecasts.

Further development and evaluation of tools like the lightning probability estimate product is certainly one area of future recommended research. The Applied Meteorological Unit at the 45WS in FL and FAA's CIWS are two excellent avenues for our results to be studied and applied. Forecast optimization techniques—like the lightning probability estimate and the Satellite

Convective Analysis and Tracking (SATCAST) algorithm created at the University of Alabama-Huntsville—will rely heavily on being able to tag and track individual developing storms using either atmospheric motion vectors or objective tracking techniques.

Another first step toward future LI research is to build a statistically significant database of independent non-lightning producing convection for more direct comparison and potential determination of either concrete LI IF thresholds or a more solid set of IF CDFs for a probabilistic outlook. A discriminant analysis on both L-P and N-L-P could then be performed to determine precisely which IFs are most useful in nowcasting lightning. Additionally, a more thorough comparison of the storm environment in conjunction with IF behavior is needed. For instance, the OK distribution may have been affected by a few stronger storms. Environmental parameters such as Convective Available Potential Energy, Convective Inhibition, freezing level, and 500-mb Omega or other indicators identified by Williams et al. (2005) may well provide more beneficial information as a part of the LI IF discriminant analysis. High temporal and spatial resolution model data like the High Resolution Rapid Refresh model is a perfect conduit for this recommended work. Since this study was limited to summertime convection, future study is recommended to interseasonally compare IF behavior to see if IFs change significantly from one season to the next. We also recommend future research to connect the lightning flash-growth rate to Tb107 cloud-top cooling trends and other IF trends to try and nowcast storm severity.

Case studies in varying geographical regions are also recommended. For instance, the MSG satellite data in Europe could be used in conjunction with Blitz Informations Dienst von Siemens (BLIDS) CG lightning data for a comparison similar to the one used in this study. MSG has the advent of more IR channels to analyze, and while BLIDS detects mainly CG strikes, the average time between IC and CG strikes could be used in place of requiring 4-D lightning data. The proposed work can build on the MSG CI work conducted by Siewert et al. (2010). Finally, some of the cases in this study—particularly at CCAFS/KSC—had higher

temporal resolution satellite imagery. Further study is recommended to see what additional IF behavior information can be identified on shorter time scales, especially as the satellite community approaches the launch of GOES-R in 2015. Shorter time intervals between satellite scans may also decrease the inherent analysis error caused by non-linear storm development. GOES-R will provide higher temporal and spatial resolution that will help overcome the pixel inhomogeneity error—for instance when a small 1-km convective cloud experiences background contamination within the larger 4-km pixel—which we possibly have in this study. GOES-R will also likely improve LI nowcast optimization products like the proposed lightning probability estimate. LI research stands to aid GOES-R and the development of its Geostationary Lightning Mapper before it is launched and reap the benefits of the new satellite after its launch.

APPENDIX A. 4-D LIGHTNING DATA FORMATS

Table 31. Original 4DLSS data format.

JDAY	TIME(UTC)	X(M)	Y(M)	Z(M)	EVENT TYPE
153	17:00:47:411087	-0019889	-0069277	+06669	LDAR EVENT
153	17:00:47:416894	-0020316	-0068869	+06875	LDAR EVENT
153	17:00:47:418110	-0020373	-0068222	+04990	LDAR EVENT
153	17:00:47:430498	-0020994	-0068609	+06542	LDAR EVENT
153	17:00:47:434779	-0021416	-0071995	+07264	LDAR EVENT
153	17:00:48:937787	-0001300	-0001500	+00500	CAL EVENT
153	17:00:52:957771	-0001300	-0001500	+00500	CAL EVENT
153	17:00:54:182885	+0012417	-0119079	-01097	CGLSS EVENT
153	17:00:54:226570	+0014065	-0118618	-01091	CGLSS EVENT
153	17:00:54:243442	+0013908	-0119129	-01101	CGLSS EVENT
153	17:01:04:957892	-0001300	-0001500	+00500	CAL EVENT
153	17:01:08:957929	-0001300	-0001500	+00500	CAL EVENT

Table 32. 4DLSS converted to old LDAR Format.

Day	Hour	Min	Sec	Microsec	X(M)	Y(M)	Z(M)
2	17	0	47	318359	-18463	-66967	7106
2	17	0	47	321328	-18084	-67912	6931
2	17	0	47	322118	-18528	-61640	2398
2	17	0	47	325315	-19008	-66084	7166
2	17	0	47	325551	-18268	-68405	10070
2	17	0	47	326676	-18253	-67598	7334
2	17	0	47	327651	-18184	-67275	7266
2	17	0	47	329609	-18138	-68120	7556
2	17	0	47	331278	-18113	-67715	7366
2	17	0	47	335237	-18198	-67670	7898

Table 33. Final 4DLSS format used to analyze storms in McIDAS-V.

Year	Month	Day	Hour	Min	Sec	Latitude	Longitude	Alt (m)	Num Flash	Num Sources
2009	6	2	17	5	40.872	29.1	-81.268	9202	1971	43
2009	6	2	17	5	45.493	27.333	-80.604	9593	1972	7
2009	6	2	17	6	19.285	28.433	-80.921	9296	1974	154
2009	6	2	17	6	38.164	29.061	-81.238	11452	1976	66
2009	6	2	17	6	38.819	28.424	-80.915	7635	1977	86
2009	6	2	17	7	11.553	29.072	-81.244	9844	1978	49
2009	6	2	17	7	21.874	28.422	-80.916	8418	1979	120
2009	6	2	17	7	27.293	27.32	-80.597	10938	1980	4
2009	6	2	17	7	57.489	28.423	-80.914	7989	1981	133
2009	6	2	17	7	58.078	27.306	-80.596	13245	1982	4

Table 34. Original decimated LMA data format.

time (UT sec of day)	lat	lon	alt(m)	reduced chi^2	P(dBW)	mask
61201.85547	36.271479	-86.617409	4037.5	2.67	14.6	02f5
61201.85685	36.249189	-86.620898	5379.5	0.3	14.9	02d5
61201.86135	36.217382	-86.620618	6736.6	1.53	9.8	12d5
61201.99988	36.237293	-86.623992	5725.6	0.41	13.6	02d5
61202.00854	36.210919	-86.618764	6307.2	0.08	8.6	02d5
61202.11041	36.309568	-86.661755	3700.1	3.12	8.4	02d7
61204.90182	36.273583	-86.634705	14279.9	0.01	15.1	555
61204.9069	36.261285	-86.636049	18576.1	1.11	20.1	07d5
61204.9097	36.254606	-86.637543	12374.4	1.11	23.7	715
61204.94684	36.336072	-86.652044	26967.7	4.45	18.8	07c4

Table 35. LMA format after flash-grouping algorithm applied.

Source Num	Time (UT sec of day)	Lat	Lon	Alt (m)	Reduced chi^2	P (dBW)	Range	Sensors	Flash Num
1	61201.85547	36.27148	-86.61741	4037.5	2.67	14.6	171.7396	7	1
2	61201.85685	36.24919	-86.6209	5379.5	0.3	14.9	169.2613	6	1
3	61201.86135	36.21738	-86.62062	6736.6	1.53	9.8	165.7314	7	1
4	61201.99988	36.23729	-86.62399	5725.6	0.41	13.6	167.9376	6	1
5	61202.00854	36.21092	-86.61876	6307.2	0.08	8.6	165.0164	6	1
6	61202.11041	36.30957	-86.66175	3700.1	3.12	8.4	175.9553	7	1
7	61204.90182	36.27358	-86.6347	14279.9	0.01	15.1	171.9574	6	2
8	61204.9069	36.26129	-86.63605	18576.1	1.11	20.1	170.5917	8	2
9	61204.9097	36.25461	-86.63754	12374.4	1.11	23.7	169.8497	6	2
10	61204.94684	36.33607	-86.65204	26967.7	4.45	18.8	178.892	6	2

Table 36. Final LMA format used to analyze storms in McIDAS-V.

Year	Month	Day	Hour	Min	Sec	Latitude	Longitude	Alt (m)	Num Flash	Num Sources
2009	6	2	17	0	1.8555	36.271	-86.617	4037.5	1	6
2009	6	2	17	0	4.9018	36.274	-86.635	14280	2	12
2009	6	2	17	0	7.3909	35.752	-87.629	13861	3	101
2009	6	2	17	0	7.6831	36.294	-86.68	11089	5	6
2009	6	2	17	0	8.9486	35.435	-87.731	8483.8	6	51
2009	6	2	17	0	10.167	36.196	-86.596	11792	9	50
2009	6	2	17	0	13.097	36.288	-86.679	5763.2	11	4
2009	6	2	17	0	14.253	36.248	-86.633	14419	12	31
2009	6	2	17	0	15.869	36.237	-86.673	11990	13	19
2009	6	2	17	0	17.468	35.44	-87.726	7700.8	14	109

THIS PAGE INTENTIONALLY LEFT BLANK

APPENDIX B. GOES IR CLOUD-TOP STATISTICS

Table 37. Median, mean, interquartile range (IQR) and standard deviation (std dev) statistics are listed for each IF at five different times: first lightning (LI-0), 15 minutes before first lightning (LI-15), 30 minutes before first lightning (LI-30), 45 minutes before first lightning (LI-45) and 60 minutes before first lightning (LI-60). Statistics are also broken down by region: AL, FL, OK and DC. LI IF statistics continue on the next page.

Statistics: All Regions and Interest Fields		*Tb107*				*Tb107_trend*				*Tb65-107*			
		AL	**FL**	**OK**	**DC**	**AL**	**FL**	**OK**	**DC**	**AL**	**FL**	**OK**	**DC**
FIRST LTG	*median*	252.94	253.16	252.10	255.34	-13.37	-16.55	-14.95	-14.96	-17.80	-17.27	-14.21	-18.91
	mean	250.70	252.04	252.97	253.88	-14.15	-17.20	-14.55	-15.66	-17.25	-17.64	-15.48	-18.10
	iqr	13.99	11.06	7.63	10.64	7.64	9.84	9.22	8.72	6.19	4.89	4.47	6.06
	std dev	9.74	8.90	6.06	7.90	7.47	7.78	6.65	6.92	5.15	3.89	3.68	4.78
LTG-15min	*median*	266.41	269.28	267.30	268.22	-8.16	-8.46	-10.39	-7.24	-24.15	-25.87	-20.74	-26.12
	mean	264.88	268.07	266.73	268.43	-8.31	-9.25	-10.95	-7.82	-24.65	-26.19	-21.69	-26.21
	iqr	9.24	7.01	5.58	8.19	6.02	4.55	6.54	4.48	6.68	5.06	5.76	9.01
	std dev	7.38	7.80	4.95	5.59	4.38	4.12	5.42	4.53	5.39	4.79	4.90	5.54
LTG-30min	*median*	273.50	277.88	277.73	275.47	-5.05	-5.89	-7.62	-4.93	-31.42	-33.13	-29.91	-32.59
	mean	273.42	276.89	277.48	275.88	-5.02	-6.05	-8.02	-5.33	-30.87	-33.08	-30.00	-32.34
	iqr	7.20	5.72	7.92	7.78	3.32	4.56	5.41	4.45	7.86	6.68	11.68	11.49
	std dev	6.66	6.76	7.35	6.06	2.75	3.27	4.26	3.68	5.94	5.29	7.16	6.85
LTG-45min	*median*	279.01	283.01	285.52	281.94	-3.80	-2.94	-6.17	-3.89	-35.71	-38.88	-37.20	-37.41
	mean	278.72	282.69	285.52	280.84	-3.86	-3.44	-7.17	-4.24	-35.39	-38.15	-37.49	-37.09
	iqr	6.97	4.88	12.97	8.77	3.11	2.83	4.63	5.30	8.63	6.36	14.99	13.65
	std dev	6.50	4.91	8.74	6.20	2.68	2.45	5.07	3.04	6.20	4.77	9.02	7.41
LTG-60min	*median*	284.10	286.74	292.70	285.28	-2.80	-2.17	-2.61	-1.72	-39.75	-41.69	-42.84	-40.96
	mean	282.84	286.23	291.45	284.81	-2.82	-2.37	-3.60	-2.13	-38.87	-41.44	-43.16	-40.91
	iqr	9.13	5.70	14.20	6.96	2.41	2.24	4.87	2.32	7.27	5.40	13.79	10.44
	std dev	6.47	4.05	8.06	5.76	1.87	1.78	3.90	2.78	6.00	4.28	8.66	7.02

Statistics: All Regions and Interest Fields		*Tb133-107*				*Tb65-107_trend*				*Tb133-107_trend*			
		AL	**FL**	**OK**	**DC**	**AL**	**FL**	**OK**	**DC**	**AL**	**FL**	**OK**	**DC**
FIRST LTG	*median*	-2.84	-2.30	-3.87	-4.08	7.23	9.11	6.01	8.45	5.28	6.05	3.89	6.06
	mean	-2.49	-2.26	-3.81	-3.82	7.51	8.61	6.47	8.83	5.76	6.53	3.91	6.52
	iqr	5.55	5.34	3.69	4.13	4.53	4.52	4.36	4.41	4.03	4.19	5.14	5.12
	std dev	4.06	4.41	2.52	3.46	4.26	3.29	3.62	3.45	4.16	6.04	3.68	5.04
LTG-15min	*median*	-8.64	-8.70	-7.78	-9.81	6.02	6.97	8.11	6.17	3.76	4.50	6.39	4.26
	mean	-8.01	-8.13	-7.99	-10.17	6.12	7.23	8.28	6.47	3.86	4.62	6.13	4.24
	iqr	5.29	4.59	3.06	4.93	4.15	3.39	6.07	4.44	3.52	4.12	5.21	3.36
	std dev	3.74	3.48	2.73	3.23	2.98	3.02	4.42	3.58	3.64	3.90	4.14	3.48
LTG-30min	*median*	-11.85	-12.40	-13.62	-13.51	4.32	5.63	6.41	4.13	3.17	3.83	4.60	2.74
	mean	-11.87	-12.57	-14.30	-14.14	4.35	5.27	7.44	5.11	3.08	3.95	4.97	3.44
	iqr	5.00	4.41	5.56	5.15	2.92	3.25	4.76	4.03	2.54	2.53	5.22	3.79
	std dev	4.02	3.94	4.00	4.14	2.40	2.20	4.00	3.47	2.27	2.18	3.94	3.48
LTG-45min	*median*	-14.92	-16.40	-19.34	-17.32	3.53	2.94	6.36	3.55	2.27	2.37	4.60	3.64
	mean	-15.03	-16.43	-19.42	-17.28	3.55	3.19	6.75	4.05	2.42	2.66	5.19	3.20
	iqr	4.91	4.37	9.01	5.90	2.62	2.69	4.74	4.70	2.36	2.16	3.91	4.50
	std dev	4.07	3.72	6.00	4.56	2.41	2.01	4.62	2.91	1.93	2.20	3.55	2.49
LTG-60min	*median*	-18.37	-18.90	-24.57	-20.06	2.41	2.35	2.84	1.41	1.69	1.77	2.25	0.99
	mean	-17.60	-18.81	-23.66	-20.28	2.68	2.31	3.68	2.05	1.72	1.81	2.46	1.60
	iqr	5.62	4.07	10.00	6.20	2.36	2.10	4.89	2.27	1.89	1.97	4.35	2.51
	std dev	4.38	3.19	5.89	4.51	1.65	1.75	3.64	2.71	1.39	1.62	2.89	2.29

Statistics: All Regions and Interest Fields		Tb39-107				Tb39-107_trend				ref39			
		AL	FL	OK	DC	AL	FL	OK	DC	AL	FL	OK	DC
FIRST LTG	median	22.49	20.07	23.72	21.90	4.02	2.33	2.71	3.29	5.28%	4.99%	7.37%	5.64%
	mean	21.75	20.72	23.19	21.28	4.43	4.49	3.26	2.37	5.80%	5.08%	7.41%	6.46%
	iqr	8.62	9.07	3.37	8.74	5.84	8.09	8.17	7.09	3.25%	1.37%	3.17%	3.39%
	std dev	6.17	6.30	4.06	5.45	4.70	6.02	5.85	6.20	2.15%	1.10%	2.06%	2.24%
LTG-15min	median	16.65	17.68	19.69	19.51	1.95	1.37	2.66	1.49	8.14%	8.55%	9.98%	10.13%
	mean	17.13	16.85	19.35	19.12	1.94	1.25	1.56	1.65	8.35%	8.34%	10.75%	10.53%
	iqr	6.10	5.94	4.84	4.42	4.02	4.81	5.68	3.88	3.76%	3.74%	3.99%	4.84%
	std dev	4.45	4.49	3.09	4.36	3.32	5.46	5.77	4.05	2.77%	2.61%	3.39%	3.31%
LTG-30min	median	15.35	14.75	18.44	18.06	0.90	1.64	2.21	1.02	10.45%	10.98%	14.30%	13.01%
	mean	15.12	14.75	17.89	18.19	1.14	1.02	1.74	0.78	10.49%	10.77%	15.04%	13.23%
	iqr	6.25	4.36	6.25	4.19	3.70	3.20	3.28	3.37	3.93%	3.83%	4.38%	4.09%
	std dev	4.19	3.17	3.93	3.82	2.58	3.77	2.83	3.32	3.04%	2.65%	4.69%	3.34%
LTG-45min	median	13.65	13.46	16.76	16.35	1.11	0.68	1.05	2.38	12.20%	12.57%	17.70%	14.41%
	mean	13.87	13.20	16.32	17.21	0.57	0.57	1.92	2.40	12.12%	12.45%	18.73%	14.95%
	iqr	4.04	3.32	5.85	3.71	2.82	2.44	3.32	3.72	3.98%	2.41%	6.85%	3.98%
	std dev	3.43	2.67	4.15	3.37	2.69	1.88	2.97	2.93	3.04%	2.43%	5.42%	2.95%
LTG-60min	median	13.18	12.53	15.28	14.63	0.76	0.54	1.13	0.97	13.74%	13.52%	21.01%	15.17%
	mean	13.03	12.42	14.57	15.11	0.65	0.43	1.25	1.29	13.63%	13.85%	21.10%	15.30%
	iqr	4.28	3.94	3.64	4.24	1.90	1.73	1.99	2.00	3.01%	2.62%	9.24%	3.79%
	std dev	3.35	2.83	3.25	3.19	1.72	1.64	1.83	2.01	3.16%	2.67%	5.85%	2.81%

Statistics: All Regions and Interest Fields		ref39_Trend			
		AL	FL	OK	DC
FIRST LTG	median	-2.78%	-3.16%	-3.97%	-4.11%
	mean	-2.62%	-3.22%	-3.77%	-4.06%
	iqr	2.21%	3.58%	2.25%	2.11%
	std dev	1.87%	2.68%	2.07%	3.00%
LTG-15min	median	-2.38%	-2.71%	-4.67%	-2.22%
	mean	-2.11%	-3.05%	-4.27%	-2.22%
	iqr	2.62%	2.42%	4.78%	2.49%
	std dev	2.01%	2.64%	4.71%	1.94%
LTG-30min	median	-1.54%	-1.93%	-2.98%	-1.61%
	mean	-1.51%	-2.23%	-3.54%	-2.18%
	iqr	1.38%	2.17%	5.00%	2.68%
	std dev	1.52%	2.84%	4.29%	2.49%
LTG-45min	median	-1.46%	-1.49%	-3.07%	-0.18%
	mean	-1.48%	-1.56%	-2.97%	-0.22%
	iqr	2.22%	2.50%	5.45%	2.03%
	std dev	2.11%	1.90%	3.29%	1.81%
LTG-60min	median	-1.08%	-0.83%	-0.17%	0.06%
	mean	-1.06%	-1.25%	-0.69%	-0.04%
	iqr	2.28%	2.28%	2.79%	0.84%
	std dev	1.60%	1.77%	3.41%	1.05%

APPENDIX C. DISTRIBUTION AND CURVE FIT INFORMATION

As discussed in Section III E, Matlab's distribution and curve fit tools were used to establish characteristic CDF equations for each IF: a) Tb107, b) Tb107 trend, c) Tb65107 difference, d) Tb133107 difference, e) Tb65107 trend, f) Tb133107 trend, g) Tb39107 difference, h) Tb39107 trend, i) ref39 and j) ref39 trend. Each set of IF data were (1) fit to a non-parametric distribution, and the resulting data were then (2) matched with an appropriate Fourier series to form the CDF equations. The non-parametric distribution bandwidth, maxima, minima and step increments are listed for each IF under (1). The Fourier series coefficients and the goodness of fit statistics for each IF are listed under (2). The Fourier series coefficients are described further in Section III E.

Tb107: 1) Bandwidth = 4.62767,
Max:Step:Min = 200:0.0625:325

2) Coefficients (with 95% confidence bounds):
a0 = 0.4982 (0.4978, 0.4986)
a1 = 0.515 (0.5108, 0.5192)
b1 = -0.2782 (-0.2861, -0.2703)
a2 = 0.04718 (0.04677, 0.04759)
b2 = 0.01568 (0.01415, 0.01722)
a3 = -0.01901 (-0.02386, -0.01415)
b3 = 0.1065 (0.1055, 0.1074)
a4 = -0.0319 (-0.03366, -0.03014)
b4 = 0.02683 (0.02495, 0.0287)
a5 = -0.01699 (-0.01836, -0.01562)
b5 = -0.01868 (-0.01996, -0.0174)
a6 = 0.0001764 (-0.001392, 0.001745)
b6 = -0.017 (-0.01709, -0.01691)
a7 = 0.00443 (0.00422, 0.00464)
b7 = -0.001656 (-0.002102, -0.00121)
a8 = 0.002864 (0.002527, 0.0032)
b8 = 0.002803 (0.002451, 0.003154)
w = 0.03993 (0.03987, 0.03998)

Goodness of fit:
SSE: 0.0002792
R-square: 1
Adjusted R-square: 1
RMSE: 0.0003752

a)

Tb107_trend: 1) Bandwidth = 1.78544,
Max:Step:Min = -40:0.0383:30

2) Coefficients (with 95% confidence bounds):
a0 = 0.5424 (0.5313, 0.5535)
a1 = 0.2833 (0.2775, 0.2891)
b1 = 0.5132 (0.5113, 0.5152)
a2 = 0.006789 (-0.0002191, 0.0138)
b2 = -0.05005 (-0.07362, -0.02648)
a3 = 0.1195 (0.1087, 0.1302)
b3 = 0.02796 (0.01774, 0.03818)
a4 = -0.01082 (-0.03388, 0.01224)
b4 = -0.01081 (-0.02011, -0.001504)
a5 = 0.02766 (0.01184, 0.04348)
b5 = -0.01711 (-0.01942, -0.0148)
a6 = 0.0008925 (-0.0132, 0.01498)
b6 = -4.73e-05 (-0.006741, 0.006646)
a7 = 0.002538 (-0.003587, 0.008663)
b7 = -0.006044 (-0.01276, 0.0006726)
a8 = 0.002148 (-0.0007484, 0.005044)
b8 = -0.004143 (-0.009178, 0.0008911)
w = 0.07121 (0.06644, 0.07598)

Goodness of fit:
SSE: 0.0122
R-square: 1
Adjusted R-square: 1
RMSE: 0.002596

b)

Tb65107_diff: 1) Bandwidth = 3.14819,
Max:Step:Min = -50:0.0418:30

2) 6-coefficient Fourier Series used since a better fit than 8

Coefficients (with 95% confidence bounds):

a0 =	0.628	(0.6276, 0.6285)
a1 =	0.4419	(0.4412, 0.4426)
b1 =	0.3078	(0.3069, 0.3087)
a2 =	-0.07753	(-0.07819, -0.07686)
b2 =	-0.1445	(-0.1451, -0.1439)
a3 =	0.03432	(0.03418, 0.03445)
b3 =	-0.03056	(-0.03103, -0.03008)
a4 =	-0.03191	(-0.0322, -0.03162)
b4 =	0.02492	(0.02464, 0.02519)
a5 =	0.001765	(0.00159, 0.001939)
b5 =	-0.01107	(-0.01116, -0.01099)
a6 =	0.0005664	(0.0004813, 0.0006516)
b6 =	0.006497	(0.006452, 0.006543)
w =	0.0568	(0.0567, 0.05689)

Goodness of fit:
SSE: 0.0001562
R-square: 1
Adjusted R-square: 1
RMSE: 0.0002867

c)

Tb133107_diff: 1) Bandwidth = 2.18439,
Max:Step:Min = -25:0.0238:40

2) Coefficients (with 95% confidence bounds):

a0 =	-163.5	(-389, 61.94)
a1 =	282.9	(-106.4, 672.2)
b1 =	109.5	(-33.84, 252.9)
a2 =	-176.4	(-421.6, 68.84)
b2 =	-159.9	(-369, 49.17)
a3 =	70.81	(-31.56, 173.2)
b3 =	141.2	(-41.46, 323.8)
a4 =	-7.977	(-25.36, 9.405)
b4 =	-86.4	(-196.8, 23.96)
a5 =	-10.75	(-20.26, -1.236)
b5 =	36.9	(-9.638, 83.45)
a6 =	8.086	(-0.03429, 16.21)
b6 =	-10.26	(-23.16, 2.634)
a7 =	-2.686	(-5.333, -0.03846)
b7 =	1.485	(-0.5004, 3.469)
a8 =	0.3799	(0.02481, 0.7351)
b8 =	-0.03038	(-0.13, 0.06923)
w =	0.04761	(0.04421, 0.05101)

Goodness of fit:
SSE: 0.005974
R-square: 1
Adjusted R-square: 1
RMSE: 0.001484

d)

Tb65107_diff_trend: 1) Bandwidth = 1.12691,
Max:Step:Min = 0:0.0243:60

2) Coefficients (with 95% confidence bounds):

a0 =	131.7	(95.3, 168.2)
a1 =	-22.43	(-33.5, -11.37)
b1 =	-242.2	(-308.8, -175.5)
a2 =	-191.6	(-242.4, -140.8)
b2 =	35.03	(17.7, 52.36)
a3 =	34.8	(17.68, 51.92)
b3 =	128.3	(96.37, 160.1)
a4 =	71.59	(55.43, 87.75)
b4 =	-25.72	(-38.15, -13.29)
a5 =	-14.39	(-21.19, -7.59)
b5 =	-32.6	(-38.98, -26.22)
a6 =	-11.58	(-13.43, -9.736)
b6 =	5.825	(3.102, 8.548)
a7 =	1.526	(0.7978, 2.254)
b7 =	2.893	(2.546, 3.241)
a8 =	0.3842	(0.3529, 0.4154)
b8 =	-0.1964	(-0.2961, -0.09662)
w =	0.05197	(0.05116, 0.05279)

Goodness of fit:
SSE: 0.01331
R-square: 1
Adjusted R-square: 1
RMSE: 0.002238

e)

Tb133107_diff_trend: 1) Bandwidth = 1.03561,
Max:Step:Min = -15:0.0290:60

2) Coefficients (with 95% confidence bounds):

a0 =	0.6375	(0.6181, 0.657)
a1 =	-0.3858	(-0.3908, -0.3808)
b1 =	0.426	(0.3874, 0.4647)
a2 =	0.04417	(0.009577, 0.07876)
b2 =	0.2432	(0.236, 0.2503)
a3 =	-0.002342	(-0.01209, 0.00741)
b3 =	-0.04491	(-0.0725, -0.01733)
a4 =	-0.1279	(-0.1493, -0.1066)
b4 =	0.003924	(-0.007, 0.01485)
a5 =	-0.03963	(-0.04891, -0.03035)
b5 =	0.07224	(0.0573, 0.08718)
a6 =	0.0154	(0.006901, 0.0239)
b6 =	-0.001672	(-0.008711, 0.005367)
a7 =	-0.02506	(-0.03027, -0.01984)
b7 =	-0.02779	(-0.03193, -0.02365)
a8 =	-0.02484	(-0.02681, -0.02288)
b8 =	0.001094	(-0.001679, 0.003867)
w =	0.06755	(0.06692, 0.06817)

Goodness of fit:
SSE: 0.1084
R-square: 0.9997
Adjusted R-square: 0.9997
RMSE: 0.006497

f)

Tb39107_diff*: 1) Bandwidth = 1.91934,
Max:Step:Min = 0:0.0329:70

2) Coefficients (with 95% confidence bounds):

a0 =	0.4335	(0.2211, 0.6459)
a1 =	-0.7575	(-0.9497, -0.5654)
b1 =	0.3435	(-0.03417, 0.7212)
a2 =	-0.06018	(-0.2511, 0.1307)
b2 =	0.3301	(0.02764, 0.6325)
a3 =	0.2848	(0.01924, 0.5504)
b3 =	0.04679	(0.01469, 0.07888)
a4 =	0.1826	(0.1129, 0.2523)
b4 =	-0.1472	(-0.3242, 0.02984)
a5 =	-0.006523	(-0.07645, 0.06341)
b5 =	-0.1174	(-0.2026, -0.03221)
a6 =	-0.05507	(-0.1074, -0.002772)
b6 =	-0.01829	(-0.03205, -0.004525)
a7 =	-0.02143	(-0.02593, -0.01693)
b7 =	0.01862	(-0.003043, 0.04028)
a8 =	-0.001177	(-0.005813, 0.003459)
b8 =	0.008472	(0.004266, 0.01268)
w =	0.06129	(0.05905, 0.06353)

Goodness of fit:
SSE: 0.003209
R-square: 1
Adjusted R-square: 1
RMSE: 0.001233

g)

Tb39107_diff_trend*: 1) Bandwidth = 1.18528,
Max:Step:Min = -15:0.0273:60

2) Coefficients (with 95% confidence bounds):

a0 =	0.6554	(0.6508, 0.66)
a1 =	-0.335	(-0.3379, -0.332)
b1 =	0.4346	(0.4257, 0.4435)
a2 =	0.07176	(0.06466, 0.07886)
b2 =	0.2322	(0.2276, 0.2368)
a3 =	-0.0056	(-0.01134, 0.000145)
b3 =	-0.01647	(-0.02087, -0.01208)
a4 =	-0.08813	(-0.09039, -0.08588)
b4 =	0.04935	(0.04357, 0.05514)
a5 =	0.0006808	(-0.003804, 0.005165)
b5 =	0.06387	(0.06307, 0.06468)
a6 =	0.004394	(0.003348, 0.00544)
b6 =	-0.005495	(-0.008412, -0.002577)
a7 =	-0.02631	(-0.02804, -0.02458)
b7 =	0.003903	(0.002676, 0.005131)
a8 =	-0.006381	(-0.007192, -0.00557)
b8 =	0.01645	(0.01568, 0.01721)
w =	0.06525	(0.06495, 0.06555)

Goodness of fit:
SSE: 0.0896
R-square: 0.9998
Adjusted R-square: 0.9998
RMSE: 0.005546

h)

ref39*: Bandwidth = 1) 0.014239,
Max:Step:Min = 0:0.00014148:0.16

2) Coefficients (with 95% confidence bounds):

a0 =	-41.65	(-57.62, -25.69)
a1 =	-14.82	(-17.35, -12.29)
b1 =	77.45	(47.94, 107)
a2 =	58.15	(34.94, 81.36)
b2 =	22.75	(18.72, 26.78)
a3 =	22.38	(18.32, 26.44)
b3 =	-35.89	(-51.28, -20.5)
a4 =	-17.53	(-26, -9.051)
b4 =	-16.42	(-19.46, -13.38)
a5 =	-9.004	(-10.74, -7.271)
b5 =	6.335	(2.579, 10.09)
a6 =	1.522	(0.2509, 2.794)
b6 =	3.566	(2.837, 4.296)
a7 =	0.9389	(0.7305, 1.147)
b7 =	-0.1737	(-0.4717, 0.1244)
a8 =	0.008288	(-0.02845, 0.04503)
b8 =	-0.1251	(-0.1567, -0.09348)
w =	6.753	(6.599, 6.907)

Goodness of fit:
SSE: 0.004985
R-square: 1
Adjusted R-square: 1
RMSE: 0.001191

i)

ref39_trend*: 1) Bandwidth = 0.00615824,
Max:Step:Min = -0.16:0.00010312:0.20

2) Coefficients (with 95% confidence bounds):

a0 =	0.4458	(0.4452, 0.4464)
a1 =	0.2402	(0.2393, 0.2412)
b1 =	0.5657	(0.5651, 0.5664)
a2 =	-0.0702	(-0.07075, -0.06965)
b2 =	0.06846	(0.0675, 0.06941)
a3 =	0.1443	(0.1439, 0.1447)
b3 =	0.05338	(0.05242, 0.05435)
a4 =	-0.0001784	(-0.0008019, 0.0004451)
b4 =	0.0724	(0.07167, 0.07313)
a5 =	0.04455	(0.04383, 0.04528)
b5 =	-0.02353	(-0.02405, -0.02301)
a6 =	0.03235	(0.0317, 0.03299)
b6 =	0.02913	(0.02872, 0.02955)
a7 =	0.003921	(0.003423, 0.00442)
b7 =	-0.01196	(-0.01246, -0.01146)
a8 =	0.02102	(0.02064, 0.02141)
b8 =	-0.003284	(-0.003732, -0.002837)
w =	11.08	(11.06, 11.1)

Goodness of fit:
SSE: 0.3325
R-square: 0.9997
Adjusted R-square: 0.9997
RMSE: 0.008297

j)

*Equations for 3.9 fields likely only valid during daytime (i.e. solar zenith angle <68deg) as Tb39107diff changes with loss of reflectance/solar component.

THIS PAGE INTENTIONALLY LEFT BLANK

LIST OF REFERENCES

Adler, R. F., and D. D. Fenn, 1979: Thunderstorm intensity as determined from satellite data. *J. Appl. Meteor.*, **18**, 502–517.

Byers, H.R., and R.R. Braham, 1948: Thunderstorm structure and circulation. *J. Atmos. Sci.*, **5**, 71–86.

Changnon, S. A., 2001: Thunderstorm rainfall in the conterminous United States. *Bull. Amer. Meteor. Soc.*, **82**, 1925-1940.

———— , 2003: Geographical and temporal variations in thunderstorms in the contiguous United States during the 20th Century. *Phys. Geog.,* **24**, 138-152.

Cooperative Institute for Meteorological Satellite Studies (CIMMS) / SSEC—UW-Madison, cited Jan. 2010: GOES Activities - - CIMMS/SSEC: Technical Info. [Available online at http://cimss.ssec.wisc.edu/goes/calibration/.]

Cooperative Program for Operational Meteorological Education and Training (COMET), cited Feb. 2005: Topics in lake effect snow forecasting, Section 1.5 Cloud and precipitation microphysics. [Available online at http://www.meted.ucar.edu/norlat/snow/lake_effect/1.5_microphysics.htm.]

Cummins K. L., J. A. Cramer, C. J. Biagi, E. P. Krider, J. Jerauld, M. Uman, and V. Rakov, 2006: The U.S. National Lightning Detection Network: Post-upgrade status. Preprints, *Second Conf. on the Meteorological Applications of Lightning Data,* Atlanta, GA, Amer. Meteor. Soc., CD-ROM, P6.1.

Curran, E. B., R. L. Holle, and R. E. López, 2000: Lightning casualties and damages in the United States from 1959 to 1994. *J. Climate*, **13**, 3448–3464.

DC Lightning Mapping Array (DCLMA), cited Jan. 2010: DCLMA Network. [Available online at http://branch.nsstc.nasa.gov/PUBLIC/DCLMA/.]

Dye J. E., W. P. Winn, J. J. Jones, and D. W. Breed, 1989: The electrification of New Mexico thunderstorms. Part I: The relationship between precipitation development and the onset of electrification. *J. Geophys. Res.*, **94**, 8643–8656.

Easterling, D. R., 1989: Regionalization of thunderstorm rainfall in the contiguous U.S. *Int. J. Climatol.,* **9**, 567-579.

Federal Aviation Administration (FAA), United States Department of Transportation, 2003: Commercial space transportation quarterly launch report. FAA 2nd Quarter Rep., 18 pp.

Goodman, S. J., D. E. Buechler, and P. J. Meyer, 1988: Convective tendency images derived from a combination of lightning and satellite data. *Wea. Forecasting*, **3**, 173–188.

———— and Coauthors, 2005: The north Alabama lightning mapping array: recent severe storm observations and future prospects. *Atmos. Res.,* **76**, 423-237.

Gremillion, M. S., and R. E. Orville, 1999: Thunderstorm characteristics of cloud-to-ground lightning at the Kennedy Space Center, Florida: A study of lightning initiation signatures as indicated by the WSR-88D. *Wea. Forecasting*, **14**, 640–649.

Houze, R. A., Jr., 1993: *Cloud Dynamics.* Academic Press, 573 pp.

Kaplan M. L, A. W. Huffman, K. M. Lux, J. D. Cetola, J. J. Charney, A. J. Riordan, Y-L Lin, and K. T. Waight III, 2005: Characterizing the severe turbulence environments associated with commercial aviation accidents. A 44-case study synoptic observational analysis. *Meteorol. Atmos. Phys.*, **88**, 129-152.

Kidder, S. Q. and T. H. Vonder Haar, 1995: *Satellite Meteorology: An Introduction*. Academic Press, 466 pp.

Koshak, W. J., R. J. Solakiewicz, R. J. Blakeslee, S. J. Goodman, H. J. Christian, J. M. Hall, J. C. Bailey, E. P. Krider, M. G. Bateman, D. J. Boccippio, D. M. Mach, E. W. McCaul, M. F. Stewart, D. E. Buechler, W. A. Petersen, and D. J. Cecil, 2004: North Alabama lightning mapping array (LMA): VHF source retrieval algorithm and error analyses. *J. Atmos. Oceanic Technol.*, **21**, 543–558.

Krehbiel, P.R., 1986: The electrical structure of thunderstorms. *The Earth's Electrical Environment*, E. P. Krider and R. G. Roble, Eds., National Academy Press, 90-113.

————, P. R., R. J. Thomas, W. Rison, T. Hamlin, J. Harlin, and M. Davis, 2000: GPS-based mapping system reveals lightning inside storms. *Eos, Trans. Amer. Geophys. Union,* **81**, 21-25.

———— and Coauthors, 2006: The Washington DC metro area lightning mapping array. *Eos, Trans. Amer. Geophys. Union,* **87** (Fall Meeting Suppl.), Abstract AE33A-1053.

Lindsey, D. T., D. W. Hillger, L. Grasso, J. A. Knaff, and J. F. Dostalek, 2006: GOES climatology and analysis of thunderstorms with enhanced 3.9-μm reflectivity. *Mon. Wea. Rev.,* **134**, 2342-2353.

MacGorman, D. R., W. D. Rust, T. J. Schuur, M. I. Biggerstaff, J. M. Straka, C. L. Ziegler, E. R. Mansell, E. C. Bruning, K. M. Kuhlman, N. R. Lund, N. S. Biermann, C. Payne, L. D. Carey, P. R. Krehbiel, W. Rison, K. B. Eack, and W. H. Beasley, 2008: TELEX The Thunderstorm Electrification and Lightning Experiment. *Bull. Amer. Meteor. Soc.*, **89**, 997–1013.

McCaul, E. W., S. J. Goodman, K. M. LaCasse, and D. J. Cecil, 2009: Forecasting lightning threat using cloud-resolving model simulations. *Wea. Forecasting*, **24**, 709–729.

McNamara, T. M., 2002: The horizontal extent of cloud-to-ground lightning over the Kennedy Space Center., M.S. thesis, Dept. of Engineering Physics, Air Force Institute of Technology, 114 pp.

Mecikalski, J. R., and K. M. Bedka, 2006: Forecasting convective initiation by monitoring the evolution of moving cumulus in daytime GOES imagery. *Mon. Wea. Rev.*, **134**, 49–78.

————, ————, S. J. Paech, and L. A. Litten, 2008: A statistical evaluation of GOES cloud-top properties for nowcasting convective initiation. *Mon. Wea. Rev.*, **136**, 4899–4914.

Murphy, M. J., K. L. Cummins, N. W. S. Demetriades, W. P. Roeder, 2008: Performance of the new Four-Dimensional Lightning Surveillance System (4DLSS) at the Kennedy Space Center/Cape Canaveral Air Force Station complex. *Extended Abstracts, 13th Conf. on Aviation, Range and Aerospace Meteorology*, New Orleans, LA, *Amer. Meteor. Soc.*, 7.6.

National Oceanic and Atmospheric Administration Comprehensive Large Array-Data Stewardship System (NOAA-CLASS), cited Jan. 2010: NOAA CLASS. [Available online at http://www.class.ncdc.noaa.gov.]

National Oceanic and Atmospheric Administration (NOAA) Hazard Statistics, cited Jan. 2010: National Weather Service (NWS) Weather Fatality, Injury and Damage Statistics. [Available online at http://www.nws.noaa.gov/om/hazstats.shtml.]

National Renewable Energy Laboratory (NREL), cited Jan. 2010: MIDC: Solar Position Algorithm (SPA) Calculator. [Available online at http://www.nrel.gov/midc/solpos/spa.html.]

Nelson, L. A., 2002: Synthesis of 3-dimensional lightning data and weather radar data to determine the distance that naturally occurring lightning travels from thunderstorms., M.S. thesis, Dept. of Engineering Physics, Air Force Institute of Technology, 85 pp.

North Alabama Lightning Mapping Array (NALMA), cited Jan. 2010: NALMA Network. [Available online at http://branch.nsstc.nasa.gov/PUBLIC/NALMA/.]

Rison, W., S. Miller, S. Hunyday, 2003: New Mexico Tech Lightning Mapping Array: Real-time system monitoring and data display. *Eos, Trans. Amer. Geophys. Union,* Fall Meeting, Abstract AE22A-1108.

Roberts R. D., and S. Rutledge, 2003: Nowcasting storm initiation and growth using *GOES-8* and WSR-88D data. *Wea. Forecasting*, **18**, 562–584.

Robinson, M., J. Evans, B. Crowe, D. Klingle-Wilson, S. Allan, 2004: Corridor Integrated Weather System operational benefits 2002-2003: Initial estimates of convective weather delay reduction, MIT Lincoln Laboratory Project Report ATC-313.

Roeder, W. P., J. E. Sardonia, S. C. Jacobs, M. S. Hinson, A. A. Guiffrida, and J. T. Madura, 1999: Lightning Launch Commit Criteria at the Eastern Range/Kennedy Space Center, *37th AIAA Aerospace Sciences Meeting and Exhibit*, Reno, NV, American Institute of Aeronautics and Astronautics, 99-0890.

Roohr, P. B., and T. H. Vonder Haar, 1994: A comparative analysis of the temporal variability of lightning observation and GOES imagery. *J. Appl. Meteor.,* **33,** 1271–1290.

Rosenfeld, D., W. L. Woodley, A. Lerner, G. Kelman, and D. T. Lindsey, 2008: Satellite detection of severe convective storms by their retrieved vertical profiles of cloud particle effective radius and thermodynamic phase, *J. Geophys. Res.,* 113, D04208, doi:10.1029/2007JD008600.

Royal Astronomical Society of Canada (RASC) Calgary Centre, cited Jan. 2010: RASC Calgary Centre—Latitude and Longitude. [Available online at http://calgary.rasc.ca/latlong.htm.]

Saunders, C. P. R., 1993: A review of thunderstorm electrification processes. *J. Appl. Meteor.,* **32**, 642-655.

Setvak, M., and C. A. Doswell III, 1991: The AVHRR channel 3 cloud top reflectivity of convective storms. *Mon. Wea. Rev.,* **119,** 841–847.

Siewert, C., 2008: Nowcasting lightning initiation through the use of infrared observations from the GOES satellite. M.S. Thesis, Univ. of Alabama in Huntsville, 105 pp.

————, M. Koenig and J. R. Mecikalski, 2010: Application of Meteosat second generation data towards improving the nowcasting of convective initiation. *Meteor. Appl.*, Published online in Wiley InterScience [Available at http://www.interscience.wiley.com], doi:10.1002/met.176.

Thomas, R. J., P. R. Krehbiel, W. Rison, T. Hamlin, J. Harlin, and D. Shown, 2001: Observations of VHF source powers radiated by lightning. *Geophys. Res. Lett.*, **28**, 143-146.

————, ————, ————, S. J. Hunyady, W. P. Winn, T. Hamlin, and J. Harlin, 2004: Accuracy of the Lightning Mapping Array. *J. Geophys. Res.*, **109**, D14207, doi:10.1029/2004JD004549.

TRMM-4DLSS ftp, cited Jan. 2010: [Available online at ftp://trmm.ksc.nasa.gov/lightning/archives/4DLSS.]

Twain, Mark. [Samuel Clemens.] *Mark Twain's Letters*. Vol. 1. Ed. Albert Bigelow Paine. New York: Harper & Bros., 1917, 818.

Ward, J. G., K. L. Cummins, and E. P. Krider, 2008: Comparison of the KSC-ER Cloud-to-Ground Lightning Surveillance System (CGLSS) and the U.S. National Lightning Detection Network^{TM} (NLDN), *20th Intl. Lightning Detection Conf.,* Atlanta, GA, Amer. Meteor. Soc., 7 pp.

Wilks, D. S., 2006: *Statistical Methods in the Atmospheric Sciences*. 2nd ed. Academic Press, 627 pp.

Williams, E. R., 1988: The electrification of thunderstorms. *Sci. Amer.,* Nov., **259**, 48-65.

————, and R. E. Orville, 1989: The relationship between lightning type and convective state of thunderclouds. *J. Geophys. Res.*, **94**, 13213–13220.

————, V. Mushtak, D. Rosenfeld, S. Goodman, and D. Boccippio, 2005: Thermodynamic conditions favorable to superlative thunderstorm updraft, mixed phase microphysics and lightning flash rate. *Atmos. Res.*, **76**, 288–306.

THIS PAGE INTENTIONALLY LEFT BLANK

INITIAL DISTRIBUTION LIST

1. Defense Technical Information Center
   Ft. Belvoir, Virginia

2. Dudley Knox Library
   Naval Postgraduate School
   Monterey, California

3. Prof. Philip A. Durkee
   Naval Postgraduate School
   Monterey, California

4. Mr. Kurt E. Nielsen
   Naval Postgraduate School
   Monterey, California

5. Mr. William Roeder
   45WS
   Patrick AFB, Florida

6. Prof. John R. Mecikalski
   University of Alabama – Huntsville
   Huntsville, Alabama

7. Air Force Weather Technical Library
   Asheville, North Carolina